Search for heavy pseudoscalar and scalar bosons decaying to a top quark pair in proton–proton collisions at $\sqrt{s} = 13\,\text{TeV}$

OPEN ACCESS
IOP Publishing
Reports on Progress in Physics
Rep. Prog. Phys. **88** (2025) 127801 (38pp)
https://doi.org/10.1088/1361-6633/ae2207

Search for heavy pseudoscalar and scalar bosons decaying to a top quark pair in proton–proton collisions at $\sqrt{s} = 13\,\text{TeV}$

The CMS Collaboration

CERN, Geneva, Switzerland

E-mail: cms-publication-committee-chair@cern.ch

Received 7 July 2025, revised 31 October 2025
Accepted for publication 20 November 2025
Published 5 December 2025

Corresponding editor: Dr Lorna Brigham

Abstract

A search for pseudoscalar or scalar bosons decaying to a top quark pair ($\mathrm{t\bar{t}}$) in final states with one or two charged leptons is presented. The analyzed proton–proton collision data was recorded at $\sqrt{s} = 13\,\text{TeV}$ by the CMS experiment at the CERN LHC and corresponds to an integrated luminosity of $138\,\text{fb}^{-1}$. The invariant mass $m_{\mathrm{t\bar{t}}}$ of the reconstructed $\mathrm{t\bar{t}}$ system and variables sensitive to its spin and parity are used to discriminate against the standard model $\mathrm{t\bar{t}}$ background. Interference between pseudoscalar or scalar boson production and the standard model $\mathrm{t\bar{t}}$ continuum is included, leading to peak-dip structures in the $m_{\mathrm{t\bar{t}}}$ distribution. An excess of the data above the background prediction, based on perturbative quantum chromodynamics (QCD) calculations, is observed near the kinematic $\mathrm{t\bar{t}}$ production threshold, while good agreement is found for high $m_{\mathrm{t\bar{t}}}$. The data are consistent with the background prediction if the contribution from a simplified model of a color-singlet ${}^1\mathrm{S}_0^{[1]}$ $\mathrm{t\bar{t}}$ quasi-bound state η_t, inspired by nonrelativistic QCD, is added. Upper limits at 95% confidence level are set on the coupling between the pseudoscalar or scalar bosons and the top quark for boson masses in the range 365–1000 GeV, relative widths between 0.5% and 25%, and two background scenarios with or without η_t contribution.

Keywords: CMS, top quark, scalar boson, pseudoscalar boson

1. Introduction

The observation of a Higgs boson with mass of 125 GeV by the ATLAS and CMS Collaborations in 2012 [1–3] confirmed the existence of an elementary spin-0 state, a crucial ingredient of the standard model (SM) of particle physics. While only one such state is required in the SM, many beyond-the-SM (BSM) extensions predict additional spin-0 states, such as two Higgs doublet models (2HDMs) [4] and models predicting a new electroweak pseudoscalar or scalar singlet [5], including models with a combination of a Higgs doublet and such singlet(s) [6]. These additional bosons may also provide a portal to dark matter by acting as mediators between SM and dark matter particles [7, 8]. The new states introduced in these BSM extensions usually include pseudoscalar (CP-odd) neutral bosons, scalar (CP-even) neutral bosons, and charged bosons. We use the symbol A to denote pseudoscalar neutral states, H for scalar neutral states not identified as the one with a mass of 125 GeV, and Φ as a common symbol to refer to either A or H bosons.

As the heaviest elementary particles, top quarks have a pivotal role in the search for BSM physics, serving as sensitive probes. Provided that additional Φ bosons couple to fermions via a Yukawa interaction with coupling strength proportional to the fermion mass, Φ bosons with mass larger than twice the top quark mass m_{t} may decay to a top quark pair ($\mathrm{t\bar{t}}$) as the dominant channel. This is true especially for A bosons with suppressed decays to weak vector bosons due to CP symmetry, as well as for H bosons in 2HDMs in the vicinity of the alignment limit [9].

In this paper, we consider a Yukawa-like coupling between Φ bosons and top quarks. The corresponding terms in the Lagrangian for the two CP eigenstates are:

$$\mathcal{L}_{\mathrm{Yukawa,A}} = i g_{\mathrm{A t\bar{t}}} \frac{m_{\mathrm{t}}}{v} \bar{\mathrm{t}} \gamma_5 \mathrm{t}\, \mathrm{A},$$
$$\mathcal{L}_{\mathrm{Yukawa,H}} = -g_{\mathrm{H t\bar{t}}} \frac{m_{\mathrm{t}}}{v} \bar{\mathrm{t}}\mathrm{t}\, \mathrm{H}, \qquad (1)$$

where $g_{\Phi \mathrm{t\bar{t}}} \geqslant 0$ is the real-valued coupling strength modifier and v is the vacuum expectation value of the SM Higgs field. We probe Φ boson masses m_Φ in the range $365 < m_\Phi < 1000\,\mathrm{GeV}$ and total widths Γ_Φ relative to m_Φ in the range $0.5 < \Gamma_\Phi/m_\Phi < 25\%$.

The production of Φ bosons is dominated by the gluon fusion process via a top quark loop, followed by a decay into a $\mathrm{t\bar{t}}$ pair, as illustrated in figure 1(upper). This process interferes with SM $\mathrm{t\bar{t}}$ production through gluon fusion, an example of which is depicted in figure 1(lower). While the pure Φ resonance component results in a Breit–Wigner peak in the $\mathrm{t\bar{t}}$ invariant mass ($m_{\mathrm{t\bar{t}}}$) distribution, the interference terms may be either destructive or constructive, with the shape and magnitude of the $m_{\mathrm{t\bar{t}}}$ distribution depending on the phase space region under consideration, the specific signal model, and the types of particles that appear in the loop of the production diagram [10, 11]. In general, the sum of the components produce a peak-dip structure in the $m_{\mathrm{t\bar{t}}}$ distribution [12–16], which is shown in figure 2 for two example choices of m_Φ and Γ_Φ.

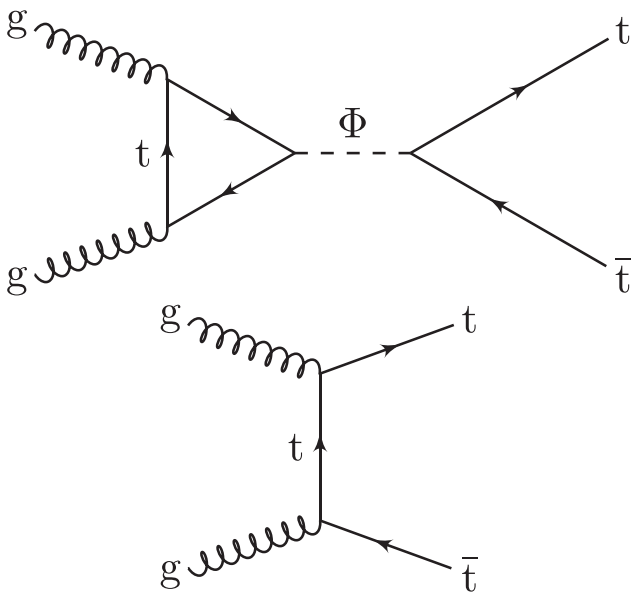

Figure 1. Example Feynman diagrams for the signal process (upper) and for SM $\mathrm{t\bar{t}}$ production (lower).

Decays of the A and H bosons produce $\mathrm{t\bar{t}}$ systems in the $^1\mathrm{S}_0$ and $^3\mathrm{P}_0$ states, respectively [14]. The SM $\mathrm{t\bar{t}}$ production comprises a mixture of spin states, with their relative contributions varying as a function of the partonic center-of-mass energy. Due to the short lifetime of top quarks, the information about their spin and polarization states is preserved in the angular distributions of their decay products [17–19]. Therefore, in addition to analyzing the $m_{\mathrm{t\bar{t}}}$ distribution, we utilize angular observables to investigate the differences in the $\mathrm{t\bar{t}}$ spin states between signal and background processes.

In the SM, $\mathrm{t\bar{t}}$ production is described by quantum chromodynamics (QCD). State-of-the-art cross section predictions rely on fixed-order (FO) perturbative QCD (pQCD) calculations and include electroweak (EW) corrections. An additional enhancement of $\mathrm{t\bar{t}}$ production below the kinematic threshold is predicted in nonrelativistic QCD, dominated by the production of color-singlet $\mathrm{t\bar{t}}$ quasi-bound states (toponium) [20–25]. We account for this effect by using a simplified model of the production of the color-singlet pseudoscalar quasi-bound state $^1\mathrm{S}_0^{[1]}$, referred to as η_{t} [25].

This paper describes a search for pseudoscalar and scalar bosons produced in proton–proton collisions at $\sqrt{s} = 13\,\mathrm{TeV}$ and decaying to $\mathrm{t\bar{t}}$. The analyzed data were recorded using the CMS detector at the CERN LHC in 2016–2018 and corresponds to an integrated luminosity of $138\,\mathrm{fb}^{-1}$ [26–28]. The single-lepton (ℓj) and dilepton ($\ell\ell$) channels are considered, corresponding to the $\mathrm{t\bar{t}} \to \mathrm{b\bar{b}WW} \to \mathrm{b\bar{b}}\ell\nu\mathrm{jj}$ and $\mathrm{b\bar{b}}\ell\nu\ell\nu$ decay chains of the $\mathrm{t\bar{t}}$ system, respectively. Events in the ℓj channel are selected with exactly one electron or muon and at least three jets (at least two of which are b tagged), and in the $\ell\ell$ channel with exactly two oppositely charged leptons (electrons and/or muons) and at least two jets (at least one of which is b tagged). The top quark four-momenta are estimated using

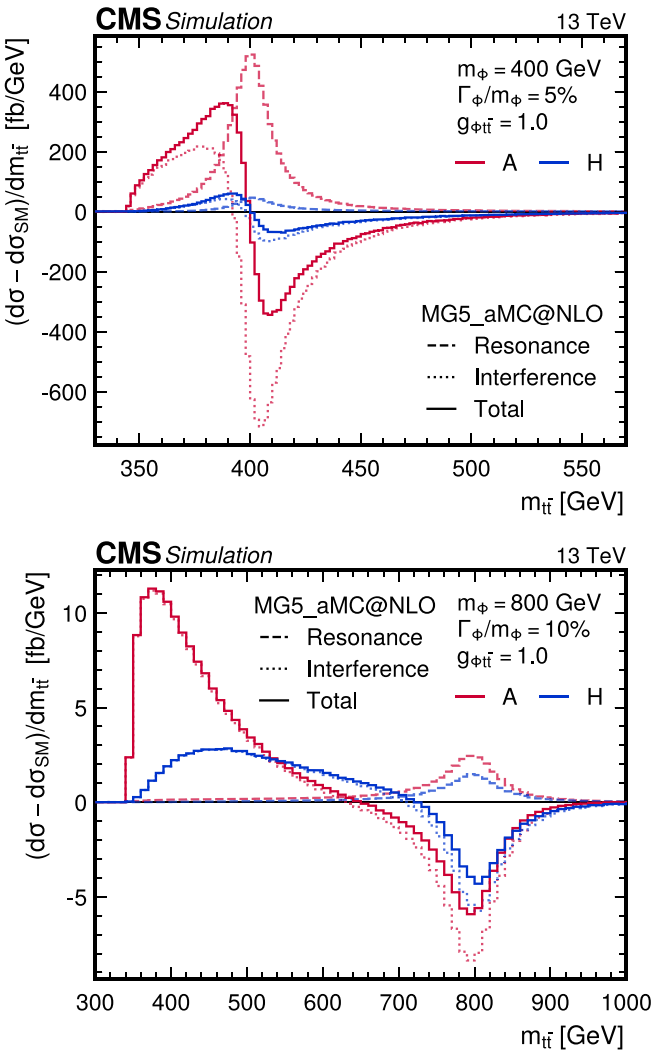

Figure 2. Differential cross section of $t\bar{t}$ production at parton level as a function of $m_{t\bar{t}}$, shown as difference between various BSM scenarios and the SM prediction. Shown are the cases of a single A (red) or H (blue) boson for two example configurations: $m_\Phi = 400\,\text{GeV}$ and $\Gamma_\Phi/m_\Phi = 5\%$ (upper), or $m_\Phi = 800\,\text{GeV}$ and $\Gamma_\Phi/m_\Phi = 10\%$ (lower), with $g_{\Phi t\bar{t}} = 1$ in both cases. Separately shown are the cases where only the resonant $\Phi \to t\bar{t}$ contribution is added to the SM prediction (dashed), where only the interference between SM and Φ boson contributions is added (dotted), and where both contributions are added (solid). The distributions have been calculated using MadGraph5_aMC@NLO as described in section 3.

kinematic reconstruction algorithms and the resulting $m_{t\bar{t}}$ distribution together with additional observables sensitive to the spin state of the $t\bar{t}$ system are used to search for Φ bosons.

The data are interpreted in terms of Φ boson production, quantified via the coupling $g_{\Phi t\bar{t}}$ for given values of m_Φ and Γ_Φ, in three signal configurations: one A boson, one H boson, or both of them. A combined maximum likelihood fit to all channels is used to extract the signals. Two different background scenarios are investigated: one consists of FO pQCD predictions alone, and the other includes η_t production as part of the background.

Near the $t\bar{t}$ threshold, there is an excess of the data with respect to the background predicted in FO pQCD alone, with a structure that favors an additional pseudoscalar contribution [29]. In [29], the companion paper to this publication, we perform an identical analysis to the one presented in this paper in the $\ell\ell$ channel only, to demonstrate that the observed excess can be explained by η_t production without the need for BSM A boson contributions. We note that the current experimental resolution does not allow for a significant distinction between the η_t and the A boson production scenarios, nor any potential mixtures of both, if the A boson is produced sufficiently close to the $t\bar{t}$ production threshold with a width of $\sim$5% or less.

This search updates a similar analysis performed by the CMS experiment using $35.9\,\text{fb}^{-1}$ of data collected in 2016, where a moderate signal-like deviation compatible with A boson production with a mass of 400 GeV was found [30], without inclusion of any contribution from $t\bar{t}$ bound states as background. Searches for $\Phi \to t\bar{t}$ have also been performed by the ATLAS experiment using $20.3\,\text{fb}^{-1}$ of $\sqrt{s} = 8\,\text{TeV}$ data [31] and $140\,\text{fb}^{-1}$ of $\sqrt{s} = 13\,\text{TeV}$ data [32], where no significant deviations from the FO pQCD prediction were observed. A detailed discussion on the differences of this result and [32] is provided in [29].

2. The CMS detector and event reconstruction

The central feature of the CMS apparatus is a superconducting solenoid of 6 m internal diameter, providing a magnetic field of 3.8 T. Within the solenoid volume are a silicon pixel and strip tracker, a lead tungstate crystal electromagnetic calorimeter (ECAL), and a brass and scintillator hadron calorimeter (HCAL), each composed of a barrel and two endcap sections. Forward calorimeters extend the pseudorapidity (η) coverage provided by the barrel and endcap detectors. Muons are reconstructed using gas-ionization detectors embedded in the steel flux-return yoke outside the solenoid. More detailed descriptions of the CMS detector, together with a definition of the coordinate system used and the relevant kinematic variables, can be found in [33, 34].

Events of interest are selected using a two-tiered trigger system. The first level (L1), composed of custom hardware processors, uses information from the calorimeters and muon detectors to select events at a rate of around 100 kHz within a fixed latency of about 4 μs [35]. The second level, known as the high-level trigger, consists of a farm of processors running a version of the full event reconstruction software optimized for fast processing, and reduces the event rate to around 1 kHz before data storage [36, 37].

The primary vertex (PV) is taken to be the vertex corresponding to the hardest scattering in the event, evaluated using tracking information alone, as described in section 9.4.1 of [38]. The particle-flow (PF) algorithm [39] aims to reconstruct and identify each individual particle in an event, with an optimized combination of information from the various elements of the CMS detector. The reconstructed particles are

referred to as PF candidates in the following. The energy of photons is obtained from the ECAL measurement. The energy of electrons is determined from a combination of the electron momentum at the PV as determined by the tracker, the energy of the corresponding ECAL cluster, and the energy sum of all bremsstrahlung photons spatially compatible with originating from the electron track. The energy of muons is obtained from the curvature of the corresponding track. The energy of charged hadrons is determined from a combination of their momentum measured in the tracker and the matching ECAL and HCAL energy deposits, corrected for the response function of the calorimeters to hadronic showers. Finally, the energy of neutral hadrons is obtained from the corresponding corrected ECAL and HCAL energies.

For each event, hadronic jets are clustered from the PF candidates using the infrared and collinear safe anti-k_T algorithm [40, 41] with a distance parameter of 0.4. Jet momentum is determined as the vectorial sum of all particle momenta in the jet, and is found from simulation to be, on average, within 5%–10% of the true momentum over the entire transverse momentum (p_T) spectrum and detector acceptance. Additional proton–proton interactions within the same or nearby bunch crossings (pileup) can contribute additional tracks and calorimetric energy depositions to the jet momentum. To mitigate this effect, charged particles identified to be originating from pileup vertices are discarded and an offset correction is applied to correct for remaining contributions [42]. Jet energy corrections are derived from simulation to bring the measured response of jets to that of particle level jets on average. *In situ* measurements of the momentum balance in dijet, photon+jet, Z+jet, and multijet events are used to account for any residual differences in the jet energy scale between data and simulation [43]. The jet energy resolution amounts typically to 15%–20% at 30 GeV, 10% at 100 GeV, and 5% at 1 TeV [43]. Additional selection criteria are applied to each jet to remove jets potentially dominated by anomalous contributions from various subdetector components or reconstruction failures [42]. To be considered in the data analysis, jets are required to satisfy $\eta < 2.4$, to have $p_T > 30$ (20) GeV in the ℓj ($\ell\ell$) channel, and to be separated by $\Delta R = \sqrt{(\Delta\eta)^2 + (\Delta\phi)^2} > 0.4$ from any selected lepton, where $\Delta\eta$ and $\Delta\phi$ are the η and azimuthal angle differences between the lepton and jet, respectively.

Jets originating from b quarks are identified with the DeepJet algorithm [44–46]. The used working point has a selection efficiency for b quark jets of about 77%, and a misidentification rate of 15% for c quark jets and of 2% for light-quark and gluon jets (considered together and referred to as light jets in the following), as evaluated in simulated $\mathrm{t\bar{t}}$ samples. Differences between data and simulation in the b tagging efficiency and misidentification rate are accounted for by scale factors that depend on the jet p_T and η.

Electrons are measured in the range $\eta < 2.5$ as energy deposits in the ECAL matched to a track. The momentum resolution for electrons with p_T of around 45 GeV from $\mathrm{Z} \to$ ee decays ranges from 1.6% to 5%. It is generally better in the barrel region than in the endcaps, and also depends on the bremsstrahlung energy emitted by the electron as it traverses the material in front of the ECAL [47, 48]. Only electrons with $\eta < 2.4$ and $p_T > 20$ GeV are considered in the analysis. In the $\ell\ell$ channel, well-identified electron candidates are selected using identification criteria based on boosted decision trees with a working point targeting a 90% efficiency, with a misidentification rate of 1% and 3% in the barrel and endcap regions, respectively [47]. In the ℓj channel, well-identified electrons are selected using the 'tight' working point of the identification criteria based on sequential requirements, with an additional requirement of being consistent with originating from the PV [47]. The efficiency of the 'tight' working point is about 70%, with a misidentification rate of 1% and 2% in the barrel and endcap regions, respectively. Furthermore, the 'veto' working point of the same sequential-requirements-based identification criteria is used to define a sample of loosely identified electrons used to veto events in the ℓj channel. All three employed sets of electron identification criteria are described in detail in [47].

Muons are measured in the range $\eta < 2.4$, with detection planes made using three technologies: drift tubes covering the barrel region, cathode strip chambers covering the endcap region, and resistive-plate chambers covering both the barrel and endcap regions. Matching muons to tracks measured in the silicon tracker results in a relative p_T resolution, for muons with p_T up to 100 GeV, of 1% in the barrel and 3% in the endcaps; and of <7% in the barrel for muons with p_T up to 1 TeV. Only muons with $p_T > 20$ GeV are considered in the analysis. For use in the main event selection, well-identified muon candidates are required to pass the 'tight' working point of the identification criteria described in [49]. The selection efficiency of well-identified muons, together with the isolation requirements described below, is 75%–85%. The misidentification rate for well-identified muons is 0.1%–0.3%, and the probability to incorrectly label muons within jets as isolated is 5%–15%. Loosely identified muons are those passing the 'loose' working point of the identification criteria [49], and are used in the ℓj channel to veto events.

Lepton candidates are required to be isolated from other activity in the event. The relative isolation I_{rel} is calculated as the p_T sum of charged-hadron, neutral-hadron, and photon PF candidates inside a cone of $\Delta R = 0.4$ around the lepton, divided by the lepton p_T. An estimated contribution from pileup is subtracted in this calculation [47, 49]. In the ℓj channel, well-identified muons are required to have $I_{rel} < 0.15$, while loosely identified muons are required to have $I_{rel} < 0.25$. The same criteria of $I_{rel} < 0.25$ are used for well-identified muons in the $\ell\ell$ channel, where separate collections of loosely identified leptons are not introduced. For electrons, isolation requirements are already included in the identification criteria defined in [47]. Scale factors that depend on the lepton p_T and η are used to correct the simulation for small differences in lepton trigger, identification, and isolation efficiency with respect to data.

The missing transverse momentum vector $\vec{p}_T^{\,\mathrm{miss}}$ is computed as the negative vector sum of the transverse momenta of all the PF candidates in an event, and its magnitude is denoted as

$p_{\mathrm{T}}^{\mathrm{miss}}$ [50]. The $\vec{p}_{\mathrm{T}}^{\mathrm{miss}}$ is modified to account for corrections to the energy scale of the reconstructed jets in the event.

3. Data and simulated event samples

The analyzed data were recorded in 2016–2018 using triggers that require the presence of a single isolated electron or muon, or the presence of two such leptons including all possible flavor combinations. Four independent data-taking eras are considered: 2016pre (19.5 fb^{-1}), 2016post (16.8 fb^{-1}), 2017 (41.5 fb^{-1}), and 2018 (59.8 fb^{-1}). The 2016 data set is split into two eras because of a modification of the APV strip tracker readout chip settings that affects the efficiency of the track hit reconstruction during the 2016 data-taking period [51], where the identifiers 'pre' and 'post' refer to the periods before and after this modification. The 2016pre, 2016post, and 2017 eras are also affected by an inefficiency caused by the gradual shift in the timing of the inputs to the ECAL L1 trigger in the regions $\eta > 2.0$ [35]. Correction factors are computed from data and applied to the acceptance evaluated by simulation to account for this effect.

In order to compare the collected data to theoretical predictions, Monte Carlo (MC) samples are produced with events simulating the signal and background processes. Various programs are used to evaluate matrix elements (MEs) and generate events at parton level. In all cases, the generators employ the next-to-next-to-leading order (NNLO) NNPDF3.1 parton distribution functions (PDFs) [52] and are interfaced with PYTHIA 8.240 [53] for fragmentation and hadronization using the CP5 underlying event tune [54, 55]. The nominal value of m_{t} is set to 172.5 GeV in all samples involving top quarks, as well as in the computation of theoretical corrections that are applied to them. The simulated events are processed through the CMS detector simulation based on the GEANT4 program [56]. Separate MC samples are generated corresponding to the data-taking conditions of each of the four eras. Pileup interactions are generated with PYTHIA and overlaid in all samples. The simulated events are weighted to reproduce the distribution of the number of pileup interactions observed in data, assuming a total inelastic cross section of 69.2 mb. On average, there are 23 collisions per bunch crossing in 2016 data and 32 in 2017–2018 data [42].

The $\Phi \to \mathrm{t\bar{t}}$ signal process is simulated at leading-order (LO) accuracy using a custom model in the MADGRAPH5_aMC@NLO2.6.5 event generator [57]. It implements the full kinematics of the top quark loop of the gluon fusion production, including finite m_{t} effects, via a form factor that is implemented as an effective coupling between the Φ bosons and gluons [58]. Event samples are produced for different m_{Φ} and Γ_{Φ}/m_{Φ} values, such that a good coverage throughout the region of phase space probed in this search is obtained. They are reweighted to target signal hypotheses by the event-by-event ratios of the squared MEs of the target signal hypothesis and the one used in the original event simulation. The target signal hypotheses in this search are m_{Φ} values of 365, 380, and 400–1000 GeV (in steps of 25 GeV), and Γ_{Φ}/m_{Φ} values of 0.5%–3% (in steps of 0.5), 4%–8% (in steps of 1), 10%, 13%, 15%, 18%, 21%, and 25%. We use the notation 'A/H$(400, 3\%)$' to refer to Φ bosons of a particular CP eigenstate, m_{Φ} in GeV, and Γ_{Φ}/m_{Φ}. The factorization and renormalization scales, μ_{F} and μ_{R}, are set on an event-by-event basis to $m_{\mathrm{t\bar{t}}}/2$, following the choice in [59]. The top quarks from the Φ boson decay are further decayed in MADGRAPH5_aMC@NLO, preserving their spin correlations.

Separate samples are generated for events corresponding to resonant Φ boson production, and for events corresponding to interference terms in the ME calculation between Φ boson and FO pQCD $\mathrm{t\bar{t}}$ background production. Events in the interference samples can receive negative weights, reflecting the sign of the corresponding part of the squared ME in the presence of a destructive interference. Since the Φ boson is produced via gluon fusion with a top quark loop, the $\Phi\,\mathrm{t\bar{t}}$ coupling appears twice in the ME. As a result, events originating from the resonance ME terms correspond to a cross section proportional to $g^4_{\Phi\mathrm{t\bar{t}}}$, while those from interference correspond to a cross section proportional to $g^2_{\Phi\mathrm{t\bar{t}}}$.

We calculate cross sections for resonant Φ boson production at NNLO accuracy in pQCD with the SUSHI 1.7.0 program [60, 61] in the context of Type-II 2HDM models, where the 2HDMC program [62] is used to calculate the remaining model parameters for a given signal hypothesis. The coupling modifiers of the Φ bosons to bottom and charm quarks are set to zero. The ratio of the NNLO cross section to the LO cross section calculated with MADGRAPH5_aMC@NLO is used as a K factor to normalize the resonant part of the signal samples, with typical values around 2.

For the interference component of the signal samples, we apply K factors corresponding to the geometric mean of those applied to the resonant signal and the FO pQCD $\mathrm{t\bar{t}}$ process [59]. Here, the FO pQCD $\mathrm{t\bar{t}}$ production K factor is calculated as the ratio between the $\mathrm{t\bar{t}}$ cross section at NNLO in pQCD with next-to-next-to-leading logarithmic (NNLL) soft-gluon resummation, as described below, and at LO in pQCD with leading logarithmic resummation. The nominal value of this K factor is 1.49, and is within 1.42 and 1.55 for different m_{t} values and scale choices used in the computation. For the H signal, we have compared the resonance and interference K factors with a recent explicit next-to-LO (NLO) calculation in the scope of a one-Higgs-singlet extension of the SM in [63]. We find good agreement for the resonance component and significant differences of about 20% for the interference component. However, we have verified that this discrepancy does not significantly alter the conclusions of this work by performing alternative fits using the updated K factors for the interference component, and obtaining compatible exclusion regions as those reported in section 8. All K factors derived in this analysis are available in [64].

The η_{t} contribution is implemented as a generic resonance in the MADGRAPH5_aMC@NLO 2.6.5 event generator at LO accuracy in pQCD using a custom simplified model obtained from [25]. The model is similar to the one used for the $\Phi \to \mathrm{t\bar{t}}$ signal generation, although its effective gluon-pseudoscalar coupling is implemented as an effective contact

interaction instead of via the top quark loop. Samples of resonant $\eta_t \to WbWb$ events are produced to allow contributions from off-shell top quarks. The η_t mass and width are set to 343 and 7 GeV, respectively, following [25], corresponding to the expectation that the toponium mass is twice m_t minus a binding energy of about 2 GeV. A restriction to $|m_{WbWb} - 343\,\text{GeV}| < 6\,\text{GeV}$ at the generator level is employed, as recommended in [25], in order to not influence the high $m_{t\bar{t}}$ region which is assumed to be well-described by FO pQCD. Other simulation parameters are set following the recommendations of the model authors. The version of the model used here does not include the nonrelativistic Hamiltonian reweighting mentioned in [25, 65]. This is expected to have a negligible effect on this analysis, which is performed on reconstructed distributions, considering that the reweighting has a very small effect on parton-level distributions [66]. The η_t sample used in [29] has been updated compared to the one used in this work, with the η_t width set to 2.8 GeV and removing the generator-level requirement on m_{WbWb} [67]. At the level of precision of this analysis, and comparing reconstructed distributions, both η_t models are in agreement.

The main background contribution originates from the FO pQCD $t\bar{t}$ production process, and is simulated at NLO accuracy in pQCD using the POWHEG v2 generator [68–71]. The μ_F and μ_R scales are set to $\sqrt{m_t^2 + p_{T,t}^2}$, where m_t and $p_{T,t}$ are the mass and p_T of the top quarks in the underlying Born-level configuration. Decays of the top quarks are performed using the narrow-width approximation [72]. The sample is normalized to the predicted $t\bar{t}$ production cross section of $833.9^{+20.5}_{-30.0}$ pb, as calculated with the TOP++2.0 program at NNLO in pQCD, and including soft-gluon resummation at NNLL order [73]. The quoted uncertainty is derived from the independent variations of μ_F and μ_R, though they are not the only ones that affect the value. To improve the theoretical description of the FO pQCD $t\bar{t}$ production process, the sample is further reweighted differentially to account for NNLO pQCD and NLO EW corrections. The NNLO pQCD prediction is calculated using a private version of the MATRIX program [74], and the NLO EW prediction is calculated using the HATHOR 2.1 program [75–80], both with a nominal scale choice of $0.5\left(\sqrt{m_t^2 + p_{T,t}^2} + \sqrt{m_{\bar{t}}^2 + p_{T,\bar{t}}^2}\right)$. Both predictions are computed at the level of stable top quarks, using the same PDF set as the POWHEG v2 $t\bar{t}$ sample. The weights are applied double-differentially at the generator level as a function of $m_{t\bar{t}}$ and the cosine of the angle between the direction of the top quark in the zero-momentum frame (ZMF) of the $t\bar{t}$ system and the direction of the $t\bar{t}$ system in the laboratory frame, $\cos\theta_t^*$.

Other background events originate from single top quark production (tX), single vector boson production in association with jets including b jets (Z+jets and W+jets), diboson production (WW, WZ, and ZZ), $t\bar{t}$ production in association with a vector boson (referred to as $t\bar{t}V$), and events composed uniquely of jets produced through the strong interaction, referred to as QCD multijet processes. The single top quark production processes, via the t and s channels and as tW production, are generated at NLO using POWHEG v2, POWHEG, and MADGRAPH5_aMC@NLO, respectively [81, 82]. The samples are normalized using the NLO cross section predictions for the t and s channels [79, 83], and approximate NNLO prediction for the tW channel [84]. The Z+jets process is generated with the POWHEG event generator [69, 70] with a multi-scale-improved NNLO accuracy in pQCD [85, 86], matched with PYTHIA 8 for initial-state radiation (ISR) and the PHOTOS package [87, 88] for final-state radiation (FSR). The W+jets event samples are generated using MADGRAPH5_aMC@NLO at LO with up to four additional partons, and the MLM matching scheme [89] is used to combine the different parton multiplicities. The single vector boson production cross sections are calculated at NNLO [90, 91]. However, in the $\ell\ell$ channel, the normalization of the Z+jets contribution is directly determined from a control region in data. Events simulating the diboson processes are generated using PYTHIA and normalized to the respective NNLO (WW) [92] or NLO (WZ and ZZ) [93] cross sections. For the WW process, we checked that explicitly simulating nonresonant $WWb\bar{b}$ production, which leads to the same final state as $t\bar{t}$ production, does not change the results of this work. The $t\bar{t}V$ events are generated at NLO with MADGRAPH5_aMC@NLO, and are normalized using NLO cross section predictions. The MC@NLO matching scheme [94] is used for the $t\bar{t}W$ samples, while the FxFx matching scheme [95] is used for the $t\bar{t}Z$ samples. Finally, the QCD multijet events are simulated with PYTHIA.

4. Data analysis in the ℓj channel

Events that contain exactly one well-identified lepton (as defined in section 2) with $p_T > 30\,\text{GeV}$ are selected for further analysis in the ℓj channel. For data recorded during 2018 and most of 2017, except for an early period, a higher threshold of $p_T > 34\,\text{GeV}$ is applied if the lepton is an electron, in order to account for higher trigger-level thresholds. Events containing additional loosely identified leptons (as defined in section 2) with $p_T > 20\,\text{GeV}$ are rejected. Events are required to contain at least three jets with $p_T > 30\,\text{GeV}$, of which at least two are required to be b tagged. This event selection is referred to as signal region (SR).

4.1. Kinematic reconstruction

Each selected event is reconstructed under the assumption of $t\bar{t}$ pair production with one leptonically and one hadronically decaying W boson from the top quark decays. The first step is to determine the neutrino four-momentum based on the measured p_T^{miss}, and the second step is to assign jets to the final-state quarks. Different procedures are followed for events with at least four or exactly three jets, as described below.

The neutrino four-momentum p^ν is reconstructed with the algorithm described in [96], separately using each b jet in the event as candidate for the b accompanying the leptonically decaying W boson. Mass constraints of the W boson and

leptonically decaying top quark are formulated, and for each b jet candidate the p^{ν} that satisfies these constraints and minimizes the distance $D_{\nu} = \left|p_{\mathrm{T}}^{\mathrm{miss}} - p_{\mathrm{T}}^{\nu}\right|$ is used as the solution [96]. If no solution is found for any b jet, the event is rejected.

For events with four or more jets, a likelihood function is constructed using the product of the probability density of the minimal D_{ν} and the two-dimensional (2D) probability density of the invariant masses of the hadronically decaying top quark and W boson. The probability densities are evaluated from simulated events in which all jets are correctly identified. All possible assignments of jets to the four final-state quarks are evaluated, provided that only b-tagged jets are assigned as b and $\bar{\mathrm{b}}$ quark candidates. The best jet assignment is the one that maximizes this likelihood.

For events with exactly three jets, the techniques described in [97] are applied. The likelihood function is constructed using the product of the probability density of the minimal D_{ν} and the probability density of the invariant mass of the two jets assigned as originating from the hadronically decaying top quark. As with the case of four or more jets, the best assignment is the one that maximizes this likelihood. There are two typical cases of $\mathrm{t\bar{t}}$ events that only have three jets. The first and more common case is when one or more quarks from the $\mathrm{t\bar{t}}$ decay lie below the p_{T} threshold or outside of the detector acceptance, which we refer to as lost-jet events. The second case typically occurs in the high-momentum regime, where the angular separation between the top quark decay products are lower, leading to multiple quarks being clustered into one jet. These events are referred to as partially merged events. Once the best jet assignment is identified, a correction is applied to the four-momentum of the hadronically decaying top quark as a function of its reconstructed mass. The correction factor, which is derived using simulation as described in [97], is larger for lost-jet events and is close to one for partially merged events, since a significant energy loss is expected only in the former case.

In events where the required $\mathrm{t\bar{t}}$ decay products, i.e. the lepton and either all four or at least three jets, are inside the detector acceptance and well identified, the correct combination is found in 74% of events with four or more jets and in 83% of events with three jets. With respect to all selected $\mathrm{t\bar{t}}$ events, these correspond to rates of 37% and 61%, respectively.

The signal is extracted using 2D templates built using the $m_{\mathrm{t\bar{t}}}$ and $|\cos\theta^{*}_{\mathrm{t}_{\ell}}|$ variables. The angle $\theta^{*}_{\mathrm{t}_{\ell}}$ is defined between the reconstructed leptonically decaying top quark in the ZMF and the direction of the $\mathrm{t\bar{t}}$ system in the laboratory frame, analogously to θ^{*}_{t} introduced in section 3. The spin-0 nature of the signals leads to the top quarks being emitted isotropically in the $\mathrm{t\bar{t}}$ ZMF, resulting in a flat $\cos\theta^{*}_{\mathrm{t}_{\ell}}$ distribution at the generator level in the absence of kinematic selections. The FO pQCD distribution, on the other hand, peaks toward high values of $|\cos\theta^{*}_{\mathrm{t}_{\ell}}|$, due to the contribution from other spin states. As a result, the $|\cos\theta^{*}_{\mathrm{t}_{\ell}}|$ distribution will be enriched with signal events at low values.

To assess the precision of the reconstruction algorithm, we compute the relative resolution of $m_{\mathrm{t\bar{t}}}$, which is the standard deviation (SD) of its relative difference to the generator-level $m_{\mathrm{t\bar{t}}}$, evaluated in all selected simulated $\mathrm{t\bar{t}}$ events. The resolution is in the range of 8%, for low generator-level $m_{\mathrm{t\bar{t}}}$ values near the threshold region, to 13% for high generator-level $m_{\mathrm{t\bar{t}}}$ values above 1000 GeV, and it does not strongly depend on the number of jets. Furthermore, the absolute resolution of $|\cos\theta^{*}_{\mathrm{t}_{\ell}}|$, defined similarly as the SD of the absolute difference to the generator-level value, is found to be about 0.05 for events with four or more jets and 0.08 for events with three jets.

4.2. Background estimation

The background in the ℓj channel is estimated from MC simulation for FO pQCD $\mathrm{t\bar{t}}$ and single top quark production, as well as for η_{t} production, as described in section 3. QCD multijet production and EW processes (mostly W+jets and small contributions from Z+jets, diboson, and $\mathrm{t\bar{t}V}$ production) are estimated using a control region (CR) in data with the same selection criteria as for the SR except for requiring that none of the selected jets is b tagged. The background distributions are obtained by subtracting the simulated single top quark and $\mathrm{t\bar{t}}$ contributions from the data in the CR. The ratio of simulated background events in the SR and CR is applied as a normalization factor to the obtained background distributions. This procedure has been validated in simulation, and the kinematic distributions obtained from the CR are compatible with those in the SR.

The result of the kinematic reconstruction and background estimation is shown in figure 3, showing the reconstructed hadronically decaying top quark mass for events with four or more jets as well as the p_{T} of the $\mathrm{t\bar{t}}$ system for events with exactly three jets.

5. Data analysis in the $\ell\ell$ channel

In the $\ell\ell$ channel, events are selected that contain exactly two oppositely charged well-identified leptons, one with $p_{\mathrm{T}} > 25\,\mathrm{GeV}$ and the other with $p_{\mathrm{T}} > 20\,\mathrm{GeV}$. Events are rejected if they contain additional well-identified electrons or muons with $p_{\mathrm{T}} > 20\,\mathrm{GeV}$. Furthermore, the invariant mass $m_{\ell\ell}$ of the dilepton pair is required to be larger than 20 GeV, to suppress events from low-mass dilepton resonances, and for same-flavor pairs to be outside of the Z boson mass window, $76 < m_{\ell\ell} < 106\,\mathrm{GeV}$. To further suppress Z+jets background contributions, events in the ee and $\mu\mu$ channels are required to have $p_{\mathrm{T}}^{\mathrm{miss}} > 40\,\mathrm{GeV}$. In all cases, at least two jets with $p_{\mathrm{T}} > 30\,\mathrm{GeV}$ are required, and additional jets with $p_{\mathrm{T}} > 20\,\mathrm{GeV}$ are also considered for further analysis. At least one of these jets is required to be b tagged.

5.1. Kinematic reconstruction

Each selected event is reconstructed under the assumption that the final state consists of a top quark pair that decays into two leptonically decaying W bosons. A kinematic reconstruction algorithm [98] consisting of two steps is applied to reconstruct the $\mathrm{t\bar{t}}$ system. First, of all jets in an event, two are identified as

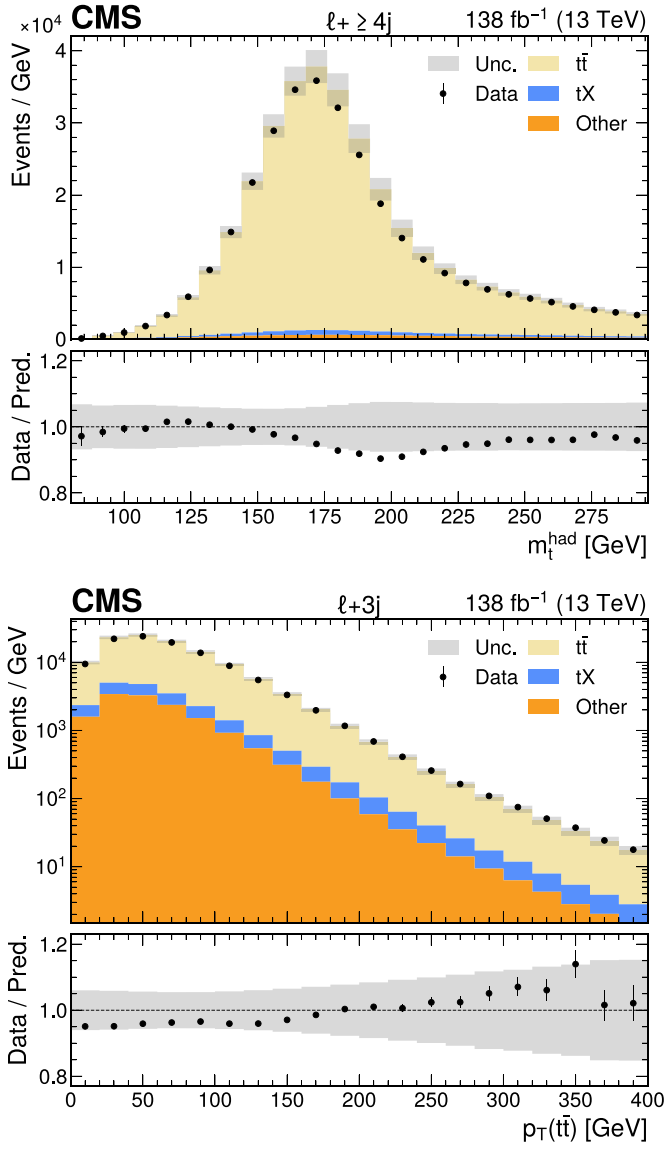

Figure 3. Comparison of the number of observed (points) and expected (colored histograms) events in the ℓj channel after the kinematic reconstruction and background estimation for the distributions of the reconstructed hadronic top quark mass $m_{\mathrm{t}}^{\mathrm{had}}$ in the region with four or more jets (upper) and the p_{T} of the $\mathrm{t\bar{t}}$ system in the region with exactly three jets (lower). The ratio to the total prediction is shown in the lower panel, and the total systematic uncertainty is shown as the gray band.

the b and $\bar{\mathrm{b}}$ quark candidates. Second, these two candidates, together with the two leptons and $p_{\mathrm{T}}^{\mathrm{miss}}$, are used to determine the t and $\bar{\mathrm{t}}$ quark four-momenta by applying mass constraints on the W bosons and top quarks, taking into account experimental resolutions.

To find the best assignment of jets to the b and $\bar{\mathrm{b}}$ quarks, candidate pairs of jets are selected based on the number of b-tagged jets in the event. For events with two or more b-tagged jets, only those jets are considered as b and $\bar{\mathrm{b}}$ quark candidates, while for events with exactly one b-tagged jet, this jet is paired with all other jets in the event. The invariant masses of the visible top quark decay products $m_{\ell^+\mathrm{b}}$ and $m_{\ell^-\bar{\mathrm{b}}}$ are calculated for each $\mathrm{b\bar{b}}$ candidate pair as well as each assignment to the b and $\bar{\mathrm{b}}$ quarks, and a likelihood is constructed as the product of the generator-level probability densities of the two invariant masses, evaluated from simulated events. The candidate pair that maximizes this likelihood is chosen for the next step of reconstruction.

Then, a system of equations for the top quark four-momenta is constructed from energy and momentum conservation as well as additional constraints [99], namely that: (i) the top quark mass is equal to 172.5 GeV, (ii) the W boson mass is equal to 80.4 GeV, (iii) the two neutrinos from the W boson decays are the sole source of $p_{\mathrm{T}}^{\mathrm{miss}}$. These equations, which are polynomials of fourth order, are solved for the neutrino momenta analytically, and the top quark four-momenta calculated as the vector sum of the decay products. To resolve ambiguities between the multiple solutions, the one with the lowest reconstructed value of $m_{\mathrm{t\bar{t}}}$ is used, which minimizes the bias with respect to the true value of $m_{\mathrm{t\bar{t}}}$ [100, 101].

In about 55% of cases, this procedure on its own does not give real solutions for the $\mathrm{t\bar{t}}$ system since it does not take into account the detector resolution. To remedy this, the system of equations is solved 100 times per event with random smearings applied to the energies and directions of the $\mathrm{b\bar{b}}$ candidates and leptons. These smearings are sampled, respectively, from distributions of the relative energy difference and angular distance between reconstructed and generator-level objects, as evaluated in simulated events. The effect of the smearing on the momenta of the $\mathrm{b\bar{b}}$ candidates and leptons is propagated to the measured $p_{\mathrm{T}}^{\mathrm{miss}}$, by adding to it the opposite of the total change in momenta along the transverse components due to the smearing. For all samplings that result in a real solution to the system of equations, weighted averages of the t and $\bar{\mathrm{t}}$ quark four-momenta are computed over all samplings, with the weight given by the same likelihood based on $m_{\ell^+\mathrm{b}}$ and $m_{\ell^-\bar{\mathrm{b}}}$ as used for the $\mathrm{b\bar{b}}$ quark candidate assignment. These averages are then considered as the final result of the reconstruction.

The performance of the $\mathrm{t\bar{t}}$ reconstruction algorithm is studied using simulated FO pQCD $\mathrm{t\bar{t}}$ events in the $\ell\ell$ final state. The algorithm produces a solution for 90% of the events. In 78% of these events, at least one b quark jet is correctly assigned, while in 61% both jets are correctly assigned. The relative $m_{\mathrm{t\bar{t}}}$ resolution, defined similarly as in section 4, is in the range of 15%, achieved at low generator-level $m_{\mathrm{t\bar{t}}}$ values near the threshold region, to around 30% at high generator-level $m_{\mathrm{t\bar{t}}}$ values above 1000 GeV. The average $m_{\mathrm{t\bar{t}}}$ resolution is 23%.

The search is performed by building three-dimensional (3D) templates using $m_{\mathrm{t\bar{t}}}$ and two observables c_{hel} and c_{han} that probe the spin correlations of the $\mathrm{t\bar{t}}$ system. Spin correlation variables have been discussed in detail in [17, 67, 102–105], and we follow the coordinate system and sign convention of [103]. The observable c_{hel} (referred to as $\cos\varphi$ in [17, 103] and $-\cos\theta_{ab}$ in [104]) is defined as the scalar product $c_{\mathrm{hel}} = \hat{\ell}_{\mathrm{t}}^{+} \cdot \hat{\ell}_{\bar{\mathrm{t}}}^{-}$, where $\hat{\ell}_{\mathrm{t}}^{+}$ and $\hat{\ell}_{\bar{\mathrm{t}}}^{-}$ are the unit vectors of the momenta of the two leptons in the rest frames of their parent t

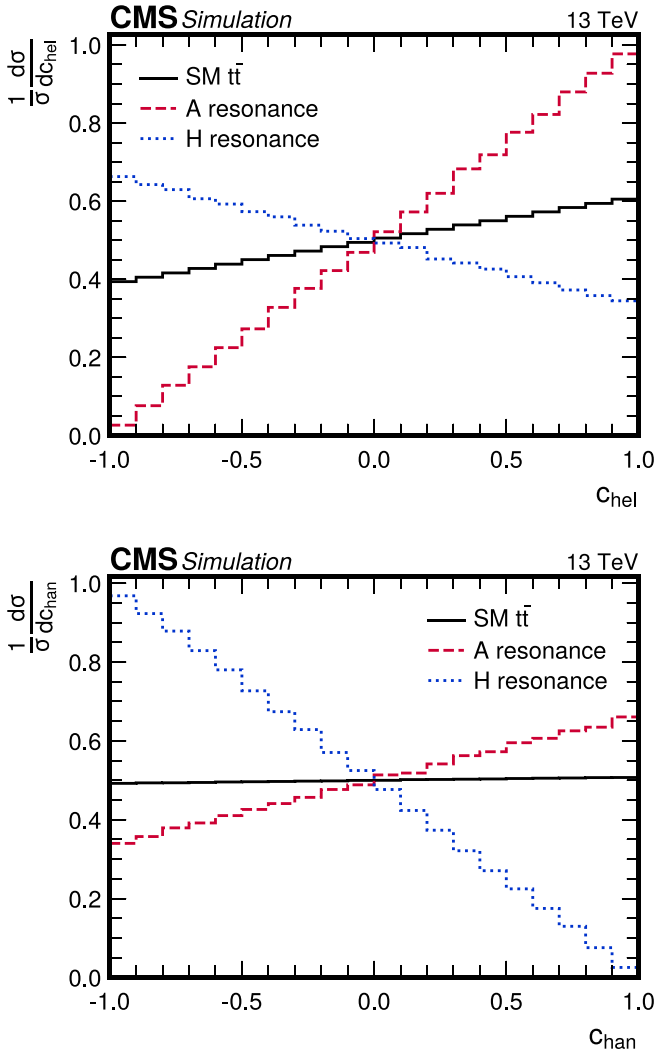

Figure 4. Normalized differential cross sections in the spin correlation observables c_{hel} (upper) and c_{han} (lower) at the parton level in the $\ell\ell$ channel, with no requirements on acceptance, for SM $\mathrm{t\bar{t}}$ production (black solid), resonant A boson production (red dashed), and resonant H boson production (blue dotted). The corresponding distributions for η_{t} are identical to those of a A boson.

and $\bar{\mathrm{t}}$, respectively, obtained by first boosting the leptons into the $\mathrm{t\bar{t}}$ ZMF and then further boosting them into the rest frames of their parent top (anti)quarks. The observable c_{han} (identified with $-\cos\theta'_{ab}$ in [104]) is obtained by flipping the sign of the component parallel to the top quark direction (the $\hat{k}$ direction in [103]) for either $\hat{\ell}_{\mathrm{t}}^{+}$ or $\hat{\ell}_{\bar{\mathrm{t}}}^{-}$, and then calculating a similar scalar product. The slopes of both distributions provide sensitivity to the degree of alignment between the t and $\bar{\mathrm{t}}$ spins. The absolute resolutions of c_{hel} and c_{han} as provided by the kinematic reconstruction, defined analogously as for $|\cos\theta^{*}_{\mathrm{t}_\ell}|$ in section 4, are found to be 0.46 for c_{hel} and 0.60 for c_{han}.

At the generator level and with no requirements on acceptance, the distributions of c_{hel} and c_{han}, integrated over the phase space of all other variables, follow a straight line, as shown in figure 4 for SM $\mathrm{t\bar{t}}$ and resonant Φ boson. For c_{hel}, the slope is maximally positive for a pseudoscalar resonance, due to the resulting $\mathrm{t\bar{t}}$ system being in the $^1\mathrm{S}_0$ state with anticorrelated t and $\bar{\mathrm{t}}$ spins. The slope for the SM $\mathrm{t\bar{t}}$ production is mildly positive, being the weighted average of all possible $\mathrm{t\bar{t}}$ spin states reachable by the initial colliding partons. Lastly, the slope of the scalar resonance is mildly negative, as a consequence of the $\mathrm{t\bar{t}}$ pair being in the $^3\mathrm{P}_0$ spin state. On the other hand, for c_{han}, the slope is mildly positive for a pseudoscalar resonance, approximately flat for the SM $\mathrm{t\bar{t}}$ production, and maximally negative for a scalar resonance. We further remark that, at generator level, the c_{hel} and c_{han} distributions for A and H resonances have the same slopes regardless of their mass and width values. The slopes of the SM $\mathrm{t\bar{t}}$ distributions on the other hand are dependent on $m_{\mathrm{t\bar{t}}}$—this is because of the change in the relative proportions of the colliding initial partons as well as their helicity combinations. These features of the c_{hel} and c_{han} distributions, when combined with $m_{\mathrm{t\bar{t}}}$, allow for discrimination between the signal and background processes and between the A and H states in a broad range of phase space.

5.2. Background estimation

All background processes in the $\ell\ell$ channel, namely FO pQCD $\mathrm{t\bar{t}}$, η_{t}, single top quark, Z+jets, diboson, and $\mathrm{t\bar{t}V}$ production, are estimated from simulated event samples. Both the $\ell\ell$ and the ℓj decay channels of $\mathrm{t\bar{t}}$ are considered for the FO pQCD $\mathrm{t\bar{t}}$ sample, and additional misidentified or nonprompt leptons are included. Contributions from W+jets events with one additional such lepton or QCD multijet events with two such leptons are found to be small in the $\ell\ell$ channel and neglected.

In the case of Z+jets production, the total yield of the simulation is corrected using data inside the Z boson mass window, which is removed in the main event selection, following a modified version of the procedure described in [106]. The same selection criteria except for the $m_{\ell\ell}$ requirements are applied to the data inside the Z boson mass window. We assume that there, the Z+jets contribution is negligible in the eμ channel compared to the ee and μμ channels, and that other backgrounds contribute equally to the three channels up to a combinatorial factor. Consequently, we can estimate the Z+jets contribution in data inside the Z boson mass window by subtracting the data yield in the eμ channel from the data yield in the ee and μμ channels while correcting for lepton reconstruction efficiencies, thus subtracting out other backgrounds.

Next, to estimate the ratio of the Z+jets contribution inside and outside the Z boson mass window, denoted as $R_{\mathrm{in/out}}$, we define a second sideband containing events with no b-tagged jets. The ratio in this region, $R^{0\mathrm{b}}_{\mathrm{in/out}}$, can be measured directly by comparing the Z+jets yields in data inside and outside the Z boson mass window. We then assume the ratio of ratios $R^{\geqslant 1\mathrm{b}}_{\mathrm{in/out}}/R^{0\mathrm{b}}_{\mathrm{in/out}}$ in the regions with $\geqslant 1$ and 0 b tags, respectively, to be well-described by simulation, which is a looser assumption compared to that in [106]. From this, we can infer $R^{\geqslant 1\mathrm{b}}_{\mathrm{in/out}}$, and thus the total Z+jets yield outside the Z boson mass window, for events with one or more b tags, as used in the main selection.

The yield is separately estimated for the ee and μμ channels, and used to normalize the simulated Z+jets contribution. Compared to the yields predicted by simulation, we find the

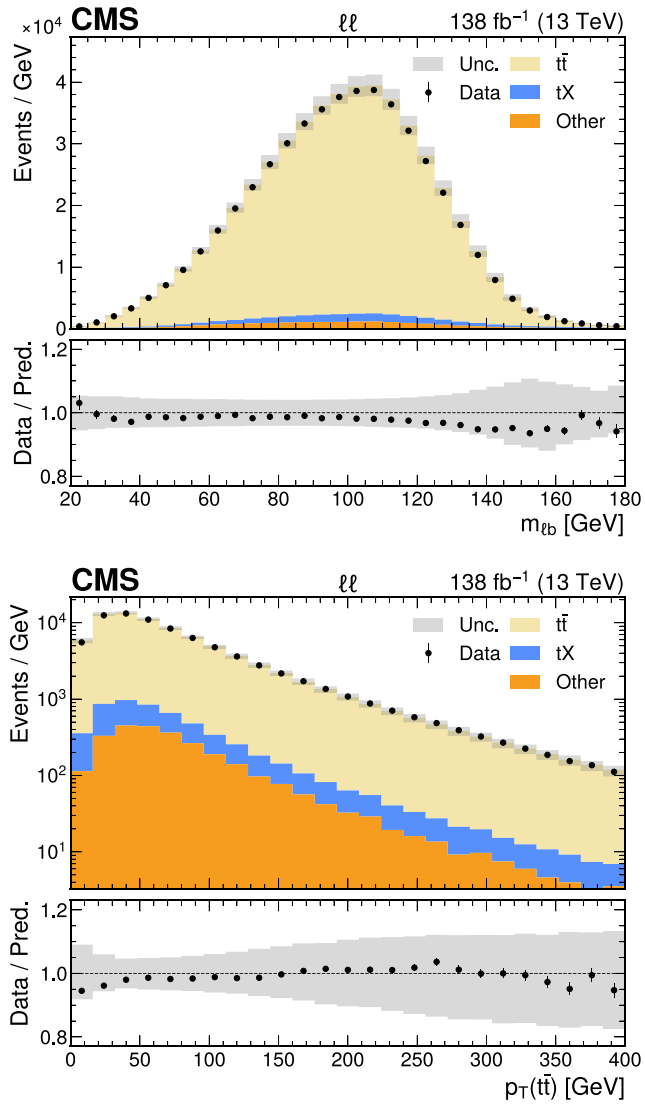

Figure 5. Comparison of the number of observed (points) and expected (colored histograms) events in the $\ell\ell$ channel after the kinematic reconstruction and background estimation for the distributions of the invariant lepton-b jet mass $m_{\ell b}$ (upper) and the p_T of the $t\bar{t}$ system (lower). The ratio to the total prediction is shown in the lower panel, and the total systematic uncertainty is shown as the gray band.

yield to be 3%–12% lower depending on analysis era and channel. For the eμ channel, where the Z+jets contribution is small, the geometric mean of the ratios to simulation is used. The level of agreement between data and MC simulation after the kinematic reconstruction and background estimation is shown in figure 5 for $m_{\ell b}$ as well as the reconstructed p_T of the $t\bar{t}$ system.

6. Systematic uncertainties

Various sources of uncertainty affect the distributions of the observables used in this analysis, and are implemented as nuisance parameters in the binned maximum likelihood fit described in section 7. For each considered experimental and theoretical systematic effect, variations of the predicted signal and background distributions are evaluated. Uncertainties that affect only the normalization of a process are modeled using log-normal constraints, as described in section 4.2 of [107]. Gaussian constraints are imposed for all other uncertainties, which are referred to as shape uncertainties and can include a log-normal-constrained variation of the overall normalization, by modifying the product of the event acceptance and the cross sections of the relevant processes. Unless stated otherwise, all uncertainties are evaluated for signal as well as background processes and treated as fully correlated among the processes, lepton channels, and eras. The uncertainties are summarized in table 1, and described in detail in the following.

The uncertainty in the jet energy scale [43] is evaluated by varying the corresponding corrections within their uncertainties, resulting in a total of 17 nuisance parameters that correspond to the absolute and relative jet energy scales, calibration uncertainties in specific detector regions, p_T balance in dijet or Z+jets events used in the jet energy calibration, and flavor-dependent jet response split into one source for b quark jets and another for all other. Of these, 12 nuisance parameters are specific to individual data-taking eras. The uncertainty in the jet energy resolution measured in calibration data is propagated to the scale correction and smearing of the jet energy resolution in simulation. An uncertainty in the unclustered component of p_T^{miss} is computed by shifting the energies of PF candidates not clustered into jets with $p_T >$ 15 GeV according to the energy resolution for each type of PF candidate [50].

Uncertainties in the scale factors to correct the b tagging efficiency in simulated events are evaluated by varying them within their respective uncertainties [44], independently for heavy-flavor (b and c quark) and light jets. We assign 20 nuisance parameters for the heavy-flavor jet scale factors that correspond to the parton shower (PS) modeling, the presence of leptons within the jet, the jet energy scale, the number of pileup interactions, and differences between different SF estimation methods. Of these, 4 nuisance parameters affect individual eras. For the light jet scale factors, 5 nuisance parameters are assigned, of which 4 affect individual eras.

Uncertainties in the trigger, electron identification, and muon identification scale factors are considered [47, 49]. For the single-muon trigger and muon identification scale factors, each uncertainty component is further split into statistical components that are uncorrelated across eras and a correlated systematic component. The effects of the inefficiency caused by the gradual shift in the timing of the inputs of the ECAL L1 trigger [35] are considered by assigning one nuisance parameter to each era except 2018, where the effect was not present.

The effective inelastic proton–proton cross section used for pileup reweighting in the simulation is varied by 4.6% from its nominal value. The uncertainty in the integrated luminosity amounts to 1.6% [26–28] and affects the normalization of all simulated processes. It is split into 5 nuisance parameters with different correlation assumptions between the eras.

Table 1. The systematic uncertainties considered in the analysis, indicating in parenthesis the number of corresponding nuisance parameters in the statistical model (if more than one), the type (affecting only normalization or also the shape of the search templates), and the affected physics processes and analysis channels they are applicable to.

Uncertainty (# of parameters)	Type	Process	Channel
Jet energy scale (17)	shape	all	all
Jet energy resolution (4)	shape	all	all
Unclustered $p_{\mathrm{T}}^{\mathrm{miss}}$ (4)	shape	all	all
b tagging heavy-flavor jets (20)	shape	all	all
b tagging light jets (5)	shape	all	all
Single-electron trigger	shape	all	ej
Single-muon trigger (5)	shape	all	μj
Dilepton triggers (12)	shape	all	ee, eμ, μμ
Electron identification (2)	shape	all	ej, ee, eμ
Muon identification (10)	shape	all	μj, eμ, μμ
ECAL L1 trigger inefficiency (3)	shape	all	all
Pileup	shape	all	all
Integrated luminosity (5)	norm.	all	all
Top quark Yukawa coupling	shape	FO pQCD $\mathrm{t\bar{t}}$	all
EW correction scheme	shape	FO pQCD $\mathrm{t\bar{t}}$	all
m_{t}	shape	FO pQCD $\mathrm{t\bar{t}}$, Φ	all
ME μ_{R} (5)	shape	FO pQCD $\mathrm{t\bar{t}}$, Φ, single t, Z+jets	all
ME μ_{F} (6)	shape	FO pQCD $\mathrm{t\bar{t}}$, Φ, η_{t}, single t, Z+jets	all
PS ISR (6)	shape	FO pQCD $\mathrm{t\bar{t}}$, Φ, η_{t}, single t, Z+jets	all
PS FSR (6)	shape	FO pQCD $\mathrm{t\bar{t}}$, Φ, η_{t}, single t, Z+jets	all
Color reconnection (2)	shape	FO pQCD $\mathrm{t\bar{t}}$	all
h_{damp}	shape	FO pQCD $\mathrm{t\bar{t}}$	all
PDF (2)	shape	FO pQCD $\mathrm{t\bar{t}}$	all
Single top quark normalization	norm.	Single t	all
EW+QCD normalization	norm.	EW+QCD	ℓj
EW+QCD shape (20)	shape	EW+QCD	ℓj
$\mathrm{t\bar{t}V}$ normalization	norm.	$\mathrm{t\bar{t}V}$	$\ell\ell$
Z+jets normalization	norm.	Z+jets	$\ell\ell$
Diboson normalization	norm.	Diboson	$\ell\ell$

The prediction of the FO pQCD $\mathrm{t\bar{t}}$ production is affected by various sources of theoretical uncertainty. The computation of the NLO EW correction, discussed in section 3, depends on the value of the SM top quark Yukawa coupling through interference with diagrams containing virtual SM Higgs bosons. This coupling is modified with respect to its SM value in many BSM scenarios relevant to this analysis, and its experimental measurement uncertainty is significantly larger than the uncertainty on the top quark mass. Thus, we consider an uncertainty in the coupling by varying its value by $1.00^{+0.11}_{-0.12}$, where the range is given by the measurement reported in [108]. Furthermore, the uncertainty in the application scheme of the NLO EW corrections when combined with NNLO pQCD corrections is considered by taking the difference between the multiplicative and additive approaches of about 1%–2%, as recommended in [80]. The uncertainty in m_{t} is considered by shifting its value in simulation by ±3 GeV, and the induced variations are then rescaled by a factor of 1/3 to emulate a more realistic top quark mass uncertainty of 1 GeV [109]. The effect of the choice of μ_{R} and μ_{F} in the ME calculation is evaluated by varying these scales independently by a factor of two up and down. The effects of the m_{t}, μ_{R}, and μ_{F} variations on the acceptance and shape of the search templates are considered at NLO accuracy, while the effects on the overall FO pQCD $\mathrm{t\bar{t}}$ normalization is considered at NNLO+NNLL accuracy [73, 110]. Decoupling the theoretical nuisance parameters based on their effects—one each for the acceptance and shape, and one additional parameter for the overall FO pQCD $\mathrm{t\bar{t}}$ normalization—does not alter the conclusions of this analysis. Unlike [29], no additional nuisance parameters comparing the predictions of different ME and PS programs are assigned to the FO pQCD $\mathrm{t\bar{t}}$ background.

The scales used to evaluate the strong coupling constant α_{S} in the PS simulation of ISR and FSR are also varied independently by a factor of two up and down. The effect of the uncertainties in the underlying event tune is estimated by varying the parameters of the CP5 tune [55]. Two uncertainties are assigned for the color reconnection model, with one based on the 'QCD-inspired' model [111], and the other by switching on the early resonance decay option in PYTHIA 8.240 [112].

The uncertainty in the matching scale between the ME and PS is evaluated by varying the POWHEG parameter h_{damp}, which

controls the suppression of radiation of additional high-p_T jets. The nominal value of h_{damp} in the simulation and its variations are $1.58\,^{+0.66}_{-0.59}\,m_t$ [113]. The uncertainty arising from the choice of the PDF set is evaluated by reweighting the simulated $t\bar{t}$ events using 100 replicas of the NNPDF3.1 set. A principal component analysis is performed on the variations from the PDF replicas to construct base variations in the space of the predicted event yields in each bin of the search templates, from which the base variation with the largest eigenvalue is used as the PDF uncertainty. The second largest eigenvalue is found to be almost two orders of magnitude smaller than the largest one, thus the base variations corresponding to it and smaller eigenvalues are not considered. The uncertainty in the α_S parameter used in the PDF set forms a second independent PDF variation uncertainty.

The μ_R and μ_F scale uncertainties in the Φ signal simulation are treated independently for the resonance and interference components. Compared to the alternative of varying the scales for the two components simultaneously, we found this to be the more conservative option. The effect on the acceptance and shapes of the search templates is considered at LO accuracy, while the effect on signal cross section is considered at NNLO accuracy. The scales used in the PS simulation of ISR and FSR are also varied independently by a factor of 2 in each direction and are treated independently for the resonant and interference components.

The uncertainty in m_t is also considered for the signal by varying its value in simulation by ± 1 GeV. Its effect on acceptance, shape, and cross section is considered in the same way as μ_R and μ_F variations. Given that this is a variation on the same physical parameter, it is treated as fully correlated with the background processes. Other theoretical uncertainties in the signal, such as the PDF, are neglected as they are small compared to those already considered.

The η_t background simulation, if applied, considers μ_F, ISR, FSR, and m_t uncertainties, affecting only the acceptance and shape. They are handled identically to the corresponding variations in the Φ signal simulation. The overall normalization of η_t is always taken to be a free parameter of the fit in this analysis. Since the used model describes effective η_t production via a contact interaction, without the emission of extra partons at the LO ME level, the model encodes no dependence on α_S. Therefore, μ_R variations have no effect on the η_t prediction.

The μ_R, μ_F, ISR, and FSR scale uncertainties are also independently considered for the Z+jets and single top quark production processes. For these processes, the μ_R and μ_F uncertainties affect only acceptance and shape, not normalization.

The expected yields for most of the non-$t\bar{t}$ background processes are derived using theoretical predictions for the cross sections at NLO or higher accuracy. The uncertainties assumed in the normalization of these processes are conservative and always exceed those of the corresponding theoretical computations. For single top quark production, we assign an uncertainty of 15%, based on relevant cross section measurements [114–116]. In the $\ell\ell$ channels, the uncertainty in the $t\bar{t}V$ production is taken to be 30% [117, 118]. The uncertainty of the Z+jets production is taken to be 5% [119]. To account for the fact that this search probes a restricted region of the phase space of the corresponding processes, we assign a normalization uncertainty of 30% for diboson production, which has little impact on the overall sensitivity due to the small contribution of these processes. All normalization uncertainties for non-$t\bar{t}$ background processes are considered uncorrelated between each other.

In the single-lepton channels, the normalization uncertainty of the EW+QCD background estimate evaluated from a CR in data is taken to be 50%. Furthermore, to estimate the effect of changing the b tagging requirements on the kinematic distributions, the estimation is repeated for three different selections of the highest allowed b tagging discriminant value in the event. The shape differences between the central selection and the selections with a higher and lower allowed value of the highest b tagging discriminant are taken into account as uncertainties in the background estimation. As an additional uncertainty, we take into account a variation of the subtracted single top quark and $t\bar{t}$ contributions, in which their expected contributions are scaled by the ratio of observed and expected events in the CR.

The nominal background prediction is affected by the limited size of the simulated MC event samples. This statistical uncertainty is evaluated using the 'light' Barlow–Beeston method [120], by introducing one additional nuisance parameter for each bin of the search templates. These parameters are uncorrelated across all channels and eras.

Several systematic variations, most notably those constructed from dedicated MC samples, are affected by statistical fluctuations. We suppress these fluctuations with a smoothing procedure, which is described in [30] and is based on the LOWESS algorithm [121, 122].

In general, the relative importance of different systematic uncertainties depends greatly on the signal hypothesis, especially the mass of the scalar bosons. Close to the $t\bar{t}$ production threshold, uncertainties due to the modeling of $t\bar{t}$ dominate the total uncertainty, in particular the top quark Yukawa coupling, the application scheme of the NLO EW corrections, μ_R, m_t, the color reconnection model, and the η_t normalization (if considered). A further nonnegligible contribution comes from the estimation of the EW+QCD background. For larger values of m_Φ, the ME-PS matching uncertainty for the FO pQCD $t\bar{t}$ background as well as experimental uncertainties due to heavy-flavor jet tagging become similarly important, while the effect of the η_t and EW+QCD contributions become small. In addition, the total MC statistical uncertainties in all bins together often outweigh every other individual uncertainty.

7. Statistical analysis

To evaluate the consistency of the observed data with the background-only hypothesis and with different signal hypotheses, we perform a statistical analysis using the search templates described in sections 4 and 5. The ℓj and $\ell\ell$ final states

do not overlap as they correspond to orthogonal lepton selection criteria.

The statistical model is defined by the likelihood function

$$L\left(\boldsymbol{p}_{\Phi},\mu\left(\eta_{\mathrm{t}}\right),\boldsymbol{\nu}\right) = \left(\prod_{i}\frac{\lambda_{i}\left(\boldsymbol{p}_{\Phi},\mu\left(\eta_{\mathrm{t}}\right),\boldsymbol{\nu}\right)^{n_{i}}}{n_{i}!}\mathrm{e}^{-\lambda_{i}\left(\boldsymbol{p}_{\Phi},\mu\left(\eta_{\mathrm{t}}\right),\boldsymbol{\nu}\right)}\right)G\left(\boldsymbol{\nu}\right),$$

where

$$\lambda_{i}\left(\boldsymbol{p}_{\Phi},\mu\left(\eta_{\mathrm{t}}\right),\boldsymbol{\nu}\right) = S_{i}^{\Phi}\left(\boldsymbol{p}_{\Phi},\boldsymbol{\nu}\right) + S_{i}^{\eta_{\mathrm{t}}}\left(\mu\left(\eta_{\mathrm{t}}\right),\boldsymbol{\nu}\right) + B_{i}\left(\boldsymbol{\nu}\right), \tag{2}$$

with B_i denoting the combined FO pQCD background yield in a given bin i, S_i^{Φ} the Φ signal yield dependent on signal model parameters $\boldsymbol{p}_{\Phi}$, $S_i^{\eta_{\mathrm{t}}}$ the η_{t} contribution dependent on the signal strength $\mu(\eta_{\mathrm{t}})$, $\boldsymbol{\nu}$ the vector of nuisance parameters on which the signal and background yields generally depend, and n_i the observed yield. The external constraints on the nuisance parameters are taken into account in this likelihood via a product of corresponding probability density functions, $G(\boldsymbol{\nu})$.

The Φ signal yield is given by

$$S_{i}^{\Phi}\left(\boldsymbol{p}_{\Phi},\boldsymbol{\nu}\right) = \sum_{\Phi=\mathrm{A,H}}\left(g_{\Phi\mathrm{t\bar{t}}}^{4}s_{\mathrm{R},i}^{\Phi}\left(m_{\Phi},\Gamma_{\Phi},\boldsymbol{\nu}\right) + g_{\Phi\mathrm{t\bar{t}}}^{2}s_{\mathrm{I},i}^{\Phi}\left(m_{\Phi},\Gamma_{\Phi},\boldsymbol{\nu}\right)\right), \tag{3}$$

where $s_{\mathrm{R},i}^{\Phi}$ and $s_{\mathrm{I},i}^{\Phi}$ are the yields for the resonant and interference part, respectively. The vector $\boldsymbol{p}_{\Phi}$ represents the signal model parameters and comprises the Φ boson mass m_{Φ}, width Γ_{Φ}, and $g_{\Phi\mathrm{t\bar{t}}}$. Equation (3) is kept generic by including contributions from both A and H. Since there is no interference between them, the corresponding signal distributions are trivially added together.

The yield of the η_{t} contribution is given by

$$S_{i}^{\eta_{\mathrm{t}}}\left(\mu\left(\eta_{\mathrm{t}}\right),\boldsymbol{\nu}\right) = \mu\left(\eta_{\mathrm{t}}\right)s_{i}^{\eta_{\mathrm{t}}}\left(\boldsymbol{\nu}\right), \tag{4}$$

where $s_i^{\eta_{\mathrm{t}}}$ are the predicted η_{t} signal yields and $\mu(\eta_{\mathrm{t}})$ is the signal strength modifier, which is a free parameter of the fit. There is no additional interference between A and η_{t} productions [67, 105, 123].

The background-only model is constructed by setting $g_{\Phi\mathrm{t\bar{t}}} = 0$. The compatibility between data and a given hypothesis is determined by performing scans over the parameters of the signal models in different scenarios, using methodologies described in the following.

7.1. Methodology for single Φ boson interpretation

In the single Φ boson interpretation, constraints on the coupling strength modifier $g_{\Phi\mathrm{t\bar{t}}}$ are derived as a function of m_{Φ} for fixed Γ_{Φ}/m_{Φ} values, separately for A and H. This is done while setting the coupling modifier for the other CP state in equation (2) to zero, thus excluding it from the statistical model. The scan is performed for the m_{Φ} and Γ_{Φ}/m_{Φ} values listed in section 3. Coupling strength values up to 3 are probed to guarantee that the amplitudes preserve perturbative unitarity for all calculations, in accordance with the lower bound $\tan\beta = 1/g_{\mathrm{At\bar{t}}} \gtrsim 0.3$ given in [4] in the context of 2HDMs, where $\tan\beta$ is the ratio of the vacuum expectation values of the Higgs doublets coupling to the up- and down-type quarks.

A variant of the LHC profile likelihood ratio test statistic $\tilde{q}_{\mu}$ equivalent to those described in [124, 125] is utilized:

$$\tilde{q}_{\mu}\left(\boldsymbol{p}_{\Phi}\right) = -2\ln\frac{L\left(\mu,\boldsymbol{p}_{\Phi},\widehat{\boldsymbol{\nu}}_{\mu,\boldsymbol{p}_{\Phi}}\right)}{L\left(\widehat{\mu},\boldsymbol{p}_{\Phi},\widehat{\boldsymbol{\nu}}_{\widehat{\mu},\boldsymbol{p}_{\Phi}}\right)}, \quad 0 \leqslant \widehat{\mu} \leqslant \mu. \tag{5}$$

Because the Φ signal scales nonlinearly with the coupling modifiers $g_{\Phi\mathrm{t\bar{t}}}$, we introduce an auxiliary overall signal strength modifier μ in terms of which the test statistic is expressed, in the same way as in [30]. This facilitates testing different Φ signal hypotheses in a computationally efficient way. The auxiliary parameter scales the overall Φ signal yield in equation (3), keeping the other parameters in $\boldsymbol{p}_{\Phi}$ fixed. The likelihood in the numerator is maximized with respect to the nuisance parameters, and $\widehat{\boldsymbol{\nu}}_{\mu,\boldsymbol{p}_{\Phi}}$ denotes the vector of their values at the maximum for a given $\boldsymbol{p}_{\Phi}$. Depending on the scenario considered, the η_{t} signal strength is kept as a free parameter of the fit and treated as part of the nuisance parameters, or it is fixed to $\mu(\eta_{\mathrm{t}}) = 0$ in both numerator and denominator. A similar notation is used in the denominator, where the likelihood is maximized with respect to both μ and $\boldsymbol{\nu}$, under the additional constraint $0 \leqslant \widehat{\mu} \leqslant \mu$. The requirement $\widehat{\mu} \geqslant 0$ excludes cases in which the shape of the overall BSM contribution gets flipped, resulting in a qualitatively different effect from what is targeted in this search. The condition $\widehat{\mu} \leqslant \mu$ prevents the exclusion of a signal hypothesis if the data are more compatible with a model that predicts the BSM contribution of a similar shape but a larger overall size.

For each signal hypothesis, we perform a test according to the $\mathrm{CL_s}$ criterion [126, 127]. An asymptotic approximation [124] is employed to efficiently construct the distributions of the adopted test statistic. We exclude a configuration $\boldsymbol{p}_{\Phi}$ at 95% confidence level (CL) if the $\mathrm{CL_s}$ value computed for $\mu = 1$, which reproduces the nominal signal expectation, is smaller than 0.05.

7.2. Methodology for A+H boson interpretation

In the A+H boson interpretation, we consider the more general case where two Φ states exist at the same time. We confine ourselves to the case with exactly one A boson and exactly one H boson, i.e. the case considered in 2HDMs [4]. Constraints in the $g_{\mathrm{At\bar{t}}}$–$g_{\mathrm{Ht\bar{t}}}$ plane are set using the following test statistic:

$$\tilde{q}_{\boldsymbol{p}_{\Phi}} = -2\ln\frac{L\left(\boldsymbol{p}_{\Phi},\widehat{\boldsymbol{\nu}}_{\boldsymbol{p}_{\Phi}}\right)}{L\left(\widehat{\boldsymbol{p}}_{\Phi},\widehat{\boldsymbol{\nu}}_{\widehat{\boldsymbol{p}}_{\Phi}}\right)}, \tag{6}$$

expressed directly in terms of $g_{\mathrm{At\bar{t}}}$ and $g_{\mathrm{Ht\bar{t}}}$. In contrast to the single A/H interpretation, the asymptotic approximation on the form of the test statistic distribution is not exploited, rendering the auxiliary parameter μ unnecessary.

For each $g_{\Phi\mathrm{t\bar{t}}}$ configuration under consideration, its compatibility with the data is evaluated with the Feldman–Cousins

prescription [128, 129]. An iterative procedure is applied to reduce the number of points for which the test statistic needs to be evaluated. An initially sparse grid of $g_{\Phi t\bar{t}}$ configurations are evaluated and refined around the region of the exclusion contour boundary at a given CL. The procedure is repeated until the minimum distance of two neighboring $g_{\Phi t\bar{t}}$ configurations in the plane is small enough. Like in the single A/H boson interpretation, we scan within the range of $g_{\Phi t\bar{t}} \leqslant 3$ in the A+H boson interpretation.

8. Results

The data are interpreted in the context of Φ boson production under two background scenarios, one including η_t production and one without. When η_t is not included, a deviation from the background prediction is observed near the $t\bar{t}$ production threshold. In section 8.1, we compare the two different background scenarios to the signal scenario corresponding to the highest local significance for this deviation. Next, in section 8.2, limits on the production of a single Φ boson are presented, assuming that the background prediction is based on FO pQCD calculations alone. Then, in section 8.3, the same Φ boson interpretations are presented, but now with η_t included as part of the background. Finally, in section 8.4, we show exclusion contours for the simultaneous presence of A and H bosons for a few examples of m_Φ and Γ_Φ/m_Φ, in the background scenario with η_t production included. Constraints on $g_{\Phi t\bar{t}}$ in the single Φ boson interpretation, as well as exclusion contours in the A+H boson interpretation, for mass and width values not included in this paper are provided in the corresponding HEPData entry [64].

We refer to the companion paper [29] for an interpretation of the excess around the threshold region in terms of a pseudoscalar $t\bar{t}$ quasi-bound state without invoking any BSM degrees of freedom, performed in the $\ell\ell$ channels only. For $m_{t\bar{t}}$ values close to the $t\bar{t}$ threshold and with the chosen analysis strategy without spin correlation observables, the ℓj channels contribute only subleading sensitivity to a $t\bar{t}$ quasi-bound state. As a result, including the ℓj channels in [29] would not significantly change the conclusions of said work.

8.1. Data compared to background scenarios with and without η_t contribution

The expected and observed distributions are shown after the fit in figures 6–8 for the three channels considered. In the middle panels, where no η_t contribution is included, a deviation from the background prediction can be seen at low values of $m_{t\bar{t}}$.

The shown fit is performed using the signal pair $A(365, 2\%)$+$H(425, 3\%)$, using the notation introduced in section 3, which corresponds to the highest observed local significance. To find this signal pair, the local significance of an A+H boson pair is estimated using the square root of the value of the test statistic from equation (6) when fixing $g_{\Phi t\bar{t}} = 0$, i.e. comparing the case of zero A+H contribution to the one that best describes the data, in the background scenario without η_t [124].

It becomes apparent in figure 8(middle) that the contributions of A/H boson production at the best fit $g_{\Phi t\bar{t}}$ values are dependent on c_{hel} and c_{han}, highlighting their sensitivity to discriminate between the signals. In general, A boson production is favored by the data over H boson production. Comparing $A(365, 2\%)$ and $H(365, 2\%)$, corresponding to the best fit mass and width for single A/H boson signals, we find a difference in negative log-likelihood of $2\Delta \ln L \approx 53$, indicating a strong preference for the CP-odd contribution.

For the lower panels of figures 6–8, η_t production was included in the fit as additional background with the normalization being a freely floating parameter of the fit, as discussed in section 7. In this case, the contributions for A and H boson production vanish, showing that the data prefers η_t production over A or H boson production. However, we note that the considered A/H masses are different from the η_t mass of 343 GeV, as described in section 3, and η_t and A are thus not directly comparable. A further difference between η_t and A/H is the inclusion of SM $t\bar{t}$–A/H interference, leading to peak-dip structures in $m_{t\bar{t}}$, while η_t is modeled as a pure resonance [123].

In addition, the Feldman–Cousins exclusion contours (as discussed in section 7.2) for the two scenarios are shown in figure 9. The expected contours are similar in shape, though the one in the background scenario including η_t (lower) is slightly wider. This is due to the fact that in the regions of $g_{At\bar{t}}$ relevant for the contours, the interference component of the signal dominates, effectively manifesting as a deficit of expected events. Since this occurs at higher $m_{t\bar{t}}$ compared to the enhancement predicted by η_t, the addition of η_t to the background does not significantly affect the expected exclusion in $g_{At\bar{t}}$. Furthermore, since H and η_t can be distinguished based on c_{hel} and c_{han}, the exclusion in $g_{Ht\bar{t}}$ is not affected either.

The observed exclusion contours are significantly different for the two background scenarios. If η_t production is not included as in figure 9(upper), the observed pseudoscalar-like excess in data manifests as a narrow strip of compatible $g_{At\bar{t}}$ values significantly different from zero. In contrast, the value of $g_{Ht\bar{t}}$ for this parameters point is compatible with zero within three SDs. This demonstrates the pseudoscalar nature of the excess.

In the η_t background scenario as presented in figure 9 (lower), the observed allowed values of both $g_{At\bar{t}}$ and $g_{Ht\bar{t}}$ are compatible with zero within two SDs, and the excess has vanished.

8.2. Single Φ boson interpretation without η_t in the background model

Combining the fit results for the 2D templates in $(m_{t\bar{t}}, |\cos\theta^*_{t_\ell}|)$ of the $\ell + 3j$ and $\ell + \geqslant 4j$ channels (as discussed in section 4), with the results derived from the 3D templates in $(m_{t\bar{t}}, c_{hel}, c_{han})$ of the $\ell\ell$ channels (as discussed in section 5),

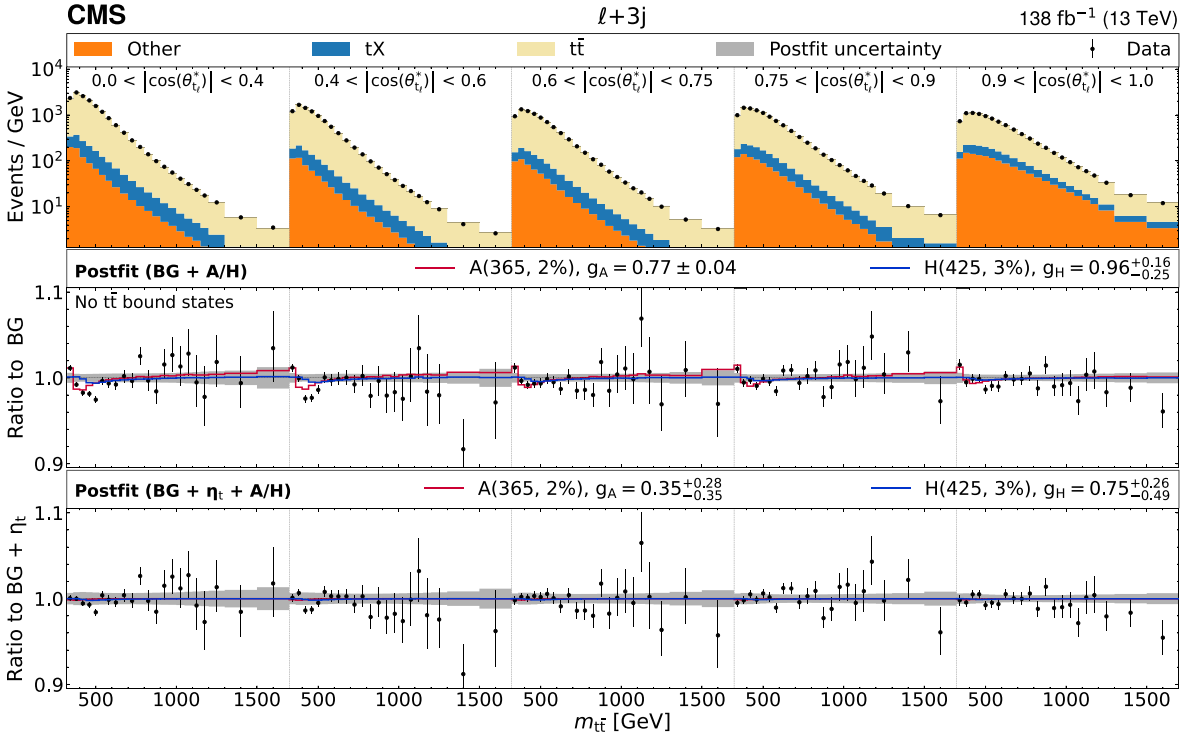

Figure 6. Observed and expected $m_{\mathrm{t\bar{t}}}$ distribution in bins of $|\cos\theta^{*}_{\mathrm{t}_\ell}|$, shown for the $\ell + 3\mathrm{j}$ channel summed over lepton flavors and eras. In the upper panel, the data (points with statistical error bars) are compared to $\mathrm{t\bar{t}}$ production in FO pQCD and other sources of background (colored histograms) after the fit to the data in the A+H interpretation. The ratio of data to the prediction is shown in the middle panel, where the two signals $\mathrm{A}(365, 2\%)$ and $\mathrm{H}(425, 3\%)$, corresponding to the best fit point, are overlaid. The lower panel shows the equivalent ratio for the fit where η_t is considered as an additional background, for the same signal points. In both cases, the gray band shows the postfit uncertainty, and the respective signals are overlaid with their best fit model parameters.

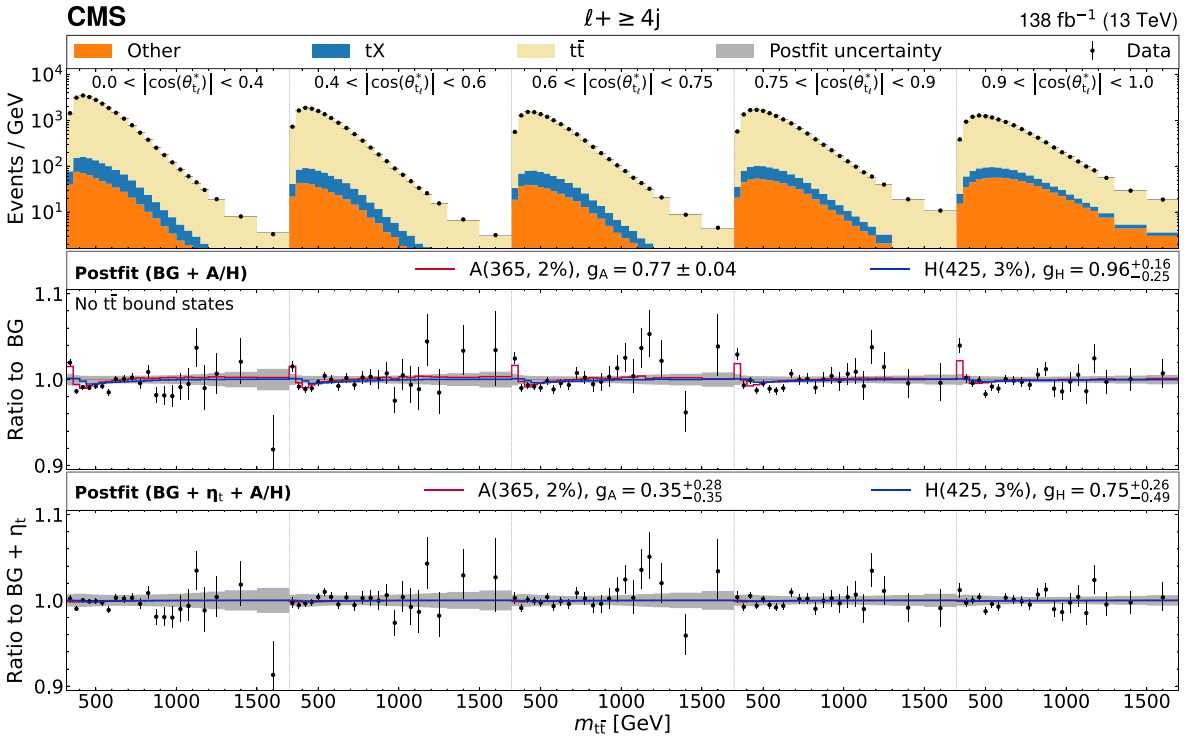

Figure 7. Observed and expected $m_{\mathrm{t\bar{t}}}$ distribution in $|\cos\theta^{*}_{\mathrm{t}_\ell}|$ bins, shown for the $\ell + \geqslant 4\mathrm{j}$ channel summed over lepton flavors and eras. Notations as in figure 6.

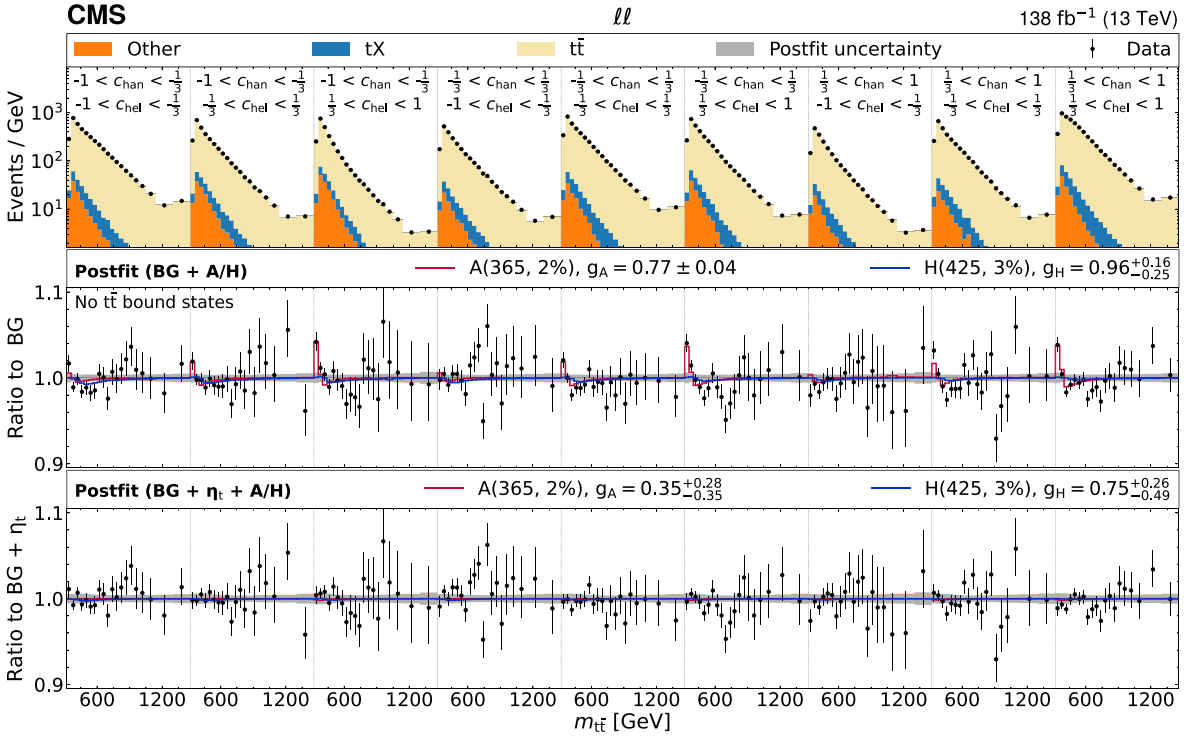

Figure 8. Observed and expected $m_{t\bar{t}}$ distribution in c_{hel} and c_{han} bins, shown for the $\ell\ell$ channel summed over lepton flavors and eras. Notations as in figure 6.

for all lepton flavors and eras, upper exclusion limits on $g_{A t\bar{t}}$ and $g_{H t\bar{t}}$ at the 95% CL are presented in figures 10 and 11, for the background scenario without η_t contribution, as functions of m_Φ for different assumptions on the Γ_Φ/m_Φ. The expected constraints on $g_{\Phi t\bar{t}}$ evolve in accordance with the signal cross section, as A/H boson mass and width values increase. The relatively sharper decline in sensitivity for A/H bosons with $700 < m_\Phi < 900\,\text{GeV}$ and larger Γ_Φ is due to cancellations in the cross sections for the resonance and interference signal components.

The expected constraints on $g_{\Phi t\bar{t}}$ obtained in this analysis improve upon the previous results presented in [30], which were based on a smaller data set and a simpler analysis strategy. In the ℓj channel, the addition of the three jets category increases the statistical power of the analysis. In the $\ell\ell$ channel, the addition of c_{han} as an observable improved sensitivity of the search, particularly for H bosons.

These improvements also result in significantly stronger observed constraints on $g_{\Phi t\bar{t}}$ compared to previous results, across most of the mass and width values in both CP scenarios. Interestingly, there is a significant deviation between observed and expected limits at low m_Φ values, for both the A and H boson interpretations. The largest differences are for A boson signal hypotheses with narrow widths. The best fit to the data is achieved for the $\mathrm{A}(365, 2\%)$ signal hypothesis, corresponding to the lowest generated A boson mass value, with an observed local significance over the background-only hypothesis in the background scenario without η_t contribution of more than five SDs. This hypothesis corresponds to the lowest m_Φ value probed in this analysis.

8.3. Single Φ boson interpretation with η_t in the background model

The same limit extraction as in section 8.2 is repeated assuming single Φ boson production as signal, but now including η_t production to the fit as additional background, with the normalization treated as an unconstrained nuisance parameter, as outlined in section 7.

The obtained 95% CL upper limits on $g_{\Phi t\bar{t}}$ as a function of m_Φ are shown in figures 12 and 13. The observed limits are consistent with the expected ones within two SDs for both CP scenarios, across all width values and the entire mass range. Notably, the excess at low masses seen in figures 10 and 11, where the background model without η_t contribution is assumed, has disappeared. This suggests that the data are well described when η_t production is included in the background model. Moreover, a comparison of the exclusion regions in figures 10–12 at low masses indicates a slight preference for the η_t hypothesis over the single A boson production hypothesis for the lowest probed mass point at $\mathrm{A}(365, 2\%)$. However, the current analysis has limited discriminatory power between these hypotheses based on their $m_{t\bar{t}}$ lineshapes due to the limited experimental resolution, preventing a definitive preference for one explanation over the other.

8.4. The A+H boson interpretation

Many extensions of the Higgs sector, such as 2HDMs [4], predict the existence of both A and H bosons, with their masses

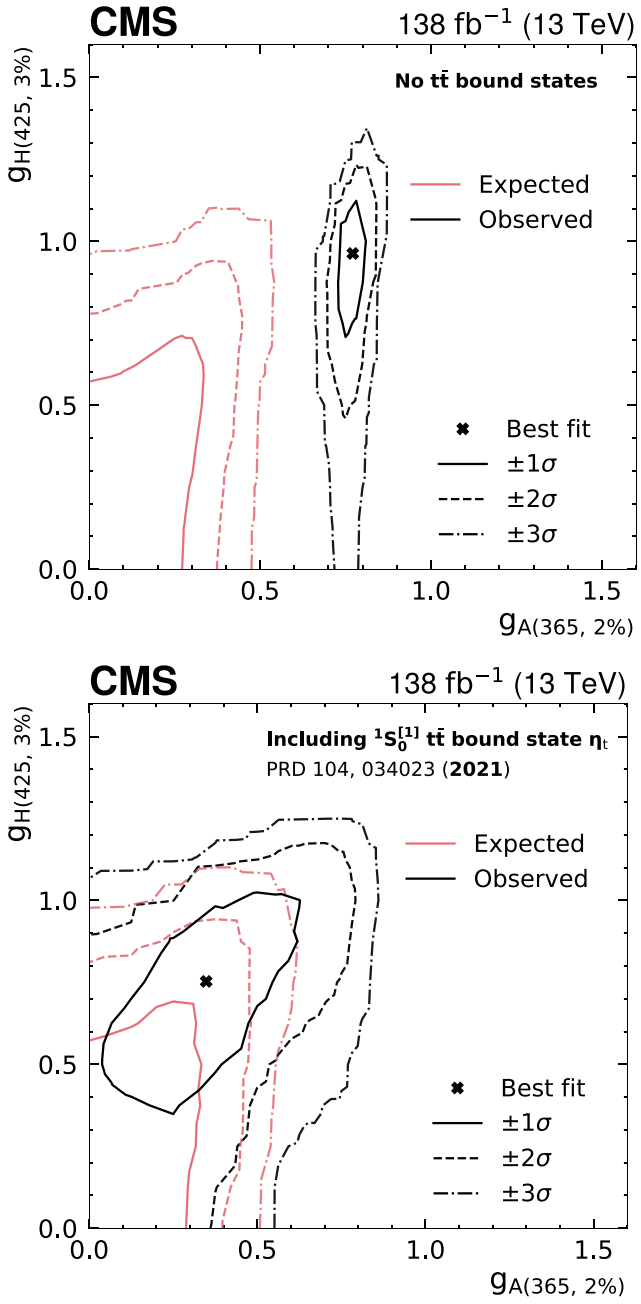

Figure 9. Frequentist 2D exclusion contours for $g_{A t\bar{t}}$ and $g_{H t\bar{t}}$ for the A(365, 2%)+H(425, 3%) signal point, in the background scenario excluding (upper) and including (lower) η_t production. The expected and observed contours, evaluated with the Feldman–Cousins prescription [128, 129], are shown in black and pink, respectively, with different line styles denoting progressively higher CLs. The regions outside of the contours are considered excluded.

and widths potentially falling within the range probed by this analysis. To investigate this possibility, we perform a simultaneous A+H boson interpretation, considering various A/H boson pairs beyond the one analyzed in section 8.1, including the η_t contribution in the background scenario.

The results are presented in figure 14 for the case of identical A and H boson masses and in figure 15 for differing masses, all assuming a width of 2%. In all cases, the observed exclusion contours are consistent with zero A+H boson contribution. We note that the difference between expected and observed contours in figure 14(lower left) corresponds to a local tension at the level of 1–2 SDs for m_H between 700 and 780 GeV and $\Gamma_H/m_H = 2\%$, similar as in figure 13 (upper left).

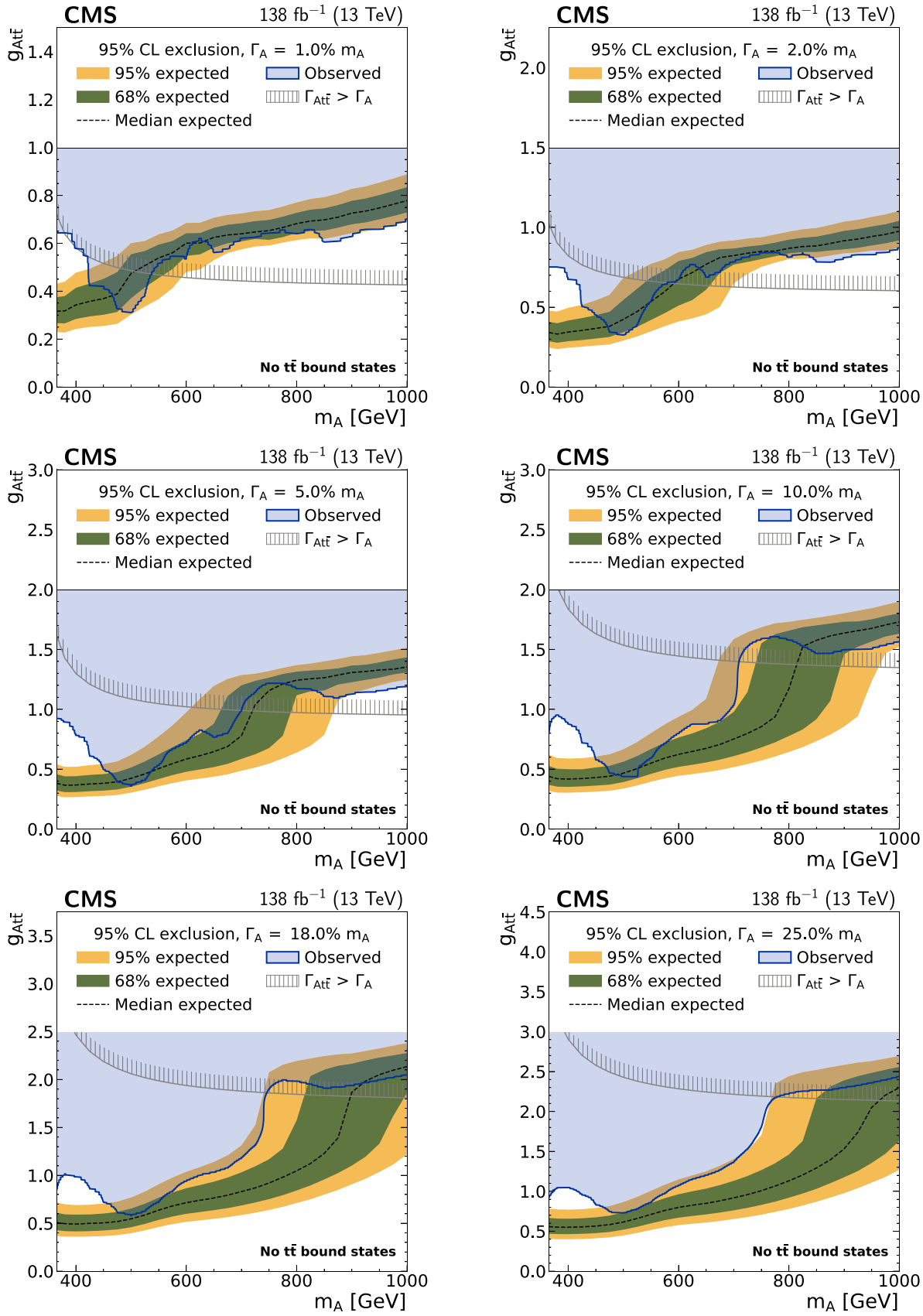

Figure 10. Model-independent constraints on $g_{A t\bar{t}}$ as functions of the A boson mass in the background scenario without η_t contribution, for Γ_Φ/m_Φ of 1%, 2%, 5%, 10%, 18%, and 25% (from upper left to lower right). The observed constraints are indicated by the shaded blue area, bounded by the solid blue curve. The inner green and outer yellow bands indicate the regions containing 68% and 95%, respectively, of the distribution of constraints expected under the background-only hypothesis. The unphysical region of phase space in which the partial width $\Gamma_{A\to t\bar{t}}$ becomes larger than the total width of the A boson is indicated by the hatched line.

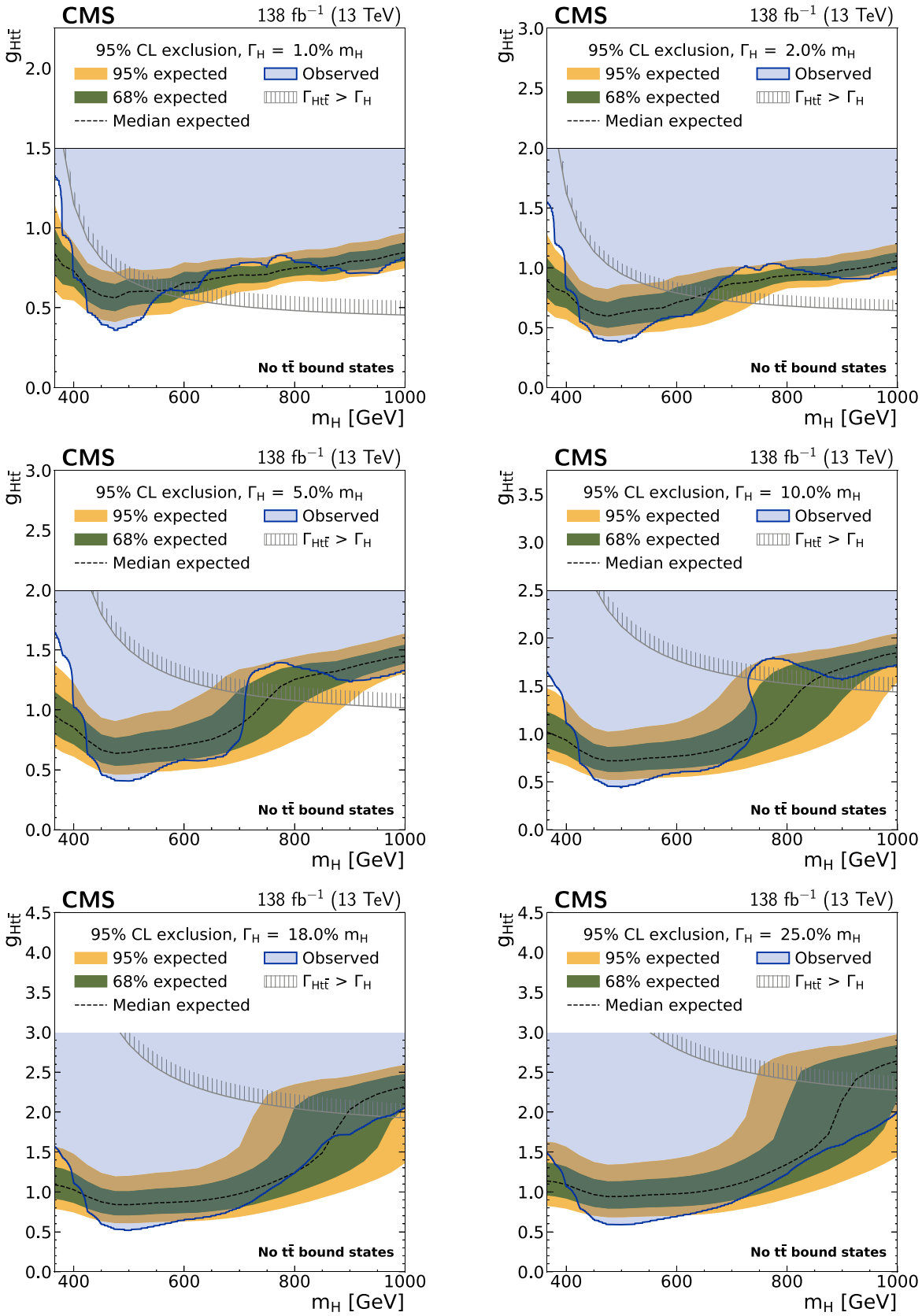

Figure 11. Model-independent constraints on $g_{Ht\bar{t}}$ as functions of the H boson mass in the background scenario without η_t contribution, shown in the same fashion as in figure 10.

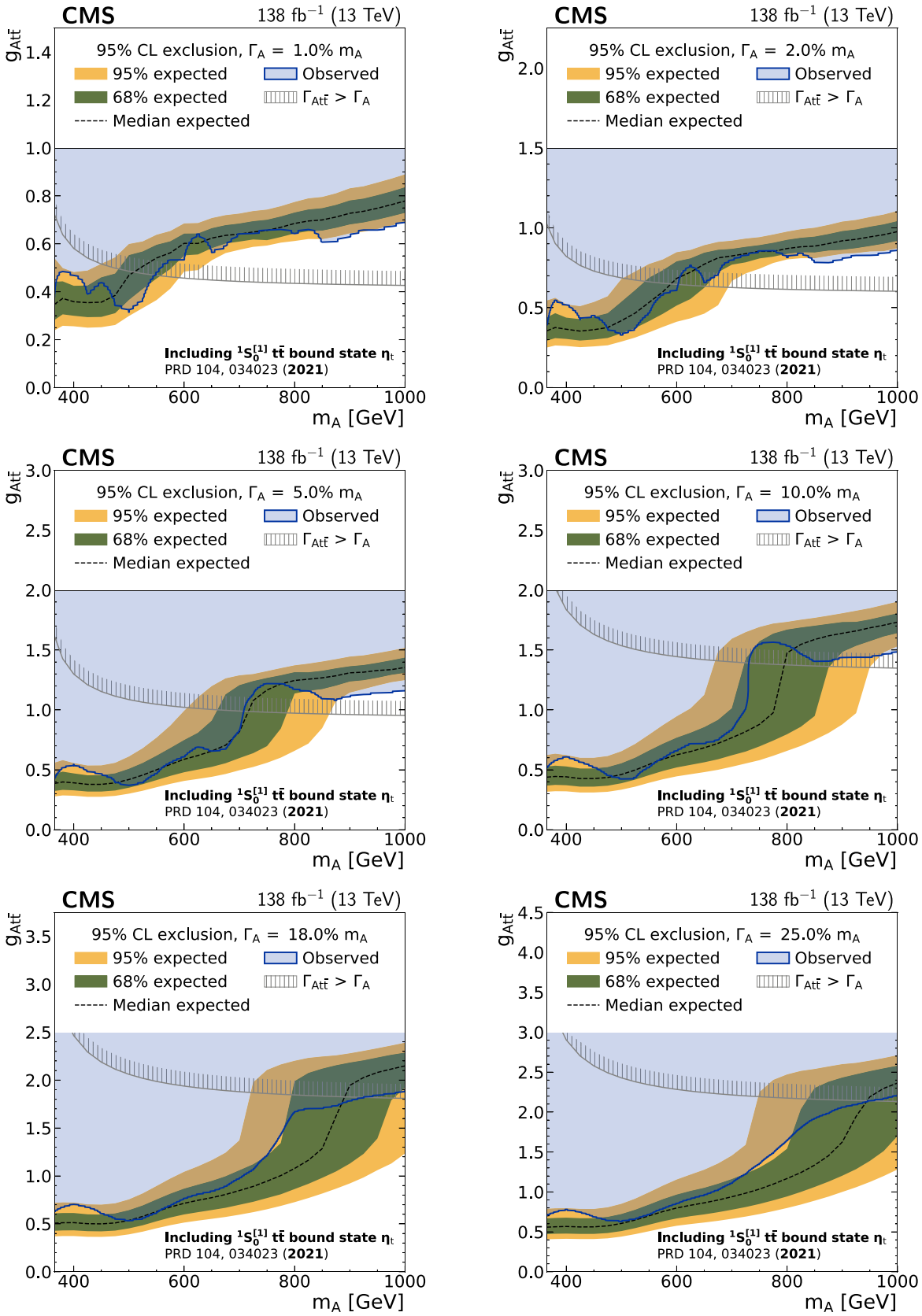

Figure 12. Model-independent constraints on $g_{At\bar{t}}$ as functions of the A boson mass in the background scenario with η_t contribution, shown in the same fashion as in figure 10.

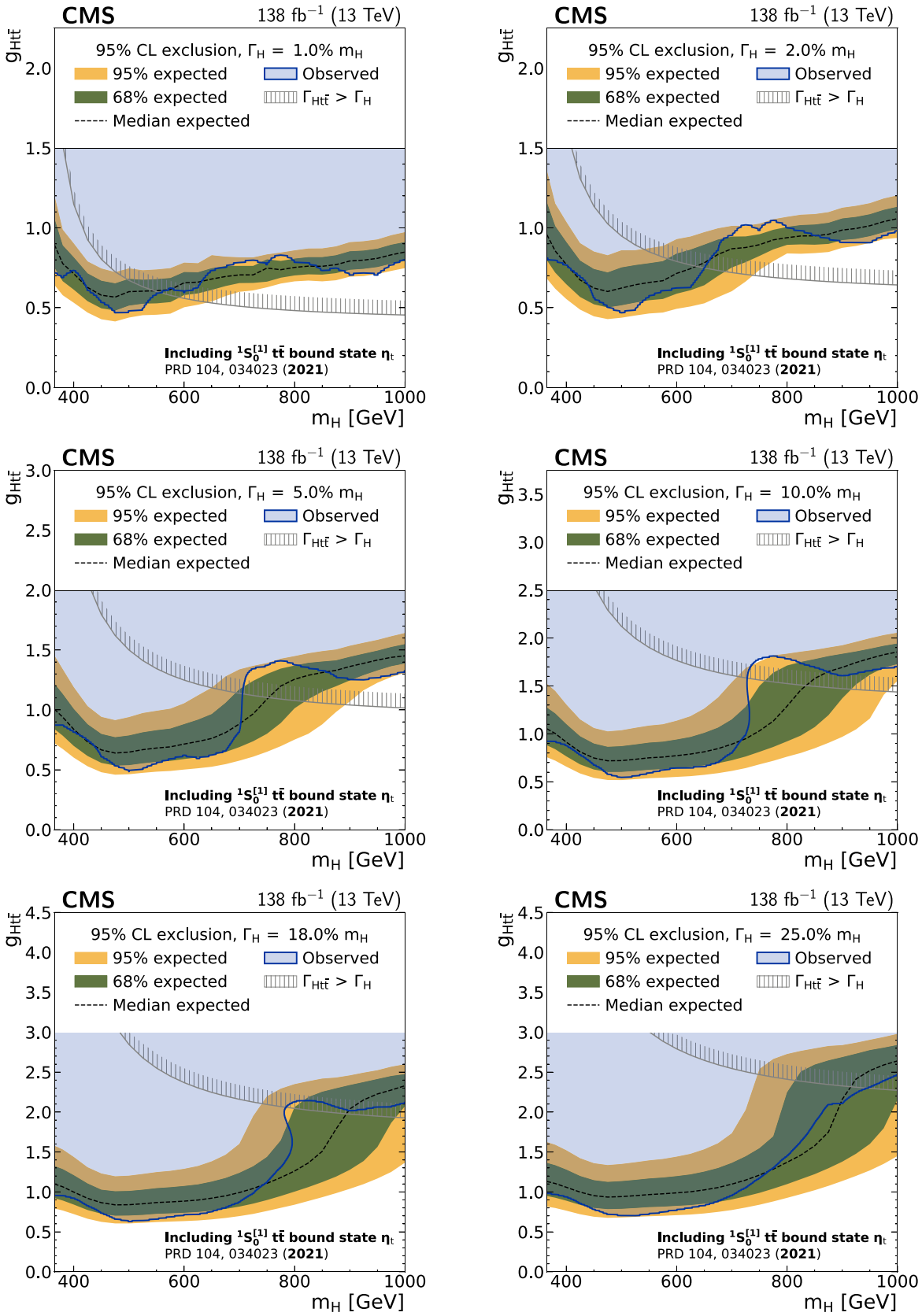

Figure 13. Model-independent constraints on $g_{Ht\bar{t}}$ as functions of the H boson mass in the background scenario with η_t contribution, shown in the same fashion as in figure 10.

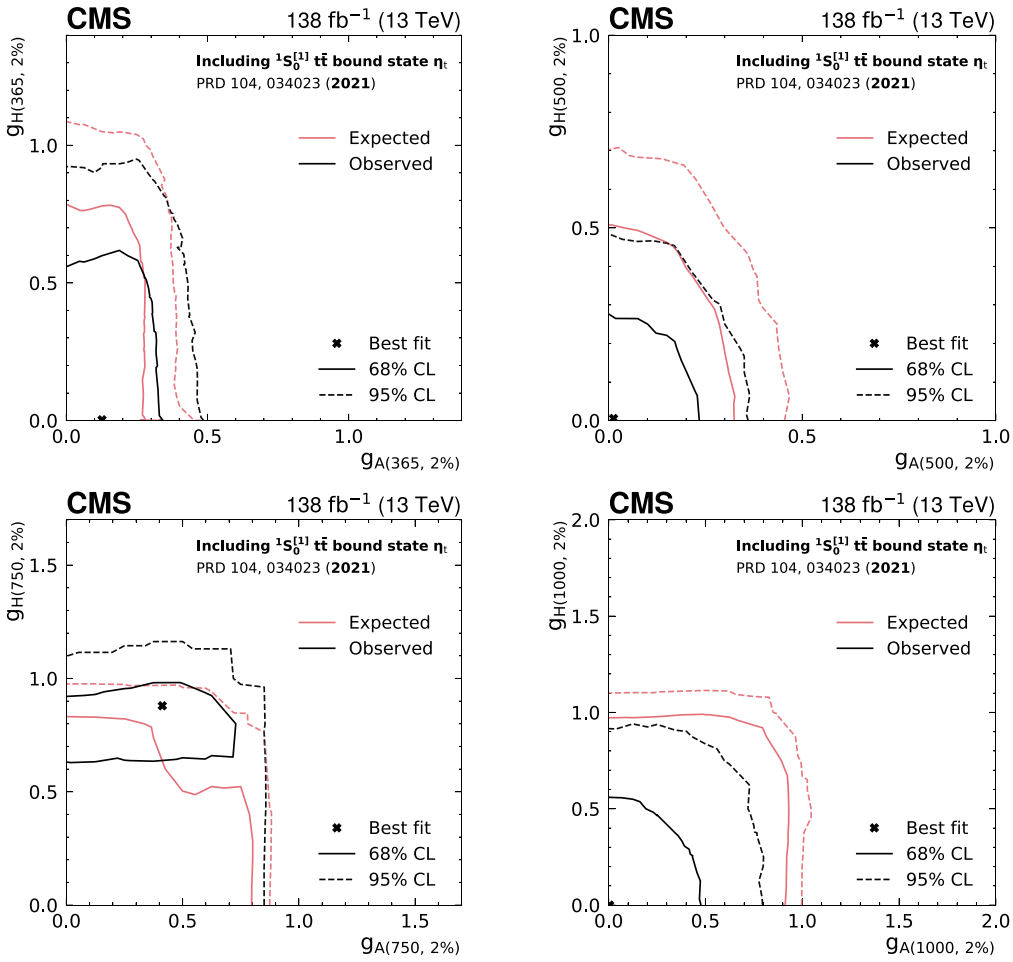

Figure 14. Frequentist 2D exclusion contours for $g_{At\bar{t}}$ and $g_{Ht\bar{t}}$ in the A+H boson interpretation for four different signal hypotheses with identical A and H boson masses of 365 GeV (upper left), 500 GeV (upper right), 750 GeV (lower left), and 1000 GeV (lower right), all assuming a relative width of 2%. The expected and observed contours, evaluated with the Feldman–Cousins prescription [128, 129], are shown in pink and black, respectively, with the solid and dashed lines corresponding to exclusions at 68% and 95% CL. The regions outside of the contours are considered excluded. In all cases, η_t production is included in the background model.

9. Summary

A search has been presented for the production of pseudoscalar or scalar bosons in proton–proton collisions at $\sqrt{s} = 13$ TeV, decaying into a top quark pair ($t\bar{t}$) in final states with one or two charged leptons. The analysis uses data collected with the CMS detector at the LHC, corresponding to an integrated luminosity of 138 fb^{-1}. To discriminate the signal from the SM $t\bar{t}$ background, the search utilizes the invariant mass of the reconstructed $t\bar{t}$ system along with angular observables sensitive to its spin and parity. The signal model accounts for both the resonant production of the new boson and its interference with the perturbative quantum chromodynamics (pQCD) $t\bar{t}$ background.

A deviation from the background prediction, modeled using FO pQCD, is observed near the $t\bar{t}$ production threshold. This deviation is similar to the moderate excess previously reported by CMS using data corresponding to an integrated luminosity of 35.9 fb^{-1} [30]. The local significance of the excess exceeds five SDs, with a strong preference for the pseudoscalar signal hypothesis over the scalar one.

Incorporating the production of a color-singlet $^1S_0^{[1]}$ $t\bar{t}$ quasi-bound state, η_t, within a simplified nonrelativistic QCD model, with an unconstrained normalization to the background, yields agreement with the observed data, eliminating the need for additional exotic pseudoscalar or scalar boson production. However, the precision of the measurement is insufficient to clearly favor either the η_t production model, or a new A boson down to a mass of 365 GeV, or any potential mixture of the two. A detailed analysis of the excess using the $t\bar{t}$ quasi-bound-state interpretation is provided in [29].

Exclusion limits at the 95% CL are set on the coupling strength between top quarks and new bosons, covering mass ranges of 365–1000 GeV and relative widths of 0.5%–25%. When the background model includes both FO pQCD $t\bar{t}$ production and η_t production, stringent constraints are obtained for three scenarios: a new pseudoscalar boson, a new scalar boson, and the simultaneous presence of both. Coupling values as low as 0.4 (0.6) are excluded

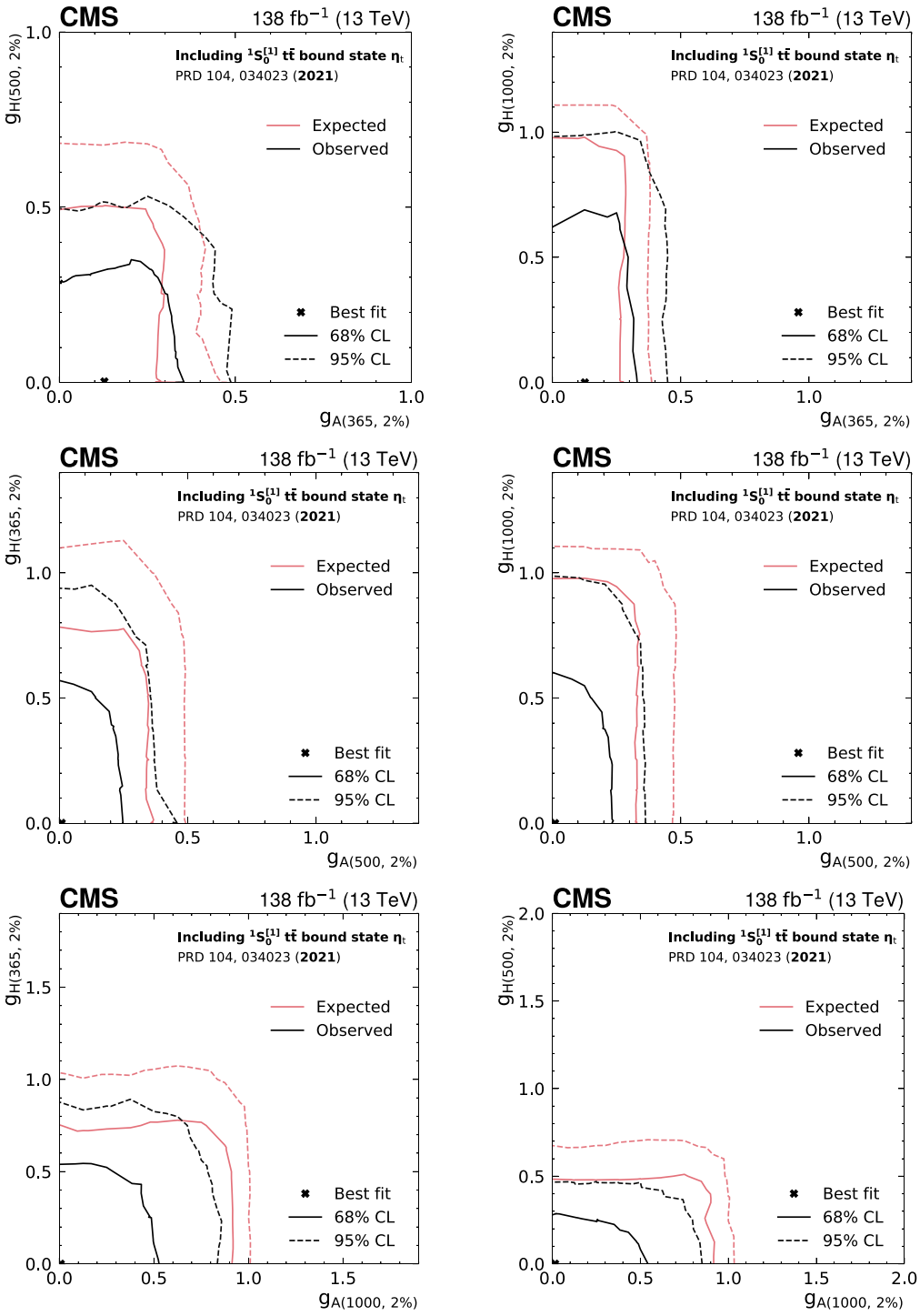

Figure 15. Frequentist 2D exclusion contours for $g_{At\bar{t}}$ and $g_{Ht\bar{t}}$ in the A+H boson interpretation for six different signal hypotheses with unequal A and H boson masses, corresponding to combinations of 365, 500, and 1000 GeV, all assuming a relative width of 2%. The expected and observed contours, evaluated with the Feldman–Cousins prescription [128, 129], are shown in pink and black, respectively, with the solid and dashed lines corresponding to exclusions at 68% and 95% CL. The regions outside of the contours are considered excluded. In all cases, η_t production is included in the background model.

for the pseudoscalar (scalar) case. These limits are similar to the ATLAS results [32] in case of pseudoscalar production, and represent the most stringent limits on scalar resonances decaying into $t\bar{t}$ over a wide range of mass and width values.

Data availability statement

Release and preservation of data used by the CMS Collaboration as the basis for publications is guided by the CMS data preservation, re-use and open access policy. The

data that support the findings of this study are available upon reasonable request from the authors.

The CMS Collaboration

A Hayrapetyan, V Makarenko, A Tumasyan[1]
Yerevan Physics Institute, Yerevan, Armenia

W Adam, J W Andrejkovic, L Benato, T Bergauer, M Dragicevic, C Giordano, P S Hussain, M Jeitler[2], N Krammer, A Li, D Liko, M Matthewman, I Mikulec, J Schieck[2], R Schöfbeck[2], D Schwarz, M Shooshtari, M Sonawane, W Waltenberger, C-E Wulz[2]
Institut für Hochenergiephysik, Vienna, Austria

T Janssen, H Kwon, D Ocampo Henao, T Van Laer, P Van Mechelen
Universiteit Antwerpen, Antwerpen, Belgium

J Bierkens, N Breugelmans, J D'Hondt, S Dansana, A De Moor, M Delcourt, F Heyen, Y Hong, P Kashko, S Lowette, I Makarenko, D Müller, J Song, S Tavernier, M Tytgat[3], G P Van Onsem, S Van Putte, D Vannerom
Vrije Universiteit Brussel, Brussel, Belgium

B Bilin, B Clerbaux, A K Das, I De Bruyn, G De Lentdecker, H Evard, L Favart, P Gianneios, A Khalilzadeh, F A Khan, A Malara, M A Shahzad, L Thomas, M Vanden Bemden, C Vander Velde, P Vanlaer, F Zhang
Université Libre de Bruxelles, Bruxelles, Belgium

M De Coen, D Dobur, G Gokbulut, J Knolle, L Lambrecht, D Marckx, K Skovpen, N Van Den Bossche, J van der Linden, J Vandenbroeck, L Wezenbeek
Ghent University, Ghent, Belgium

S Bein, A Benecke, A Bethani, G Bruno, A Cappati, J De Favereau De Jeneret, C Delaere, A Giammanco, A O Guzel, V Lemaitre, J Lidrych, P Malek, P Mastrapasqua, S Turkcapar
Université Catholique de Louvain, Louvain-la-Neuve, Belgium

G A Alves, M Barroso Ferreira Filho, E Coelho, C Hensel, T Menezes De Oliveira, C Mora Herrera[4], P Rebello Teles, M Soeiro, E J Tonelli Manganote[5], A Vilela Pereira[4]
Centro Brasileiro de Pesquisas Fisicas, Rio de Janeiro, Brazil

W L Aldá Júnior, H Brandao Malbouisson, W Carvalho, J Chinellato[6], M Costa Reis, E M Da Costa, G G Da Silveira[7], D De Jesus Damiao, S Fonseca De Souza, R Gomes De Souza, S S Jesus, T Laux Kuhn[7], M Macedo, K Mota Amarilo, L Mundim, H Nogima, J P Pinheiro, A Santoro, A Sznajder, M Thiel, F Torres Da Silva De Araujo[8]
Universidade do Estado do Rio de Janeiro, Rio de Janeiro, Brazil

C A Bernardes[7], T R Fernandez Perez Tomei, E M Gregores, B Lopes Da Costa, I Maietto Silverio, P G Mercadante, S F Novaes, B Orzari, Sandra S Padula, V Scheurer
Universidade Estadual Paulista, Universidade Federal do ABC, São Paulo, Brazil

A Aleksandrov, G Antchev, P Danev, R Hadjiiska, P Iaydjiev, M Misheva, M Shopova, G Sultanov
Institute for Nuclear Research and Nuclear Energy, Bulgarian Academy of Sciences, Sofia, Bulgaria

A Dimitrov, L Litov, B Pavlov, P Petkov, A Petrov
University of Sofia, Sofia, Bulgaria

S Keshri, D Laroze, S Thakur
Instituto De Alta Investigación, Universidad de Tarapacá, Casilla 7 D, Arica, Chile

W Brooks
Universidad Tecnica Federico Santa Maria, Valparaiso, Chile

T Cheng, T Javaid, L Wang, L Yuan
Beihang University, Beijing, People's Republic of China

Z Hu, Z Liang, J Liu, X Wang
Department of Physics, Tsinghua University, Beijing, People's Republic of China

G M Chen[9], H S Chen[9], M Chen[9], Y Chen, Q Hou, X Hou, F Iemmi, C H Jiang, A Kapoor[10], H Liao, G Liu, Z-A Liu[11], J N Song[11], S Song, J Tao, C Wang[9], J Wang, H Zhang, J Zhao
Institute of High Energy Physics, Beijing, People's Republic of China

A Agapitos, Y Ban, A Carvalho Antunes De Oliveira, S Deng, B Guo, Q Guo, C Jiang, A Levin, C Li, Q Li, Y Mao, S Qian, S J Qian, X Qin, X Sun, D Wang, J Wang, H Yang, M Zhang, Y Zhao, C Zhou
State Key Laboratory of Nuclear Physics and Technology, Peking University, Beijing, People's Republic of China

S Yang
State Key Laboratory of Nuclear Physics and Technology, Institute of Quantum Matter, South China Normal University, Guangzhou, People's Republic of China

Z You
Sun Yat-Sen University, Guangzhou, People's Republic of China

K Jaffel, N Lu
University of Science and Technology of China, Hefei, People's Republic of China

G Bauer[12], B Li[13], H Wang, K Yi[14], J Zhang
Nanjing Normal University, Nanjing, People's Republic of China

Y Li
Institute of Modern Physics and Key Laboratory of Nuclear Physics and Ion-beam Application (MOE)—Fudan University, Shanghai, People's Republic of China

Z Lin, C Lu, M Xiao[15]
Zhejiang University, Hangzhou, Zhejiang, People's Republic of China

C Avila, D A Barbosa Trujillo, A Cabrera, C Florez, J Fraga, J A Reyes Vega
Universidad de Los Andes, Bogota, Colombia

C Rendón, M Rodriguez, A A Ruales Barbosa, J D Ruiz Alvarez
Universidad de Antioquia, Medellin, Colombia

N Godinovic, D Lelas, A Sculac
University of Split, Faculty of Electrical Engineering, Mechanical Engineering and Naval Architecture, Split, Croatia

M Kovac, A Petkovic, T Sculac
University of Split, Faculty of Science, Split, Croatia

P Bargassa, V Brigljevic, B K Chitroda, D Ferencek, K Jakovcic, A Starodumov, T Susa
Institute Rudjer Boskovic, Zagreb, Croatia

A Attikis, K Christoforou, A Hadjiagapiou, C Leonidou, C Nicolaou, L Paizanos, F Ptochos, P A Razis, H Rykaczewski, H Saka, A Stepennov
University of Cyprus, Nicosia, Cyprus

M Finger[†], M Finger Jr
Charles University, Prague, Czech Republic

E Ayala
Escuela Politecnica Nacional, Quito, Ecuador

E Carrera Jarrin
Universidad San Francisco de Quito, Quito, Ecuador

S Elgammal[16], A Ellithi Kamel[17]
Academy of Scientific Research and Technology of the Arab Republic of Egypt, Egyptian Network of High Energy Physics, Cairo, Egypt

M Abdullah Al-Mashad, A Hussein, H Mohammed
Center for High Energy Physics (CHEP-FU), Fayoum University, El-Fayoum, Egypt

K Ehataht, M Kadastik, T Lange, C Nielsen, J Pata, M Raidal, N Seeba, L Tani
National Institute of Chemical Physics and Biophysics, Tallinn, Estonia

A Milieva, K Osterberg, M Voutilainen
Department of Physics, University of Helsinki, Helsinki, Finland

N Bin Norjoharuddeen, E Brücken, F Garcia, P Inkaew, K T S Kallonen, R Kumar Verma, T Lampén, K Lassila-Perini, B Lehtela, S Lehti, T Lindén, N R Mancilla Xinto, M Myllymäki, M M Rantanen, S Saariokari, N T Toikka, J Tuominiemi
Helsinki Institute of Physics, Helsinki, Finland

H Kirschenmann, P Luukka, H Petrow
Lappeenranta-Lahti University of Technology, Lappeenranta, Finland

M Besancon, F Couderc, M Dejardin, D Denegri, P Devouge, J L Faure, F Ferri, P Gaigne, S Ganjour, P Gras, G Hamel de Monchenault, M Kumar, V Lohezic, J Malcles, F Orlandi, L Portales, S Ronchi, M Ö Sahin, A Savoy-Navarro[18], P Simkina, M Titov, M Tornago
IRFU, CEA, Université Paris-Saclay, Gif-sur-Yvette, France

F Beaudette, G Boldrini, P Busson, C Charlot, M Chiusi, T D Cuisset, F Damas, O Davignon, A De Wit, T Debnath, I T Ehle, B A Fontana Santos Alves, S Ghosh, A Gilbert, R Granier de Cassagnac, L Kalipoliti, M Manoni, M Nguyen, S Obraztsov, C Ochando, R Salerno, J B Sauvan, Y Sirois, G Sokmen, L Urda Gómez, A Zabi, A Zghiche
Laboratoire Leprince-Ringuet, CNRS/IN2P3, Ecole Polytechnique, Institut Polytechnique de Paris, Palaiseau, France

J-L Agram[19], J Andrea, D Bloch, J-M Brom, E C Chabert, C Collard, G Coulon, S Falke, U Goerlach, R Haeberle, A-C Le Bihan, M Meena, O Poncet, G Saha, P Vaucelle
Université de Strasbourg, CNRS, IPHC UMR 7178, Strasbourg, France

A Di Florio
Centre de Calcul de l'Institut National de Physique Nucleaire et de Physique des Particules, CNRS/IN2P3, Villeurbanne, France

D Amram, S Beauceron, B Blancon, G Boudoul, N Chanon, D Contardo, P Depasse, C Dozen[20], H El Mamouni, J Fay, S Gascon, M Gouzevitch, C Greenberg, G Grenier, B Ille, E Jourd'huy, I B Laktineh, M Lethuillier, B Massoteau, L Mirabito, A Purohit, M Vander Donckt, J Xiao
Institut de Physique des 2 Infinis de Lyon (IP2I), Villeurbanne, France

I Lomidze, T Toriashvili[21], Z Tsamalaidze[22]
Georgian Technical University, Tbilisi, Georgia

V Botta, S Consuegra Rodríguez, L Feld, K Klein, M Lipinski, D Meuser, P Nattland, V Oppenländer, A Pauls, D Pérez Adán, N Röwert, M Teroerde
RWTH Aachen University, I. Physikalisches Institut, Aachen, Germany

C Daumann, S Diekmann, A Dodonova, N Eich, D Eliseev, F Engelke, J Erdmann, M Erdmann, B Fischer, T Hebbeker, K Hoepfner, F Ivone, A Jung, N Kumar, M Y Lee, F Mausolf, M Merschmeyer, A Meyer, F Nowotny, A Pozdnyakov, W Redjeb, H Reithler, U Sarkar, V Sarkisovi, A Schmidt, C Seth, A Sharma, J L Spah, V Vaulin, S Zaleski
RWTH Aachen University, III. Physikalisches Institut A, Aachen, Germany

M R Beckers, C Dziwok, G Flügge, N Hoeflich, T Kress, A Nowack, O Pooth, A Stahl, A Zotz
RWTH Aachen University, III. Physikalisches Institut B, Aachen, Germany

H Aarup Petersen, A Abel, M Aldaya Martin, J Alimena, S Amoroso, Y An, I Andreev, J Bach, S Baxter, M Bayatmakou, H Becerril Gonzalez, O Behnke, A Belvedere, A A Bin Anuar, F Blekman[23], K Borras[24], A Campbell, S Chatterjee, L X Coll Saravia, G Eckerlin, D Eckstein, E Gallo[23], A Geiser, V Guglielmi, M Guthoff, A Hinzmann, L Jeppe, M Kasemann, C Kleinwort, R Kogler, M Komm, D Krücker, W Lange, D Leyva Pernia, K-Y Lin, K Lipka[25], W Lohmann[26], J Malvaso, R Mankel, I-A Melzer-Pellmann, M Mendizabal Morentin, A B Meyer, G Milella, K Moral Figueroa, A Mussgiller, L P Nair, J Niedziela, A Nürnberg, J Park, E Ranken, A Raspereza, D Rastorguev, J Rübenach, L Rygaard, M Scham[27,24], S Schnake[24], P Schütze, C Schwanenberger[23], D Selivanova, K Sharko, M Shchedrolosiev, D Stafford, M Torkian, F Vazzoler, A Ventura Barroso, R Walsh, D Wang, Q Wang, K Wichmann, L Wiens[24], C Wissing, Y Yang, S Zakharov, A Zimermmane Castro Santos
Deutsches Elektronen-Synchrotron, Hamburg, Germany

A Albrecht, A R Alves Andrade, M Antonello, S Bollweg, M Bonanomi, K El Morabit, Y Fischer, M Frahm, E Garutti, A Grohsjean, A A Guvenli, J Haller, D Hundhausen, G Kasieczka, P Keicher, R Klanner, W Korcari, T Kramer, C C Kuo, F Labe, J Lange, A Lobanov, L Moureaux, M Mrowietz, A Nigamova, K Nikolopoulos, Y Nissan, A Paasch, K J Pena Rodriguez, N Prouvost, T Quadfasel, B Raciti, M Rieger, D Savoiu, P Schleper, M Schröder, J Schwandt, M Sommerhalder, H Stadie, G Steinbrück, A Tews, R Ward, B Wiederspan, M Wolf
University of Hamburg, Hamburg, Germany

S Brommer, E Butz, Y M Chen, T Chwalek, A Dierlamm, G G Dincer, U Elicabuk, N Faltermann, M Giffels, A Gottmann, F Hartmann[28], R Hofsaess, M Horzela, U Husemann, J Kieseler, M Klute, R Kunnilan Muhammed Rafeek, O Lavoryk, J M Lawhorn, A Lintuluoto, S Maier, M Mormile, Th Müller, E Pfeffer, M Presilla, G Quast, K Rabbertz, B Regnery, R Schmieder, N Shadskiy, I Shvetsov, H J Simonis, L Sowa, L Stockmeier, K Tauqeer, M Toms, B Topko, N Trevisani, C Verstege, T Voigtländer, R F Von Cube, J Von Den Driesch, M Wassmer, R Wolf, W D Zeuner, X Zuo
Karlsruher Institut fuer Technologie, Karlsruhe, Germany

G Anagnostou, G Daskalakis, A Kyriakis
Institute of Nuclear and Particle Physics (INPP), NCSR Demokritos, Aghia Paraskevi, Greece

G Melachroinos, Z Painesis, I Paraskevas, N Saoulidou, K Theofilatos, E Tziaferi, K Vellidis, I Zisopoulos
National and Kapodistrian University of Athens, Athens, Greece

T Chatzistavrou, G Karapostoli, K Kousouris, E Siamarkou, G Tsipolitis
National Technical University of Athens, Athens, Greece

I Bestintzanos, I Evangelou, C Foudas, P Katsoulis, P Kokkas, P G Kosmoglou Kioseoglou, N Manthos, I Papadopoulos, J Strologas
University of Ioánnina, Ioánnina, Greece

D Druzhkin, C Hajdu, D Horvath[29,30], K Márton, A J Rádl[31], F Sikler, V Veszpremi
HUN-REN Wigner Research Centre for Physics, Budapest, Hungary

M Csanád, K Farkas, A Fehérkuti[32], M M A Gadallah[33], Á Kadlecsik, M León Coello, G Pásztor, G I Veres
MTA-ELTE Lendület CMS Particle and Nuclear Physics Group, Eötvös Loránd University, Budapest, Hungary

B Ujvari, G Zilizi
Faculty of Informatics, University of Debrecen, Debrecen, Hungary

G Bencze, S Czellar, J Molnar, Z Szillasi
HUN-REN ATOMKI—Institute of Nuclear Research, Debrecen, Hungary

T Csorgo[32], F Nemes[32], T Novak, I Szanyi[34]
Karoly Robert Campus, MATE Institute of Technology, Gyongyos, Hungary

S Bansal, S B Beri, V Bhatnagar, G Chaudhary, S Chauhan, N Dhingra[35], A Kaur, A Kaur, H Kaur, M Kaur, S Kumar, T Sheokand, J B Singh, A Singla
Panjab University, Chandigarh, India

A Bhardwaj, A Chhetri, B C Choudhary, A Kumar, A Kumar, M Naimuddin, S Phor, K Ranjan, M K Saini
University of Delhi, Delhi, India

S Acharya[36], B Gomber[36], B Sahu[36]
University of Hyderabad, Hyderabad, India

S Mukherjee
Indian Institute of Technology Kanpur, Kanpur, India

S Baradia, S Bhattacharya, S Das Gupta, S Dutta, S Dutta, S Sarkar
Saha Institute of Nuclear Physics, HBNI, Kolkata, India

M M Ameen, P K Behera, S Chatterjee, G Dash, A Dattamunsi, P Jana, P Kalbhor, S Kamble, J R Komaragiri[37], T Mishra, P R Pujahari, A K Sikdar, R K Singh, P Verma, S Verma, A Vijay
Indian Institute of Technology Madras, Madras, India

B K Sirasva
IISER Mohali, India, Mohali, India

L Bhatt, S Dugad, G B Mohanty, M Shelake, P Suryadevara
Tata Institute of Fundamental Research-A, Mumbai, India

A Bala, S Banerjee, S Barman[38], R M Chatterjee, M Guchait, Sh Jain, A Jaiswal, B M Joshi, S Kumar, M Maity[38], G Majumder, K Mazumdar, S Parolia, R Saxena, A Thachayath
Tata Institute of Fundamental Research-B, Mumbai, India

S Bahinipati[39], D Maity[40], P Mal, K Naskar[40], A Nayak[40], S Nayak, K Pal, R Raturi, P Sadangi, S K Swain, S Varghese[40], D Vats[40]
National Institute of Science Education and Research, An OCC of Homi Bhabha National Institute, Bhubaneswar, Odisha, India

A Alpana, S Dube, P Hazarika, B Kansal, A Laha, R Sharma, S Sharma, K Y Vaish
Indian Institute of Science Education and Research (IISER), Pune, India

S Ghosh
Indian Institute of Technology Hyderabad, Telangana, India

H Bakhshiansohi[41], A Jafari[42], V Sedighzadeh Dalavi, M Zeinali[43]
Isfahan University of Technology, Isfahan, Iran

S Bashiri, S Chenarani[44], S M Etesami, Y Hosseini, M Khakzad, E Khazaie, M Mohammadi Najafabadi, S Tizchang[45]
Institute for Research in Fundamental Sciences (IPM), Tehran, Iran

M Felcini, M Grunewald
University College Dublin, Dublin, Ireland

M Abbrescia[a,b], M Barbieri[a,b], M Buonsante[a,b], A Colaleo[a,b], D Creanza[a,c], B D'Anzi[a,b], N De Filippis[a,c], M De Palma[a,b], W Elmetenawee[a,b,46], N Ferrara[a,c], L Fiore[a], L Longo[a], M Louka[a,b], G Maggi[a,c], M Maggi[a], I Margjeka[a], V Mastrapasqua[a,b], S My[a,b], F Nenna[a,b], S Nuzzo[a,b], A Pellecchia[a,b], A Pompili[a,b], G Pugliese[a,c], R Radogna[a,b], D Ramos[a], A Ranieri[a], L Silvestris[a], F M Simone[a,c], Ü Sözbilir[a], A Stamerra[a,b], D Troiano[a,b], R Venditti[a,b], P Verwilligen[a], A Zaza[a,b]
INFN Sezione di Bari[a], Università di Bari[b], Politecnico di Bari[c], Bari, Italy

G Abbiendi[a], C Battilana[a,b], D Bonacorsi[a,b], P Capiluppi[a,b], F R Cavallo[a], M Cuffiani[a,b], T Diotalevi[a,b], F Fabbri[a], A Fanfani[a,b], D Fasanella[a], P Giacomelli[a], C Grandi[a], L Guiducci[a,b], S Lo Meo[a,47], M Lorusso[a,b], L Lunerti[a], S Marcellini[a], G Masetti[a], F L Navarria[a,b], G Paggi[a,b], A Perrotta[a], F Primavera[a,b], A M Rossi[a,b], S Rossi Tisbeni[a,b], T Rovelli[a,b], G P Siroli[a,b]
INFN Sezione di Bologna[a], Università di Bologna[b], Bologna, Italy

S Costa[a,b,48], A Di Mattia[a], A Lapertosa[a], R Potenza[a,b], A Tricomi[a,b,48]
INFN Sezione di Catania[a], Università di Catania[b], Catania, Italy

J Altork[a,b], P Assiouras[a], G Barbagli[a], G Bardelli[a], M Bartolini[a,b], A Calandri[a,b], B Camaiani[a,b], A Cassese[a], R Ceccarelli[a], V Ciulli[a,b], C Civinini[a], R D'Alessandro[a,b], L Damenti[a,b], E Focardi[a,b], T Kello[a], G Latino[a,b], P Lenzi[a,b], M Lizzo[a], M Meschini[a], S Paoletti[a], A Papanastassiou[a,b], G Sguazzoni[a], L Viliani[a]

INFN Sezione di Firenze[a], Università di Firenze[b], Firenze, Italy

L Benussi, S Colafranceschi, S Meola[49], D Piccolo
INFN Laboratori Nazionali di Frascati, Frascati, Italy

M Alves Gallo Pereira[a], F Ferro[a], E Robutti[a], S Tosi[a,b]
INFN Sezione di Genova[a], Università di Genova[b], Genova, Italy

A Benaglia[a], F Brivio[a], V Camagni[a,b], F Cetorelli[a,b], F De Guio[a,b], M E Dinardo[a,b], P Dini[a], S Gennai[a], R Gerosa[a,b], A Ghezzi[a,b], P Govoni[a,b], L Guzzi[a], M R Kim[a], G Lavizzari[a,b], M T Lucchini[a,b], M Malberti[a], S Malvezzi[a], A Massironi[a], D Menasce[a], L Moroni[a], M Paganoni[a,b], S Palluotto[a,b], D Pedrini[a], A Perego[a,b], B S Pinolini[a], G Pizzati[a,b], S Ragazzi[a,b], T Tabarelli de Fatis[a,b]
INFN Sezione di Milano-Bicocca[a], Università di Milano-Bicocca[b], Milano, Italy

S Buontempo[a], C Di Fraia[a,b], F Fabozzi[a,c], L Favilla[a,d], A O M Iorio[a,b], L Lista[a,b,50], P Paolucci[a,28], B Rossi[a]
INFN Sezione di Napoli[a], Università di Napoli 'Federico II'[b], Napoli, Italy; Università della Basilicata[c], Potenza, Italy; Scuola Superiore Meridionale (SSM)[d], Napoli, Italy

P Azzi[a], N Bacchetta[a,51], D Bisello[a,b], P Bortignon[a], G Bortolato[a,b], A C M Bulla[a], R Carlin[a,b], P Checchia[a], T Dorigo[a,52], F Gasparini[a,b], U Gasparini[a,b], S Giorgetti[a], E Lusiani[a], M Margoni[a,b], M Michelotto[a], J Pazzini[a,b], P Ronchese[a,b], R Rossin[a,b], F Simonetto[a,b], M Tosi[a,b], A Triossi[a,b], S Ventura[a], P Zotto[a,b], A Zucchetta[a,b], G Zumerle[a,b]
INFN Sezione di Padova[a], Università di Padova[b], Padova, Italy; Universita degli Studi di Cagliari[c], Cagliari, Italy

A Braghieri[a], S Calzaferri[a], P Montagna[a,b], M Pelliccioni[a], V Re[a], C Riccardi[a,b], P Salvini[a], I Vai[a,b], P Vitulo[a,b]
INFN Sezione di Pavia[a], Università di Pavia[b], Pavia, Italy

S Ajmal[a,b], M E Ascioti[a,b], G M Bilei[a], C Carrivale[a,b], D Ciangottini[a,b], L Della Penna[a,b], L Fanò[a,b], V Mariani[a,b], M Menichelli[a], F Moscatelli[a,53], A Rossi[a,b], A Santocchia[a,b], D Spiga[a], T Tedeschi[a,b]
INFN Sezione di Perugia[a], Università di Perugia[b], Perugia, Italy

C Aimè[a,b], C A Alexe[a,c], P Asenov[a,b], P Azzurri[a], G Bagliesi[a], R Bhattacharya[a], L Bianchini[a,b], T Boccali[a], E Bossini[a], D Bruschini[a,c], L Calligaris[a,b], R Castaldi[a], F Cattafesta[a,c], M A Ciocci[a,d], M Cipriani[a,b], R Dell'Orso[a], S Donato[a,b], R Forti[a,b], A Giassi[a], F Ligabue[a,c], A C Marini[a,b], D Matos Figueiredo[a], A Messineo[a,b], S Mishra[a], V K Muraleedharan Nair Bindhu[a,b], S Nandan[a], F Palla[a], M Riggirello[a,c], A Rizzi[a,b], G Rolandi[a,c], S Roy Chowdhury[a,54], T Sarkar[a], A Scribano[a], P Solanki[a,b], P Spagnolo[a], F Tenchini[a,b], R Tenchini[a], G Tonelli[a,b], N Turini[a,d], F Vaselli[a,c], A Venturi[a], P G Verdini[a]
INFN Sezione di Pisa[a], Università di Pisa[b], Scuola Normale Superiore di Pisa[c], Pisa, Italy; Università di Siena[d], Siena, Italy

P Akrap[a,b], C Basile[a,b], S C Behera[a], F Cavallari[a], L Cunqueiro Mendez[a,b], F De Riggi[a,b], D Del Re[a,b], E Di Marco[a], M Diemoz[a], F Errico[a], L Frosina[a,b], R Gargiulo[a,b], B Harikrishnan[a,b], F Lombardi[a,b], E Longo[a,b], L Martikainen[a,b], J Mijuskovic[a,b], G Organtini[a,b], N Palmeri[a,b], R Paramatti[a,b], C Quaranta[a,b], S Rahatlou[a,b], C Rovelli[a], F Santanastasio[a,b], L Soffi[a], V Vladimirov[a,b]
INFN Sezione di Roma[a], Sapienza Università di Roma[b], Roma, Italy

N Amapane[a,b], R Arcidiacono[a,c], S Argiro[a,b], M Arneodo[a,c], N Bartosik[a,c], R Bellan[a,b], A Bellora[a,b], C Biino[a], C Borca[a,b], N Cartiglia[a], M Costa[a,b], R Covarelli[a,b], N Demaria[a], L Finco[a], M Grippo[a,b], B Kiani[a,b], L Lanteri[a,b], F Legger[a], F Luongo[a,b], C Mariotti[a], S Maselli[a], A Mecca[a,b], L Menzio[a,b], P Meridiani[a], E Migliore[a,b], M Monteno[a], M M Obertino[a,b], G Ortona[a], L Pacher[a,b], N Pastrone[a], M Ruspa[a,c], F Siviero[a,b], V Sola[a,b], A Solano[a,b], A Staiano[a], C Tarricone[a,b], D Trocino[a], G Umoret[a,b], E Vlasov[a,b], R White[a,b]
INFN Sezione di Torino[a], Università di Torino[b], Torino, Italy; Università del Piemonte Orientale[c], Novara, Italy

J Babbar[a,b], S Belforte[a], V Candelise[a,b], M Casarsa[a], F Cossutti[a], K De Leo[a], G Della Ricca[a,b], R Delli Gatti[a,b]
INFN Sezione di Trieste[a], Università di Trieste[b], Trieste, Italy

S Dogra, J Hong, J Kim, T Kim, D Lee, H Lee, J Lee, S W Lee, C S Moon, Y D Oh, S Sekmen, B Tae, Y C Yang
Kyungpook National University, Daegu, Republic of Korea

M S Kim
Department of Mathematics and Physics—GWNU, Gangneung, Republic of Korea

G Bak, P Gwak, H Kim, D H Moon, J Seo
Chonnam National University, Institute for Universe and Elementary Particles, Kwangju, Republic of Korea

E Asilar, F Carnevali, J Choi[55], T J Kim, Y Ryou
Hanyang University, Seoul, Republic of Korea

S Ha, S Han, B Hong, K Lee, K S Lee, S Lee, J Yoo
Korea University, Seoul, Republic of Korea

J Goh, J Shin, S Yang
Kyung Hee University, Department of Physics, Seoul, Republic of Korea

Y Kang, H S Kim, Y Kim, S Lee
Sejong University, Seoul, Republic of Korea

J Almond, J H Bhyun, J Choi, J Choi, W Jun, H Kim, J Kim, T Kim, Y Kim, Y W Kim, S Ko, H Lee, J Lee, J Lee, B H Oh, S B Oh, J Shin, U K Yang, I Yoon
Seoul National University, Seoul, Republic of Korea

W Jang, D Y Kang, D Kim, S Kim, B Ko, J S H Lee, Y Lee, I C Park, Y Roh, I J Watson
University of Seoul, Seoul, Republic of Korea

G Cho, K Hwang, B Kim, S Kim, K Lee, H D Yoo
Yonsei University, Department of Physics, Seoul, Republic of Korea

M Choi, Y Lee, I Yu
Sungkyunkwan University, Suwon, Republic of Korea

T Beyrouthy, Y Gharbia
College of Engineering and Technology, American University of the Middle East (AUM), Dasman, Kuwait

F Alazemi
Kuwait University—College of Science—Department of Physics, Safat, Kuwait

K Dreimanis, O M Eberlins, A Gaile, C Munoz Diaz, D Osite, G Pikurs, R Plese, A Potrebko, M Seidel, D Sidiropoulos Kontos
Riga Technical University, Riga, Latvia

N R Strautnieks
University of Latvia (LU), Riga, Latvia

M Ambrozas, A Juodagalvis, S Nargelas, A Rinkevicius, G Tamulaitis
Vilnius University, Vilnius, Lithuania

I Yusuff[56], Z Zolkapli
National Centre for Particle Physics, Universiti Malaya, Kuala Lumpur, Malaysia

J F Benitez, A Castaneda Hernandez, A Cota Rodriguez, L E Cuevas Picos, H A Encinas Acosta, L G Gallegos Maríñez, J A Murillo Quijada, A Sehrawat, L Valencia Palomo
Universidad de Sonora (UNISON), Hermosillo, Mexico

G Ayala, H Castilla-Valdez, H Crotte Ledesma, R Lopez-Fernandez, J Mejia Guisao, R Reyes-Almanza, A Sánchez Hernández
Centro de Investigacion y de Estudios Avanzados del IPN, Mexico City, Mexico

C Oropeza Barrera, D L Ramirez Guadarrama, M Ramírez García
Universidad Iberoamericana, Mexico City, Mexico

I Bautista, F E Neri Huerta, I Pedraza, H A Salazar Ibarguen, C Uribe Estrada
Benemerita Universidad Autonoma de Puebla, Puebla, Mexico

I Bubanja, N Raicevic
University of Montenegro, Podgorica, Montenegro

P H Butler
University of Canterbury, Christchurch, New Zealand

A Ahmad, M I Asghar, A Awais, M I M Awan, W A Khan
National Centre for Physics, Quaid-I-Azam University, Islamabad, Pakistan

V Avati, L Forthomme, L Grzanka, M Malawski, K Piotrzkowski
AGH University of Krakow, Krakow, Poland

M Bluj, M Górski, M Kazana, M Szleper, P Zalewski
National Centre for Nuclear Research, Swierk, Poland

K Bunkowski, K Doroba, A Kalinowski, M Konecki, J Krolikowski, A Muhammad
Institute of Experimental Physics, Faculty of Physics, University of Warsaw, Warsaw, Poland

P Fokow, K Pozniak, W Zabolotny
Warsaw University of Technology, Warsaw, Poland

M Araujo, D Bastos, C Beirão Da Cruz E Silva, A Boletti, M Bozzo, T Camporesi, G Da Molin, M Gallinaro, J Hollar, N Leonardo, G B Marozzo, A Petrilli, M Pisano, J Seixas, J Varela, J W Wulff
Laboratório de Instrumentacão e Física Experimental de Partículas, Lisboa, Portugal

P Adzic, L Markovic, P Milenovic, V Milosevic
Faculty of Physics, University of Belgrade, Belgrade, Serbia

D Devetak, M Dordevic, J Milosevic, L Nadderd, V Rekovic, M Stojanovic
VINCA Institute of Nuclear Sciences, University of Belgrade, Belgrade, Serbia

M Alcalde Martinez, J Alcaraz Maestre, Cristina F Bedoya, J A Brochero Cifuentes, Oliver M Carretero, M Cepeda, M Cerrada, N Colino, J Cuchillo Ortega, B De La Cruz,

A Delgado Peris, A Escalante Del Valle, D Fernández Del Val, J P Fernández Ramos, J Flix, M C Fouz, M Gonzalez Hernandez, O Gonzalez Lopez, S Goy Lopez, J M Hernandez, M I Josa, J Llorente Merino, C Martin Perez, E Martin Viscasillas, D Moran, C M Morcillo Perez, R Paz Herrera, C Perez Dengra, A Pérez-Calero Yzquierdo, J Puerta Pelayo, I Redondo, J Vazquez Escobar
Centro de Investigaciones Energéticas Medioambientales y Tecnológicas (CIEMAT), Madrid, Spain

J F de Trocóniz
Universidad Autónoma de Madrid, Madrid, Spain

B Alvarez Gonzalez, J Ayllon Torresano, A Cardini, J Cuevas, J Del Riego Badas, D Estrada Acevedo, J Fernandez Menendez, S Folgueras, I Gonzalez Caballero, P Leguina, M Obeso Menendez, E Palencia Cortezon, J Prado Pico, A Soto Rodríguez, C Vico Villalba, P Vischia
Universidad de Oviedo, Instituto Universitario de Ciencias y Tecnologías Espaciales de Asturias (ICTEA), Oviedo, Spain

S Blanco Fernández, I J Cabrillo, A Calderon, J Duarte Campderros, M Fernandez, G Gomez, C Lasaosa García, R Lopez Ruiz, C Martinez Rivero, P Martinez Ruiz del Arbol, F Matorras, P Matorras Cuevas, E Navarrete Ramos, J Piedra Gomez, C Quintana San Emeterio, L Scodellaro, I Vila, R Vilar Cortabitarte, J M Vizan Garcia
Instituto de Física de Cantabria (IFCA), CSIC-Universidad de Cantabria, Santander, Spain

B Kailasapathy[57], D D C Wickramarathna
University of Colombo, Colombo, Sri Lanka

W G D Dharmaratna[58], K Liyanage, N Perera
University of Ruhuna, Department of Physics, Matara, Sri Lanka

D Abbaneo, C Amendola, R Ardino, E Auffray, J Baechler, D Barney, M Bianco, A Bocci, L Borgonovi, C Botta, A Bragagnolo, C E Brown, C Caillol, G Cerminara, P Connor, D d'Enterria, A Dabrowski, A David, A De Roeck, M M Defranchis, M Deile, M Dobson, W Funk, A Gaddi, S Giani, D Gigi, K Gill, F Glege, M Glowacki, A Gruber, J Hegeman, J K Heikkilä, B Huber, V Innocente, T James, P Janot, O Kaluzinska, O Karacheban[26], G Karathanasis, S Laurila, P Lecoq, C Lourenco, A-M Lyon, M Magherini, L Malgeri, M Mannelli, A Mehta, F Meijers, J A Merlin, S Mersi, E Meschi, M Migliorini, F Monti, F Moortgat, M Mulders, M Musich, I Neutelings, S Orfanelli, F Pantaleo, M Pari, G Petrucciani, A Pfeiffer, M Pierini, M Pitt, H Qu, D Rabady, B Ribeiro Lopes, F Riti, P Rosado, M Rovere, H Sakulin, R Salvatico, S Sanchez Cruz, S Scarfi, M Selvaggi, A Sharma, K Shchelina, P Silva, P Sphicas[59], A G Stahl Leiton, A Steen, S Summers, D Treille, P Tropea, E Vernazza, J Wanczyk[60], J Wang, S Wuchterl, M Zarucki, P Zehetner, P Zejdl, G Zevi Della Porta
CERN European Organization for Nuclear Research, Geneva, Switzerland

T Bevilacqua[61], L Caminada[61], W Erdmann, R Horisberger, Q Ingram, H C Kaestli, D Kotlinski, C Lange, U Langenegger, M Missiroli[61], L Noehte[61], T Rohe, A Samalan
PSI Center for Neutron and Muon Sciences, Villigen, Switzerland

T K Aarrestad, M Backhaus, G Bonomelli, C Cazzaniga, K Datta, P De Bryas Dexmiers D'archiacchiac[60], A De Cosa, G Dissertori, M Dittmar, M Donegà, F Eble, K Gedia, F Glessgen, C Grab, N Härringer, T G Harte, W Lustermann, M Malucchi, R A Manzoni, M Marchegiani, L Marchese, A Mascellani[60], F Nessi-Tedaldi, F Pauss, V Perovic, B Ristic, R Seidita, J Steggemann[60], A Tarabini, D Valsecchi, R Wallny
ETH Zurich—Institute for Particle Physics and Astrophysics (IPA), Zurich, Switzerland

C Amsler[62], P Bärtschi, F Bilandzija, M F Canelli, G Celotto, K Cormier, M Huwiler, W Jin, A Jofrehei, B Kilminster, T H Kwok, S Leontsinis, V Lukashenko, A Macchiolo, F Meng, J Motta, A Reimers, P Robmann, M Senger, E Shokr, F Stäger, R Tramontano
Universität Zürich, Zurich, Switzerland

D Bhowmik, C M Kuo, P K Rout, S Taj, P C Tiwari[37]
National Central University, Chung-Li, Taiwan

L Ceard, K F Chen, Z G Chen, A De Iorio, W-S Hou, T H Hsu, Y W Kao, S Karmakar, G Kole, Y Y Li, R-S Lu, E Paganis, X F Su, J Thomas-Wilsker, L S Tsai, D Tsionou, H Y Wu, E Yazgan
National Taiwan University (NTU), Taipei, Taiwan

C Asawatangtrakuldee, N Srimanobhas
High Energy Physics Research Unit, Department of Physics, Faculty of Science, Chulalongkorn University, Bangkok, Thailand

Y Maghrbi
Tunis El Manar University, Tunis, Tunisia

D Agyel, F Dolek, I Dumanoglu[63], Y Guler[64], E Gurpinar Guler[64], C Isik, O Kara, A Kayis Topaksu, Y Komurcu, G Onengut, K Ozdemir[65], B Tali[66], U G Tok, E Uslan, I S Zorbakir

Cukurova University, Physics Department, Science and Art Faculty, Adana, Turkey

M Yalvac[67]
Middle East Technical University, Physics Department, Ankara, Turkey

B Akgun, I O Atakisi[68]**, E Gülmez, M Kaya**[69]**, O Kaya**[70]**, M A Sarkisla**[71]**, S Tekten**[72]
Bogazici University, Istanbul, Turkey

A Cakir, K Cankocak[63,73]**, S Sen**[74]
Istanbul Technical University, Istanbul, Turkey

O Aydilek[75]**, B Hacisahinoglu, I Hos**[76]**, B Kaynak, S Ozkorucuklu, O Potok, H Sert, C Simsek, C Zorbilmez**
Istanbul University, Istanbul, Turkey

S Cerci, B Isildak[77]**, E Simsek, D Sunar Cerci, T Yetkin**[20]
Yildiz Technical University, Istanbul, Turkey

A Boyaryntsev, O Dadazhanova, B Grynyov
Institute for Scintillation Materials of National Academy of Science of Ukraine, Kharkiv, Ukraine

L Levchuk
National Science Centre, Kharkiv Institute of Physics and Technology, Kharkiv, Ukraine

J J Brooke, A Bundock, F Bury, E Clement, D Cussans, D Dharmender, H Flacher, J Goldstein, H F Heath, M-L Holmberg, L Kreczko, S Paramesvaran, L Robertshaw, M S Sanjrani[41]**, J Segal, V J Smith**
University of Bristol, Bristol, United Kingdom

A H Ball, K W Bell, A Belyaev[78]**, C Brew, R M Brown, D J A Cockerill, A Elliot, K V Ellis, J Gajownik, K Harder, S Harper, J Linacre, K Manolopoulos, M Moallemi, D M Newbold, E Olaiya, D Petyt, T Reis, A R Sahasransu, G Salvi, T Schuh, C H Shepherd-Themistocleous, I R Tomalin, K C Whalen, T Williams**
Rutherford Appleton Laboratory, Didcot, United Kingdom

I Andreou, R Bainbridge, P Bloch, O Buchmuller, C A Carrillo Montoya, D Colling, J S Dancu, I Das, P Dauncey, G Davies, M Della Negra, S Fayer, G Fedi, G Hall, H R Hoorani, A Howard, G Iles, C R Knight, P Krueper, J Langford, K H Law, J León Holgado, E Leutgeb, L Lyons, A-M Magnan, B Maier, S Mallios, A Mastronikolis, M Mieskolainen, J Nash[79]**, M Pesaresi, P B Pradeep, B C Radburn-Smith, A Richards, A Rose, L Russell, K Savva, C Seez, R Shukla, A Tapper, K Uchida, G P Uttley, T Virdee**[28]**, M Vojinovic, N Wardle, D Winterbottom**
Imperial College, London, United Kingdom

J E Cole, A Khan, P Kyberd, I D Reid
Brunel University, Uxbridge, United Kingdom

S Abdullin, A Brinkerhoff, E Collins, M R Darwish, J Dittmann, K Hatakeyama, V Hegde, J Hiltbrand, B McMaster, J Samudio, S Sawant, C Sutantawibul, J Wilson
Baylor University, Waco, TX, United States of America

J M Hogan[80]
Bethel University, St. Paul, MN, United States of America

R Bartek, A Dominguez, S Raj, A E Simsek, S S Yu
Catholic University of America, Washington, DC, United States of America

B Bam, A Buchot Perraguin, S Campbell, R Chudasama, S I Cooper, C Crovella, G Fidalgo, S V Gleyzer, A Khukhunaishvili, K Matchev, E Pearson, C U Perez, P Rumerio[81]**, E Usai, R Yi**
The University of Alabama, Tuscaloosa, AL, United States of America

S Cholak, G De Castro, Z Demiragli, C Erice, C Fangmeier, C Fernandez Madrazo, E Fontanesi, J Fulcher, F Golf, S Jeon, J O'Cain, I Reed, J Rohlf, K Salyer, D Sperka, D Spitzbart, I Suarez, A Tsatsos, E Wurtz, A G Zecchinelli
Boston University, Boston, MA, United States of America

G Barone, G Benelli, D Cutts, S Ellis, L Gouskos, M Hadley, U Heintz, K W Ho, T Kwon, G Landsberg, K T Lau, J Luo, S Mondal, J Roloff, T Russell, S Sagir[82]**, X Shen, M Stamenkovic, N Venkatasubramanian**
Brown University, Providence, RI, United States of America

S Abbott, B Barton, R Breedon, H Cai, M Calderon De La Barca Sanchez, M Chertok, M Citron, J Conway, P T Cox, R Erbacher, O Kukral, G Mocellin, S Ostrom, I Salazar Segovia, W Wei, S Yoo
University of California, Davis, Davis, CA, United States of America

K Adamidis, M Bachtis, D Campos, R Cousins, A Datta, G Flores Avila, J Hauser, M Ignatenko, M A Iqbal, T Lam, Y F Lo, E Manca, A Nunez Del Prado, D Saltzberg, V Valuev
University of California, Los Angeles, CA, United States of America

R Clare, J W Gary, G Hanson
University of California, Riverside, Riverside, CA, United States of America

A Aportela, A Arora, J G Branson, S Cittolin, S Cooperstein, D Diaz, J Duarte, L Giannini, Y Gu, J Guiang, V Krutelyov, R Lee, J Letts, H Li, M Masciovecchio, F Mokhtar, S Mukherjee, M Pieri, D Primosch, M Quinnan, V Sharma, M Tadel, E Vourliotis, F Würthwein, A Yagil, Z Zhao
University of California, San Diego, La Jolla, CA, United States of America

A Barzdukas, L Brennan, C Campagnari, S Carron Montero[83], K Downham, C Grieco, M M Hussain, J Incandela, J Kim, M W K Lai, A J Li, P Masterson, J Richman, S N Santpur, U Sarica, R Schmitz, F Setti, J Sheplock, D Stuart, T Á Vámi, X Yan, D Zhang
University of California, Santa Barbara—Department of Physics, Santa Barbara, CA, United States of America

A Albert, S Bhattacharya, A Bornheim, O Cerri, R Kansal, J Mao, H B Newman, G Reales Gutiérrez, T Sievert, M Spiropulu, J R Vlimant, R A Wynne, S Xie
California Institute of Technology, Pasadena, CA, United States of America

J Alison, S An, M Cremonesi, V Dutta, E Y Ertorer, T Ferguson, T A Gómez Espinosa, A Harilal, A Kallil Tharayil, M Kanemura, C Liu, P Meiring, T Mudholkar, S Murthy, P Palit, K Park, M Paulini, A Roberts, A Sanchez, W Terrill
Carnegie Mellon University, Pittsburgh, PA, United States of America

J P Cumalat, W T Ford, A Hart, A Hassani, S Kwan, J Pearkes, C Savard, N Schonbeck, K Stenson, K A Ulmer, S R Wagner, N Zipper, D Zuolo
University of Colorado Boulder, Boulder, CO, United States of America

J Alexander, X Chen, D J Cranshaw, J Dickinson, J Fan, X Fan, J Grassi, S Hogan, P Kotamnives, J Monroy, G Niendorf, M Oshiro, J R Patterson, M Reid, A Ryd, J Thom, P Wittich, R Zou, L Zygala
Cornell University, Ithaca, NY, United States of America

M Albrow, M Alyari, O Amram, G Apollinari, A Apresyan, L A T Bauerdick, D Berry, J Berryhill, P C Bhat, K Burkett, J N Butler, A Canepa, G B Cerati, H W K Cheung, F Chlebana, C Cosby, G Cummings, I Dutta, V D Elvira, J Freeman, A Gandrakota, Z Gecse, L Gray, D Green, A Grummer, S Grünendahl, D Guerrero, O Gutsche, R M Harris, T C Herwig, J Hirschauer, B Jayatilaka, S Jindariani, M Johnson, U Joshi, T Klijnsma, B Klima, K H M Kwok, S Lammel, C Lee, D Lincoln, R Lipton, T Liu, K Maeshima, D Mason, P McBride, P Merkel, S Mrenna, S Nahn, J Ngadiuba, D Noonan, S Norberg, V Papadimitriou, N Pastika, K Pedro, C Pena[84], C E Perez Lara, F Ravera, A Reinsvold Hall[85], L Ristori, M Safdari, E Sexton-Kennedy, N Smith, A Soha, L Spiegel, S Stoynev, J Strait, L Taylor, S Tkaczyk, N V Tran, L Uplegger, E W Vaandering, C Wang, I Zoi
Fermi National Accelerator Laboratory, Batavia, IL, United States of America

C Aruta, P Avery, D Bourilkov, P Chang, V Cherepanov, R D Field, C Huh, E Koenig, M Kolosova, J Konigsberg, A Korytov, N Menendez, G Mitselmakher, K Mohrman, A Muthirakalayil Madhu, N Rawal, S Rosenzweig, V Sulimov, Y Takahashi, J Wang
University of Florida, Gainesville, FL, United States of America

T Adams, A Al Kadhim, A Askew, S Bower, R Hashmi, R S Kim, T Kolberg, G Martinez, M Mazza, H Prosper, P R Prova, M Wulansatiti, R Yohay
Florida State University, Tallahassee, FL, United States of America

B Alsufyani, S Butalla, S Das, M Hohlmann, M Lavinsky, E Yanes
Florida Institute of Technology, Melbourne, FL, United States of America

M R Adams, N Barnett, A Baty, C Bennett, R Cavanaugh, R Escobar Franco, O Evdokimov, C E Gerber, H Gupta, M Hawksworth, A Hingrajiya, D J Hofman, J H Lee, D S Lemos, C Mills, S Nanda, G Nigmatkulov, B Ozek, T Phan, D Pilipovic, R Pradhan, E Prifti, P Roy, T Roy, N Singh, M B Tonjes, N Varelas, M A Wadud, J Yoo
University of Illinois Chicago, Chicago, IL, United States of America

M Alhusseini, D Blend, K Dilsiz[86], O K Köseyan, A Mestvirishvili[87], O Neogi, H Ogul[88], Y Onel, A Penzo, C Snyder, E Tiras[89]
The University of Iowa, Iowa City, IA, United States of America

B Blumenfeld, J Davis, A V Gritsan, L Kang, S Kyriacou, P Maksimovic, M Roguljic, S Sekhar, M V Srivastav, M Swartz
Johns Hopkins University, Baltimore, MD, United States of America

A Abreu, L F Alcerro Alcerro, J Anguiano, S Arteaga Escatel, P Baringer, A Bean, Z Flowers,

D Grove, J King, G Krintiras, M Lazarovits, C Le Mahieu, J Marquez, M Murray, M Nickel, S Popescu[90], C Rogan, C Royon, S Rudrabhatla, S Sanders, C Smith, G Wilson
The University of Kansas, Lawrence, KS, United States of America

B Allmond, R Gujju Gurunadha, N Islam, A Ivanov, K Kaadze, Y Maravin, J Natoli, D Roy, G Sorrentino
Kansas State University, Manhattan, KS, United States of America

A Baden, A Belloni, J Bistany-riebman, S C Eno, N J Hadley, S Jabeen, R G Kellogg, T Koeth, B Kronheim, S Lascio, P Major, A C Mignerey, C Palmer, C Papageorgakis, M M Paranjpe, E Popova[91], A Shevelev, L Zhang
University of Maryland, College Park, MD, United States of America

C Baldenegro Barrera, J Bendavid, H Bossi, S Bright-Thonney, I A Cali, Y C Chen, P C Chou, M D'Alfonso, J Eysermans, C Freer, G Gomez-Ceballos, M Goncharov, G Grosso, P Harris, D Hoang, G M Innocenti, D Kovalskyi, J Krupa, L Lavezzo, Y-J Lee, K Long, C Mcginn, A Novak, M I Park, C Paus, C Reissel, C Roland, G Roland, S Rothman, T A Sheng, G S F Stephans, D Walter, Z Wang, B Wyslouch, T J Yang
Massachusetts Institute of Technology, Cambridge, MA, United States of America

B Crossman, W J Jackson, C Kapsiak, M Krohn, D Mahon, J Mans, B Marzocchi, R Rusack, O Sancar, R Saradhy, N Strobbe
University of Minnesota, Minneapolis, MN, United States of America

K Bloom, D R Claes, G Haza, J Hossain, C Joo, I Kravchenko, A Rohilla, J E Siado, W Tabb, A Vagnerini, A Wightman, F Yan
University of Nebraska-Lincoln, Lincoln, NE, United States of America

H Bandyopadhyay, L Hay, H W Hsia, I Iashvili, A Kalogeropoulos, A Kharchilava, A Mandal, M Morris, D Nguyen, S Rappoccio, H Rejeb Sfar, A Williams, P Young, D Yu
State University of New York at Buffalo, Buffalo, NY, United States of America

G Alverson, E Barberis, J Bonilla, B Bylsma, M Campana, J Dervan, Y Haddad, Y Han, I Israr, A Krishna, M Lu, N Manganelli, R Mccarthy, D M Morse, T Orimoto, A Parker, L Skinnari, C S Thoreson, E Tsai, D Wood
Northeastern University, Boston, MA, United States of America

S Dittmer, K A Hahn, Y Liu, M Mcginnis, Y Miao, D G Monk, M H Schmitt, A Taliercio, M Velasco, J Wang
Northwestern University, Evanston, IL, United States of America

G Agarwal, R Band, R Bucci, S Castells, A Das, A Ehnis, R Goldouzian, M Hildreth, K Hurtado Anampa, T Ivanov, C Jessop, A Karneyeu, K Lannon, J Lawrence, N Loukas, L Lutton, J Mariano, N Marinelli, I Mcalister, T McCauley, C Mcgrady, C Moore, Y Musienko[22], H Nelson, M Osherson, A Piccinelli, R Ruchti, A Townsend, Y Wan, M Wayne, H Yockey
University of Notre Dame, Notre Dame, IN, United States of America

A Basnet, M Carrigan, R De Los Santos, L S Durkin, C Hill, M Joyce, M Nunez Ornelas, D A Wenzl, B L Winer, B R Yates
The Ohio State University, Columbus, OH, United States of America

H Bouchamaoui, K Coldham, P Das, G Dezoort, P Elmer, A Frankenthal, M Galli, B Greenberg, N Haubrich, K Kennedy, G Kopp, Y Lai, D Lange, A Loeliger, D Marlow, I Ojalvo, J Olsen, F Simpson, D Stickland, C Tully
Princeton University, Princeton, NJ, United States of America

S Malik, R Sharma
University of Puerto Rico, Mayaguez, PR, United States of America

S Chandra, R Chawla, A Gu, L Gutay, M Jones, A W Jung, D Kondratyev, M Liu, G Negro, N Neumeister, G Paspalaki, S Piperov, N R Saha, J F Schulte, F Wang, A Wildridge, W Xie, Y Yao, Y Zhong
Purdue University, West Lafayette, IN, United States of America

N Parashar, A Pathak, E Shumka
Purdue University Northwest, Hammond, IN, United States of America

D Acosta, A Agrawal, C Arbour, T Carnahan, K M Ecklund, P J Fernández Manteca, S Freed, P Gardner, F J M Geurts, T Huang, I Krommydas, N Lewis, W Li, J Lin, O Miguel Colin, B P Padley, R Redjimi, J Rotter, E Yigitbasi, Y Zhang
Rice University, Houston, TX, United States of America

O Bessidskaia Bylund, A Bodek, P de Barbaro[†], R Demina, A Garcia-Bellido, H S Hare, O Hindrichs, N Parmar, P Parygin[91], H Seo, R Taus
University of Rochester, Rochester, NY, United States of America

B Chiarito, J P Chou, S V Clark, S Donnelly, D Gadkari, Y Gershtein, E Halkiadakis, M Heindl, C Houghton, D Jaroslawski, S Konstantinou, I Laflotte, A Lath, J Martins, B Rand, J Reichert, P Saha, S Salur, S Schnetzer, S Somalwar, R Stone, S A Thayil, S Thomas, J Vora
Rutgers, The State University of New Jersey, Piscataway, NJ, United States of America

D Ally, A G Delannoy, S Fiorendi, J Harris, S Higginbotham, T Holmes, A R Kanuganti, N Karunarathna, J Lawless, L Lee, E Nibigira, B Skipworth, S Spanier
University of Tennessee, Knoxville, TN, United States of America

D Aebi, M Ahmad, T Akhter, K Androsov, A Bolshov, O Bouhali[92], A Cagnotta, V D'Amante, R Eusebi, P Flanagan, J Gilmore, Y Guo, T Kamon, S Luo, R Mueller, A Safonov
Texas A&M University, College Station, TX, United States of America

N Akchurin, J Damgov, Y Feng, N Gogate, Y Kazhykarim, K Lamichhane, S W Lee, C Madrid, A Mankel, T Peltola, I Volobouev
Texas Tech University, Lubbock, TX, United States of America

E Appelt, Y Chen, S Greene, A Gurrola, W Johns, R Kunnawalkam Elayavalli, A Melo, D Rathjens, F Romeo, P Sheldon, S Tuo, J Velkovska, J Viinikainen, J Zhang
Vanderbilt University, Nashville, TN, United States of America

B Cardwell, H Chung, B Cox, J Hakala, R Hirosky, M Jose, A Ledovskoy, C Mantilla, C Neu, C Ramón Álvarez
University of Virginia, Charlottesville, VA, United States of America

S Bhattacharya, P E Karchin
Wayne State University, Detroit, MI, United States of America

A Aravind, S Banerjee, K Black, T Bose, E Chavez, S Dasu, P Everaerts, C Galloni, H He, M Herndon, A Herve, C K Koraka, S Lomte, R Loveless, A Mallampalli, A Mohammadi, S Mondal, T Nelson, G Parida, L Pétré, D Pinna, A Savin, V Shang, V Sharma, W H Smith, D Teague, H F Tsoi, W Vetens, A Warden
University of Wisconsin—Madison, Madison, WI, United States of America

S Afanasiev, V Alexakhin, Yu Andreev, T Aushev, D Budkouski, R Chistov[93], M Danilov[93], T Dimova[93], A Ershov[93], S Gninenko, I Gorbunov, A Gribushin[93], A Kamenev, V Karjavine, M Kirsanov, V Klyukhin[93], O Kodolova[94,91], V Korenkov, A Kozyrev[93], N Krasnikov, A Lanev, A Malakhov, V Matveev[93], A Nikitenko[95,94], V Palichik, V Perelygin, S Petrushanko[93], S Polikarpov[93], O Radchenko[93], M Savina, V Shalaev, S Shmatov, S Shulha, Y Skovpen[93], V Smirnov, O Teryaev, I Tlisova[93], A Toropin, N Voytishin, B S Yuldashev[†,96], A Zarubin, I Zhizhin
Authors affiliated with an international laboratory covered by a cooperation agreement with CERN

E Boos, V Bunichev, M Dubinin[84], V Savrin, A Snigirev, L Dudko, K Ivanov, V Kim[22], V Murzin, V Oreshkin, D Sosnov
Authors affiliated with an institute formerly covered by a cooperation agreement with CERN

[†]Deceased
[1]Also at Yerevan State University, Yerevan, Armenia
[2]Also at TU Wien, Vienna, Austria
[3]Also at Ghent University, Ghent, Belgium
[4]Also at Universidade do Estado do Rio de Janeiro, Rio de Janeiro, Brazil
[5]Also at FACAMP—Faculdades de Campinas, Sao Paulo, Brazil
[6]Also at Universidade Estadual de Campinas, Campinas, Brazil
[7]Also at Federal University of Rio Grande do Sul, Porto Alegre, Brazil
[8]Also at The University of the State of Amazonas, Manaus, Brazil
[9]Also at University of Chinese Academy of Sciences, Beijing, People's Republic of China
[10]Also at China Center of Advanced Science and Technology, Beijing, People's Republic of China
[11]Also at University of Chinese Academy of Sciences, Beijing, People's Republic of China
[12]Now at Henan Normal University, Xinxiang, People's Republic of China
[13]Also at University of Shanghai for Science and Technology, Shanghai, People's Republic of China
[14]Now at The University of Iowa, Iowa City, IA, United States of America
[15]Also at Center for High Energy Physics, Peking University, Beijing, People's Republic of China
[16]Now at British University in Egypt, Cairo, Egypt
[17]Now at Cairo University, Cairo, Egypt
[18]Also at Purdue University, West Lafayette, IN, United States of America
[19]Also at Université de Haute Alsace, Mulhouse, France
[20]Also at Istinye University, Istanbul, Turkey
[21]Also at Tbilisi State University, Tbilisi, Georgia
[22]Also at an institute formerly covered by a cooperation agreement with CERN
[23]Also at University of Hamburg, Hamburg, Germany
[24]Also at RWTH Aachen University, III. Physikalisches Institut A, Aachen, Germany

[25]Also at Bergische University Wuppertal (BUW), Wuppertal, Germany
[26]Also at Brandenburg University of Technology, Cottbus, Germany
[27]Also at Forschungszentrum Jülich, Juelich, Germany
[28]Also at CERN European Organization for Nuclear Research, Geneva, Switzerland
[29]Also at HUN-REN ATOMKI—Institute of Nuclear Research, Debrecen, Hungary
[30]Now at Universitatea Babes-Bolyai—Facultatea de Fizica, Cluj-Napoca, Romania
[31]Also at MTA-ELTE Lendület CMS Particle and Nuclear Physics Group, Eötvös Loránd University, Budapest, Hungary
[32]Also at HUN-REN Wigner Research Centre for Physics, Budapest, Hungary
[33]Also at Physics Department, Faculty of Science, Assiut University, Assiut, Egypt
[34]Also at The University of Kansas, Lawrence, KS, United States of America
[35]Also at Punjab Agricultural University, Ludhiana, India
[36]Also at University of Hyderabad, Hyderabad, India
[37]Also at Indian Institute of Science (IISc), Bangalore, India
[38]Also at University of Visva-Bharati, Santiniketan, India
[39]Also at IIT Bhubaneswar, Bhubaneswar, India
[40]Also at Institute of Physics, Bhubaneswar, India
[41]Also at Deutsches Elektronen-Synchrotron, Hamburg, Germany
[42]Also at Isfahan University of Technology, Isfahan, Iran
[43]Also at Sharif University of Technology, Tehran, Iran
[44]Also at Department of Physics, University of Science and Technology of Mazandaran, Behshahr, Iran
[45]Also at Department of Physics, Faculty of Science, Arak University, ARAK, Iran
[46]Also at Helwan University, Cairo, Egypt
[47]Also at Italian National Agency for New Technologies, Energy and Sustainable Economic Development, Bologna, Italy
[48]Also at Centro Siciliano di Fisica Nucleare e di Struttura Della Materia, Catania, Italy
[49]Also at Università degli Studi Guglielmo Marconi, Roma, Italy
[50]Also at Scuola Superiore Meridionale, Università di Napoli 'Federico II', Napoli, Italy
[51]Also at Fermi National Accelerator Laboratory, Batavia, IL, United States of America
[52]Also at Lulea University of Technology, Lulea, Sweden
[53]Also at Consiglio Nazionale delle Ricerche—Istituto Officina dei Materiali, Perugia, Italy
[54]Also at UPES—University of Petroleum and Energy Studies, Dehradun, India
[55]Also at Institut de Physique des 2 Infinis de Lyon (IP2I), Villeurbanne, France
[56]Also at Department of Applied Physics, Faculty of Science and Technology, Universiti Kebangsaan Malaysia, Bangi, Malaysia
[57]Also at Trincomalee Campus, Eastern University, Sri Lanka, Nilaveli, Sri Lanka
[58]Also at Saegis Campus, Nugegoda, Sri Lanka
[59]Also at National and Kapodistrian University of Athens, Athens, Greece
[60]Also at Ecole Polytechnique Fédérale Lausanne, Lausanne, Switzerland
[61]Also at Universität Zürich, Zurich, Switzerland
[62]Also at Stefan Meyer Institute for Subatomic Physics, Vienna, Austria
[63]Also at Near East University, Research Center of Experimental Health Science, Mersin, Turkey
[64]Also at Konya Technical University, Konya, Turkey
[65]Also at Izmir Bakircay University, Izmir, Turkey
[66]Also at Adiyaman University, Adiyaman, Turkey
[67]Also at Bozok Universitetesi Rektörlügü, Yozgat, Turkey
[68]Also at Istanbul Sabahattin Zaim University, Istanbul, Turkey
[69]Also at Marmara University, Istanbul, Turkey
[70]Also at Milli Savunma University, Istanbul, Turkey
[71]Also at Informatics and Information Security Research Center, Gebze/Kocaeli, Turkey
[72]Also at Kafkas University, Kars, Turkey
[73]Now at Istanbul Okan University, Istanbul, Turkey
[74]Also at Hacettepe University, Ankara, Turkey
[75]Also at Erzincan Binali Yildirim University, Erzincan, Turkey
[76]Also at Istanbul University—Cerrahpasa, Faculty of Engineering, Istanbul, Turkey
[77]Also at Yildiz Technical University, Istanbul, Turkey
[78]Also at School of Physics and Astronomy, University of Southampton, Southampton, United Kingdom
[79]Also at Monash University, Faculty of Science, Clayton, Australia
[80]Also at Bethel University, St. Paul, MN, United States of America
[81]Also at Università di Torino, Torino, Italy
[82]Also at Karamanoğlu Mehmetbey University, Karaman, Turkey
[83]Also at California Lutheran University, Thousand Oaks, CA, United States of America
[84]Also at California Institute of Technology, Pasadena, CA, United States of America
[85]Also at United States Naval Academy, Annapolis, MD, United States of America
[86]Also at Bingol University, Bingol, Turkey
[87]Also at Georgian Technical University, Tbilisi, Georgia
[88]Also at Sinop University, Sinop, Turkey
[89]Also at Erciyes University, Kayseri, Turkey
[90]Also at Horia Hulubei National Institute of Physics and Nuclear Engineering (IFIN-HH), Bucharest, Romania
[91]Now at another institute formerly covered by a cooperation agreement with CERN
[92]Also at Hamad Bin Khalifa University (HBKU), Doha, Qatar
[93]Also at another institute formerly covered by a cooperation agreement with CERN
[94]Also at Yerevan Physics Institute, Yerevan, Armenia
[95]Also at Imperial College, London, United Kingdom
[96]Also at Institute of Nuclear Physics of the Uzbekistan Academy of Sciences, Tashkent, Uzbekistan

References

[1] ATLAS Collaboration 2012 Observation of a new particle in the search for the standard model Higgs boson with the ATLAS detector at the LHC *Phys. Lett. B* **716** 1

[2] CMS Collaboration 2012 Observation of a new boson at a mass of 125 GeV with the CMS experiment at the LHC *Phys. Lett. B* **716** 30

[3] CMS Collaboration 2013 Observation of a new boson with mass near 125 GeV in pp collisions at $\sqrt{s} = 7$ and 8 TeV *J. High Energy Phys.* JHEP06(2013)081

[4] Branco G C *et al* 2012 Theory and phenomenology of two-Higgs-doublet models *Phys. Rep.* **516** 1

[5] Huitu K, Koivunen N, Lebedev O, Mondal S and Toma T 2019 Probing pseudo-Goldstone dark matter at the LHC *Phys. Rev. D* **100** 015009

[6] Mühlleitner M, Sampaio M O P, Santos R and Wittbrodt J 2017 Phenomenological comparison of models with extended Higgs sectors *J. High Energy Phys.* JHEP08(2017)132

[7] Abdallah J *et al* 2015 Simplified models for dark matter searches at the LHC *Phys. Dark Univ.* **9–10** 8

[8] Arina C *et al* 2016 A comprehensive approach to dark matter studies: exploration of simplified top-philic models *J. High Energy Phys.* JHEP11(2016)111

[9] Craig N, Galloway J and Thomas S 2013 Searching for signs of the second Higgs doublet (arXiv:1305.2424)

[10] Carena M and Liu Z 2016 Challenges and opportunities for heavy scalar searches in the $\mathrm{t\bar{t}}$ channel at the LHC *J. High Energy Phys.* JHEP11(2016)159

[11] Djouadi A, Ellis J, Popov A and Quevillon J 2019 Interference effects in $\mathrm{t\bar{t}}$ production at the LHC as a window on new physics *J. High Energy Phys.* JHEP03(2019)119

[12] Gaemers K J F and Hoogeveen F 1984 Higgs production and decay into heavy flavours with the gluon fusion mechanism *Phys. Lett. B* **146** 347

[13] Dicus D, Stange A and Willenbrock S 1994 Higgs decay to top quarks at hadron colliders *Phys. Lett. B* **333** 126

[14] Bernreuther W, Flesch M and Haberl P 1998 Signatures of Higgs bosons in the top quark decay channel at hadron colliders *Phys. Rev. D* **58** 114031

[15] Bernreuther W, Galler P, Mellein C, Si Z-G and Uwer P 2016 Production of heavy Higgs bosons and decay into top quarks at the LHC *Phys. Rev. D* **93** 034032

[16] Bernreuther W, Galler P, Si Z-G and Uwer P 2017 Production of heavy Higgs bosons and decay into top quarks at the LHC. II. Top-quark polarization and spin correlation effects *Phys. Rev. D* **95** 095012

[17] Bernreuther W, Brandenburg A, Si Z G and Uwer P 2004 Top quark pair production and decay at hadron colliders *Nucl. Phys. B* **690** 81

[18] Bernreuther W 2008 Top-quark physics at the LHC *J. Phys. G* **35** 083001

[19] Mahlon G and Parke S J 2010 Spin correlation effects in top quark pair production at the LHC *Phys. Rev. D* **81** 074024

[20] Fadin V S and Khoze V A 1987 Threshold behavior of the cross section for the production of t quarks in $\mathrm{e^+e^-}$ annihilation *JETP Lett.* **46** 525 (available at: http://jetpletters.ru/ps/0/article_18631.shtml)

[21] Fadin V S, Khoze V A and Sjöstrand T 1990 On the threshold behaviour of heavy top production *Z. Phys. C* **48** 613

[22] Hoang A H *et al* 2000 Top-antitop pair production close to threshold: synopsis of recent NNLO results *Eur. Phys. J. Direct* **2** 1

[23] Kiyo Y, Kühn J H, Moch S, Steinhauser M and Uwer P 2009 Top-quark pair production near threshold at LHC *Eur. Phys. J. C* **60** 375

[24] Ju W-L , Wang G, Wang X, Xu X, Xu Y and Yang L L 2020 Top quark pair production near threshold: single/double distributions and mass determination *J. High Energy Phys.* JHEP06(2020)158

[25] Fuks B, Hagiwara K, Ma K and Zheng Y-J 2021 Signatures of toponium formation in LHC run 2 data *Phys. Rev. D* **104** 034023

[26] CMS Collaboration 2021 Precision luminosity measurement in proton-proton collisions at $\sqrt{s} = 13$ TeV in 2015 and 2016 at CMS *Eur. Phys. J. C* **81** 800

[27] CMS Collaboration 2018 CMS luminosity measurement for the 2017 data-taking period at $\sqrt{s} = 13$ TeV *CMS Physics Analysis Summary* CMS-PAS-LUM-17-004 (available at: https://cds.cern.ch/record/2621960)

[28] CMS Collaboration 2019 CMS luminosity measurement for the 2018 data-taking period at $\sqrt{s} = 13$ TeV *CMS Physics Analysis Summary* CMS-PAS-LUM-18-002 (available at: https://cds.cern.ch/record/2676164)

[29] CMS Collaboration 2025 Observation of a pseudoscalar excess at the top quark pair production threshold *Rep. Prog. Phys.* **88** 087801

[30] CMS Collaboration 2020 Search for heavy Higgs bosons decaying to a top quark pair in proton-proton collisions at $\sqrt{s} = 13$ TeV *J. High Energy Phys.* JHEP04(2020)171

[31] ATLAS Collaboration 2017 Search for heavy Higgs bosons A/H decaying to a top quark pair in pp collisions at $\sqrt{s} = 8$ TeV with the ATLAS detector *Phys. Rev. Lett.* **119** 191803

[32] ATLAS Collaboration 2024 Search for heavy neutral Higgs bosons decaying into a top quark pair in 140 $\mathrm{fb^{-1}}$ of proton-proton collision data at $\sqrt{s} = 13$ TeV with the ATLAS detector *J. High Energy Phys.* JHEP08(2024)013

[33] CMS Collaboration 2008 The CMS experiment at the CERN LHC *JINST* **3** S08004

[34] CMS Collaboration 2024 Development of the CMS detector for the CERN LHC Run 3 *JINST* **19** 05064

[35] CMS Collaboration 2020 Performance of the CMS Level-1 trigger in proton-proton collisions at $\sqrt{s} = 13$ TeV *JINST* **15** 10017

[36] CMS Collaboration 2017 The CMS trigger system *JINST* **12** 01020

[37] CMS Collaboration 2024 Performance of the CMS high-level trigger during LHC Run 2 *JINST* **19** 11021

[38] CMS Collaboration 2015 Technical proposal for the Phase-II upgrade of the Compact Muon Solenoid *CMS Technical Proposal* CERN-LHCC-2015-010, CMS-TDR-15-02 (https://doi.org/10.17181/CERN.VU8I.D59J)

[39] CMS Collaboration 2017 Particle-flow reconstruction and global event description with the CMS detector *JINST* **12** 10003

[40] Cacciari M, Salam G P and Soyez G 2008 The anti-k_T jet clustering algorithm *J. High Energy Phys.* JHEP04(2008)063

[41] Cacciari M, Salam G P and Soyez G 2012 FastJet user manual *Eur. Phys. J. C* **72** 1896

[42] CMS Collaboration 2020 Pileup mitigation at CMS in 13 TeV data *JINST* **15** 09018

[43] CMS Collaboration 2017 Jet energy scale and resolution in the CMS experiment in pp collisions at 8 TeV *JINST* **12** 02014

[44] CMS Collaboration 2018 Identification of heavy-flavour jets with the CMS detector in pp collisions at 13 TeV *JINST* **13** 05011

[45] Bols E , Kieseler J, Verzetti M, Stoye M and Stakia A 2020 Jet flavour classification using DeepJet *JINST* **15** 12012

[46] CMS Collaboration 2023 Performance summary of AK4 jet b tagging with data from proton-proton collisions at 13 TeV with the CMS detector *CMS Detector*

Performance Note CMS-DP-2023-005 (available at: https://cds.cern.ch/record/2854609)
[47] CMS Collaboration 2021 Electron and photon reconstruction and identification with the CMS experiment at the CERN LHC *JINST* **16** 05014
[48] CMS Collaboration 2020 ECAL 2016 refined calibration and Run 2 summary plots *CMS Detector Performance Note* CMS-DP-2020-021 (available at: https://cds.cern.ch/record/2717925)
[49] CMS Collaboration 2018 Performance of the CMS muon detector and muon reconstruction with proton-proton collisions at $\sqrt{s} = 13\,\text{TeV}$ *JINST* **13** 06015
[50] CMS Collaboration 2019 Performance of missing transverse momentum reconstruction in proton-proton collisions at $\sqrt{s} = 13\,\text{TeV}$ using the CMS detector *JINST* **14** 07004
[51] CMS Collaboration 2020 Simulation of the silicon strip tracker pre-amplifier in early 2016 data *CMS Detector Performance Note* CMS-DP-2020-045 (available at: https://cds.cern.ch/record/2740688)
[52] NNPDF Collaboration 2015 Parton distributions for the LHC run II *J. High Energy Phys.* JHEP04(2015)040
[53] Sjöstrand T *et al* 2015 An introduction to PYTHIA 8.2 *Comput. Phys. Commun.* **191** 159
[54] Skands P, Carrazza S and Rojo J 2014 Tuning PYTHIA 8.1: the Monash 2013 tune *Eur. Phys. J. C* **74** 3024
[55] CMS Collaboration 2020 Extraction and validation of a new set of CMS PYTHIA 8 tunes from underlying-event measurements *Eur. Phys. J. C* **80** 4
[56] GEANT4 Collaboration 2003 GEANT4—a simulation toolkit *Nucl. Instrum. Methods Phys. Res. A* **506** 250
[57] Alwall J *et al* 2014 The automated computation of tree-level and next-to-leading order differential cross sections and their matching to parton shower simulations *J. High Energy Phys.* JHEP07(2014)079
[58] Spira M, Djouadi A, Graudenz D and Zerwas P M 1995 Higgs boson production at the LHC *Nucl. Phys. B* **453** 17
[59] Hespel B, Maltoni F and Vryonidou E 2016 Signal background interference effects in heavy scalar production and decay to a top-anti-top pair *J. High Energy Phys.* JHEP10(2016)016
[60] Harlander R V, Liebler S and Mantler H 2013 SUSHI: a program for the calculation of Higgs production in gluon fusion and bottom-quark annihilation in the standard model and the MSSM *Comput. Phys. Commun.* **184** 1605
[61] Harlander R V, Liebler S and Mantler H 2017 SUSHI bento: beyond NNLO and the heavy-top limit *Comput. Phys. Commun.* **212** 239
[62] Eriksson D, Rathsman J and Stål O 2010 2HDMC—two-Higgs-doublet model calculator *Comput. Phys. Commun.* **181** 189
Eriksson D, Rathsman J and Stål O 2010 *Comput. Phys. Commun.* **181** 985 (erratum)
[63] Banfi A, Kauer N, Lind A, Lindert J M and Wood R 2024 Higgs interference effects in top-quark pair production in the 1HSM *J. High Energy Phys.* JHEP08(2024)112
[64] HEPData record for this analysis 2025 (available at: http://dx.doi.org/10.17182/hepdata.159298)
[65] Fuks B, Hagiwara K, Ma K and Zheng Y-J 2025 Simulating toponium formation signals at the LHC *Eur. Phys. J. C* **85** 157
[66] Sumino Y and Yokoya H 2010 Bound-state effects on kinematical distributions of top quarks at hadron colliders *J. High Energy Phys.* JHEP09(2010)034
Sumino Y and Yokoya H 2016 *J. High Energy Phys.* JHEP06(2016)037 (erratum)
[67] Maltoni F, Severi C, Tentori S and Vryonidou E 2024 Quantum detection of new physics in top-quark pair production at the LHC *J. High Energy Phys.* JHEP03(2024)099
[68] Nason P 2004 A new method for combining NLO QCD with shower Monte Carlo algorithms *J. High Energy Phys.* JHEP11(2004)040
[69] Frixione S, Nason P and Oleari C 2007 Matching NLO QCD computations with parton shower simulations: the POWHEG method *J. High Energy Phys.* JHEP11(2007)070
[70] Alioli S, Nason P, Oleari C and Re E 2010 A general framework for implementing NLO calculations in shower Monte Carlo programs: the POWHEG BOX *J. High Energy Phys.* JHEP06(2010)043
[71] Campbell J M, Ellis R K, Nason P and Re E 2015 Top-pair production and decay at NLO matched with parton showers *J. High Energy Phys.* JHEP04(2015)114
[72] Gigg M A and Richardson P 2008 Simulation of finite width effects in physics beyond the standard model (arXiv:0805.3037)
[73] Czakon M and Mitov A 2014 TOP++: a program for the calculation of the top-pair cross-section at hadron colliders *Comput. Phys. Commun.* **185** 2930
[74] Grazzini M, Kallweit S and Wiesemann M 2018 Fully differential NNLO computations with MATRIX *Eur. Phys. J. C* **78** 537
[75] Bernreuther W, Fücker M and Si Z G 2006 Mixed QCD and weak corrections to top quark pair production at hadron colliders *Phys. Lett. B* **633** 54
Bernreuther W, Fücker M and Si Z G 2007 *Phys. Lett. B* **644** 386 (erratum)
[76] Kühn J H, Scharf A and Uwer P 2006 Electroweak corrections to top-quark pair production in quark-antiquark annihilation *Eur. Phys. J. C* **45** 139
[77] Bernreuther W, Fücker M and Si Z-G 2006 Weak interaction corrections to hadronic top quark pair production *Phys. Rev. D* **74** 113005
[78] Kühn J H, Scharf A and Uwer P 2007 Electroweak effects in top-quark pair production at hadron colliders *Eur. Phys. J. C* **51** 37
[79] Aliev M *et al* 2011 HATHOR: Hadronic top and heavy quarks cross section calculator *Comput. Phys. Commun.* **182** 1034
[80] Kühn J H, Scharf A and Uwer P 2015 Weak interactions in top-quark pair production at hadron colliders: an update *Phys. Rev. D* **91** 014020
[81] Re E 2011 Single-top Wt-channel production matched with parton showers using the POWHEG method *Eur. Phys. J. C* **71** 1547
[82] Alioli S, Nason P, Oleari C and Re E 2009 NLO single-top production matched with shower in POWHEG: *s*- and *t*-channel contributions *J. High Energy Phys.* JHEP09(2009)111
Alioli S, Nason P, Oleari C and Re E 2010 *J. High Energy Phys.* JHEP02(2010)011 (erratum)
[83] Kant P *et al* 2015 HATHOR for single top-quark production: updated predictions and uncertainty estimates for single top-quark production in hadronic collisions *Comput. Phys. Commun.* **191** 74
[84] Kidonakis N and Yamanaka N 2021 Higher-order correction for tW production at high-energy hadron colliders *J. High Energy Phys.* **05** 278
[85] Monni P F *et al* 2020 MiNNLOPS: a new method to match NNLO QCD to parton showers *J. High Energy Phys.* JHEP05(2020)143
Monni P F *et al* 2022 *J. High Energy Phys.* JHEP02(2022)031 (erratum)
[86] Monni P F, Re E and Wiesemann M 2020 MiNNLOPS: optimizing $2 \to 1$ hadronic processes *Eur. Phys. J. C* **80** 1075
[87] Barberio E and Was Z 1994 PHOTOS—a universal Monte Carlo for QED radiative corrections: version 2.0 *Comput. Phys. Commun.* **79** 291

[88] Golonka P and Was Z 2006 PHOTOS Monte Carlo: a precision tool for QED corrections in Z and W decays *Eur. Phys. J. C* **45** 97

[89] Alwall J *et al* 2008 Comparative study of various algorithms for the merging of parton showers and matrix elements in hadronic collisions *Eur. Phys. J. C* **53** 473

[90] Melnikov K and Petriello F 2006 Electroweak gauge boson production at hadron colliders through $\mathcal{O}(\alpha_S^2)$ *Phys. Rev. D* **74** 114017

[91] Li Y and Petriello F 2012 Combining QCD and electroweak corrections to dilepton production in FEWZ *Phys. Rev. D* **86** 094034

[92] Gehrmann T, Grazzini M, Kallweit S, Maierhöfer P, von Manteuffel A, Pozzorini S, Rathlev D and Tancredi L 2014 W^+W^- production at hadron colliders in next to next to leading order QCD *Phys. Rev. Lett.* **113** 212001

[93] Campbell J M and Ellis R K 2010 MCFM for the Tevatron and the LHC *Nucl. Phys. B* **205–206** 10

[94] Frixione S and Webber B R 2002 Matching NLO QCD computations and parton shower simulations *J. High Energy Phys.* JHEP06(2002)029

[95] Frederix R and Frixione S 2012 Merging meets matching in MC@NLO *J. High Energy Phys.* JHEP12(2012)061

[96] Betchart B A, Demina R and Harel A 2014 Analytic solutions for neutrino momenta in decay of top quarks *Nucl. Instrum. Methods Phys. Res. A* **736** 169

[97] Demina R, Harel A and Orbaker D 2015 Reconstructing $\mathrm{t\bar{t}}$ events with one lost jet *Nucl. Instrum. Methods Phys. Res. A* **788** 128

[98] CMS Collaboration 2015 Measurement of the differential cross section for top quark pair production in pp collisions at $\sqrt{s} = 8$ TeV *Eur. Phys. J. C* **75** 542

[99] Sonnenschein L 2006 Analytical solution of $\mathrm{t\bar{t}}$ dilepton equations *Phys. Rev. D* **73** 054015
Sonnenschein L 2008 *Phys. Rev. D* **78** 079902 (erratum)

[100] CMS Collaboration 2017 Measurement of double-differential cross sections for top quark pair production in pp collisions at $\sqrt{s} = 8$ TeV and impact on parton distribution functions *Eur. Phys. J. C* **77** 459

[101] Korol I 2016 Measurement of double differential $\mathrm{t\bar{t}}$ production cross sections with the CMS detector *PhD Thesis* Universität Hamburg (https://doi.org/10.3204/DESY-THESIS-2016-011)

[102] Bernreuther W and Si Z-G 2010 Distributions and correlations for top quark pair production and decay at the Tevatron and LHC *Nucl. Phys. B* **837** 90

[103] Bernreuther W, Heisler D and Si Z-G 2015 A set of top quark spin correlation and polarization observables for the LHC: standard model predictions and new physics contributions *J. High Energy Phys.* JHEP12(2015)026

[104] Aguilar-Saavedra J A and Casas J A 2022 Improved tests of entanglement and Bell inequalities with LHC tops *Eur. Phys. J. C* **82** 666

[105] Aguilar-Saavedra J A 2024 Toponium hunter's guide *Phys. Rev. D* **110** 054032

[106] CMS Collaboration 2011 Measurement of the $\mathrm{t\bar{t}}$ production cross section and the top quark mass in the dilepton channel in pp collisions at $\sqrt{s} = 7$ TeV *J. High Energy Phys.* JHEP07(2011)049

[107] CMS Collaboration 2024 The CMS statistical analysis and combination tool: COMBINE *Comput. Softw. Big Sci.* **8** 19

[108] CMS Collaboration 2019 Combined measurements of Higgs boson couplings in proton-proton collisions at $\sqrt{s} = 13$ TeV *Eur. Phys. J. C* **79** 421

[109] CMS Collaboration 2016 Measurement of the top quark mass using proton-proton data at $\sqrt{s} = 7$ and 8 TeV *Phys. Rev. D* **93** 072004

[110] Butterworth J *et al* 2016 PDF4LHC recommendations for LHC Run 2 *J. Phys. G* **43** 023001

[111] Christiansen J R and Skands P Z 2015 String formation beyond leading colour *J. High Energy Phys.* JHEP08(2015)003

[112] CMS Collaboration 2023 CMS PYTHIA 8 colour reconnection tunes based on underlying-event data *Eur. Phys. J. C* **83** 587

[113] CMS Collaboration 2016 Investigations of the impact of the parton shower tuning in PYTHIA 8 in the modelling of $\mathrm{t\bar{t}}$ at $\sqrt{s} = 8$ and 13 TeV *CMS Physics Analysis Summary* CMS-PAS-TOP-16-021 (available at: https://cds.cern.ch/record/2235192)

[114] ATLAS Collaboration 2017 Measurement of the inclusive cross-sections of single top-quark and top-antiquark t-channel production in pp collisions at $\sqrt{s} = 13$ TeV with the ATLAS detector *J. High Energy Phys.* JHEP04(2017)086

[115] CMS Collaboration 2020 Measurement of the single top quark and antiquark production cross sections in the t channel and their ratio in proton-proton collisions at $\sqrt{s} = 13$ TeV *Phys. Lett. B* **800** 135042

[116] CMS Collaboration 2018 Measurement of the production cross section for single top quarks in association with W bosons in proton-proton collisions at $\sqrt{s} = 13$ TeV *J. High Energy Phys.* JHEP10(2018)117

[117] CMS Collaboration 2018 Measurement of the cross section for top quark pair production in association with a W or Z boson in proton-proton collisions at $\sqrt{s} = 13$ TeV *J. High Energy Phys.* JHEP08(2018)011

[118] ATLAS Collaboration 2019 Measurement of the $\mathrm{t\bar{t}Z}$ and $\mathrm{t\bar{t}W}$ cross sections in proton-proton collisions at $\sqrt{s} = 13$ TeV with the ATLAS detector *Phys. Rev. D* **99** 072009

[119] ATLAS Collaboration 2017 Measurements of top-quark pair to Z-boson cross-section ratios at $\sqrt{s} = 13$, 8, 7 TeV with the ATLAS detector *J. High Energy Phys.* JHEP02(2017)117

[120] Barlow R and Beeston C 1993 Fitting using finite Monte Carlo samples *Comput. Phys. Commun.* **77** 219

[121] Cleveland W S 1979 Robust locally weighted regression and smoothing scatterplots *J. Am. Stat. Assoc.* **74** 829

[122] Cleveland W S and Devlin S J 1988 Locally weighted regression: an approach to regression analysis by local fitting *J. Am. Stat. Assoc.* **83** 596

[123] Djouadi A, Ellis J and Quevillon J 2025 Contrasting pseudoscalar Higgs and toponium states at the LHC and beyond *Phys. Lett. B* **866** 139583

[124] Cowan G, Cranmer K, Gross E and Vitells O 2011 Asymptotic formulae for likelihood-based tests of new physics *Eur. Phys. J. C* **71** 1554
Cowan G, Cranmer K, Gross E and Vitells O 2013 *Eur. Phys. J. C* **73** 2501 (erratum)

[125] ATLAS and CMS Collaborations, and LHC Higgs Combination Group 2011 Procedure for the LHC Higgs boson search combination in Summer 2011 *Technical Report* CMS-NOTE-2011-005, ATL-PHYS-PUB-2011-11 (available at: https://cds.cern.ch/record/1379837)

[126] Junk T 1999 Confidence level computation for combining searches with small statistics *Nucl. Instrum. Methods Phys. Res. A* **434** 435

[127] Read A L 2002 Presentation of search results: the $\mathrm{CL_s}$ technique *J. Phys. G* **28** 2693

[128] Feldman G J and Cousins R D 1998 Unified approach to the classical statistical analysis of small signals *Phys. Rev. D* **57** 3873

[129] Cousins R D and Highland V L 1992 Incorporating systematic uncertainties into an upper limit *Nucl. Instrum. Methods Phys. Res. A* **320** 331